Ph.D. in Scientific Computing: Models, Structures, Algorithms and Applications

Delay Differential Equations in a Nonlinear Cochlear Model

Doctoral Thesis submitted to
Department of Science and High Technology
University of Insubria
Como, Italy

XXVI CYCLE

Supervisor
Prof. Dr. Daniele Bertaccini

Ph.D. Student
Teresa Botti

December 2014

Ph.D. in Scientific Computing:
Models, Structures, Algorithms and Applications

Department of Science and High Technology, University of Insubria
Como, Italy

Delay Differential Equations in a Nonlinear Cochlear Model
Doctoral Thesis submitted by Teresa Botti

Abstract

The human auditory system performs its primary function in the cochlea, the main organ of the inner ear, where the spectral analysis of a sound signal and its transduction into a neural signal occur. It is filled with liquid and divided in two cavities by the basilar membrane (BM). A sound stimulus propagates in air as an acoustic pressure wave through the outer and the middle ear. The pressure of the stapes on the oval window (boundary between the middle and the inner ear) causes the cochlear fluid to flow between the two cavities through a hole at the end of the BM. A spatial partial differential equation of fluid-dynamics describes this physical process. As a consequence of the differential pressure between the two cavities, each micro-element of the BM oscillates as a forced damped harmonic oscillator. The BM displacement is amplified by the overlying outer hair cells (OHCs) through a nonlinear nonlocal active feedback mechanism. The latter can be modeled by means of various representations. Among them, the delayed stiffness model of Talmadge et al. (J. Acoust. Soc. Am. 104, 1998) has been considered in this thesis. Specifically, the cochlear nonlinearity is introduced as a quadratic function of the BM displacement in the passive linear damping function. Moreover, the active mechanism is described by two additional forces, each one proportional to the BM displacement delayed by a slow and a fast feedback constant time, respectively. According to this model, a time delay differential equation (DDE) of the second order describes the oscillating dynamics of the BM. A different formulation of the nonlinear active mechanism, driven by the OHCs, is expressed as a nonlinear function of the BM velocity by the anti-damping model of Moleti et al. (J. Acoust. Soc. Am. 133, 2013). In this case the model equations do not contain time delays.

The numerical integration of the above mentioned models has been obtained by finite differencing with respect to the space variable in the state space, as introduced by Elliott et al. (J. Acoust. Soc. Am. 122, 2007), and then integrating in time with the adaptive package introduced by Bertaccini and Sisto as a modification of the popular Matlab `ode15s` package (J.

Comput. Phys. 230, 2011). The semidiscrete formulation of the delayed stiffness model and the anti-damping model has a non trivial mass matrix, and eigenvalues of the system matrix with large negative real part and imaginary part. That is why an implicit solver with an infinite region of absolute stability should be used. Therefore, the customized Matlab `ode15s` package by Bertaccini and Sisto seems to be the convenient choice to integrate the problem at hand numerically. In particular, for the delayed stiffness model, an integrator for constant DDEs (the *method of steps*; Bellen and Zennaro, Oxford University Press 2003) has been formulated and based on the customized `ode15s`.

All these topics have been discussed in this doctoral thesis, which is subdivided in the following chapters.

Chapter 1 describes the anatomy of the human ear, with special regard to the cochlea. Some experimental evidences about the cochlear mechanisms are discussed, in order to support the cochlear modeling. Two physical models with one degree of freedom are shown: the anti-damping model of Sisto et al. (J. Acoust. Soc. Am. 128, 2010) and Moleti et al. (J. Acoust. Soc. Am. 133, 2013), and the delayed stiffness model of Talmadge et al. (J. Acoust. Soc. Am. 104, 1998).

Chapter 2 discusses the general theory of DDEs, with greater reference to constant and time dependent DDEs from Bellen and Zennaro (Oxford University Press 2003). Existence and uniqueness of time dependent DDEs are briefly analyzed, while the *method of steps* is shown as a basic approach to find a numerical approximation of the DDEs solution. According to this method, IVPs of constant DDEs (as for the semidiscrete delayed stiffness model) are turned into IVPs of ODEs in a subinterval (of length less than or equal to the time delay) of the whole integration interval. Each IVP of ODEs can be integrated by means of any ODEs numerical method, and its convergence is then discussed.

Chapter 3 describes the main tools used to find an approximate solution of the considered models. In particular, the discretization for spatial partial derivatives by means of finite differences is shown. Such a representation turns a model, which is continuous in the space-time domain, into a semidiscrete model to be integrated in time. The models considered in this thesis are stiff, so the phenomenon of stiffness is discussed and the `ode15s` package of Matlab for integrating stiff ODEs is described. Nevertheless, greater benefits can be obtained by using the `ode15s` package customized by Bertaccini and Sisto as a hybrid direct-iterative solver which exploits Krylov subspace methods.

Chapter 4 shows the semidiscrete formulation of the continuous models (anti-damping model and delayed stiffness model) in the state space with

respect to the spatial variable, as introduced by Elliott et al. (J. Acoust. Soc. Am. 122, 2007). The algebraic properties of the semidiscrete models are discussed in order to show why the customized `ode15s` package may perform a faster numerical integration of the semidiscrete models and how this solver can be used in an integration numerical technique for constant DDEs (the *method of steps*).

Chapter 5 shows the results produced by the numerical experiments of the delayed stiffness model by supplying a sinusoidal tone, and compares them with the numerical results produced by the anti-damping model. Some considerations about the numerical approach of the time integration are also discussed, and a part of the simplified code used for integrating the semidiscrete delayed stiffness model, is reported. The results are comparable with those obtained by the anti-damping model, and then the numerical experimental evidences seem to justify the proposed integration technique for constant DDEs. Delayed model properties of tonotopicity, anti-damping and nonlinearity are verified, as well as the dependence of the approximate solution on some free parameters of the model. The cochlear response described by the delayed stiffness model shows a typical tall and broad BM activity pattern. This behavior is also found in the numerical results of a model with two degree of freedom produced by Neely and Kim (J. Acoust. Soc. Am. 79, 1986) and Elliott et al. (J. Acoust. Soc. Am. 122, 2007).

Contents

Chapter 1

Cochlear Models

The ear is the component of the human body performing the peripheral stage of the hearing function. Its inner part contains the cochlea, the organ of the auditory system where the spectral analysis of a sound signal and its transduction into a neural signal occur.

Cochlear modeling is an useful tool to deepen the knowledge of the human cochlear physiology. The interpretation of experimental data, and also the design of hearing diagnostic techniques and cochlear implants can improve with the use of model solutions. On the other hand, the cochlear response might even be evaluated outside the accessibility range of experimental techniques by means of cochlear models. For this reason, a fundamental stage of this study is the formulation of models which are able of predicting a realistic cochlear function.

In this Chapter a short overview about ear anatomy and function (section 1.1 and section 1.2) will be shown with the aid of some experimental evidences about cochlear mechanisms (section 1.3 and section 1.4). For further details regarding the cochlear physiology see Brown et al. (1999) [28] and Keener and Sneyd (1998) [105]. Then, modeling of the inner ear will be described by means of two different formulations: the anti-damping model and the delayed stiffness model (section 1.5). In particular, refer to Sisto et al. (2010) [180] and Moleti et al. (2013) [132] for the first model, and Talmadge et al. (1998) [189] for the second model.

1.1 Human ear function

The ear is a transducer of the mechanic energy of an incident sound wave into an electric signal sent to the brain via the auditory branch of the eighth cranial nerve. This transduction can be divided in three stages, each of these

achieved by one of the three parts of the ear: outer ear, middle ear and inner ear.

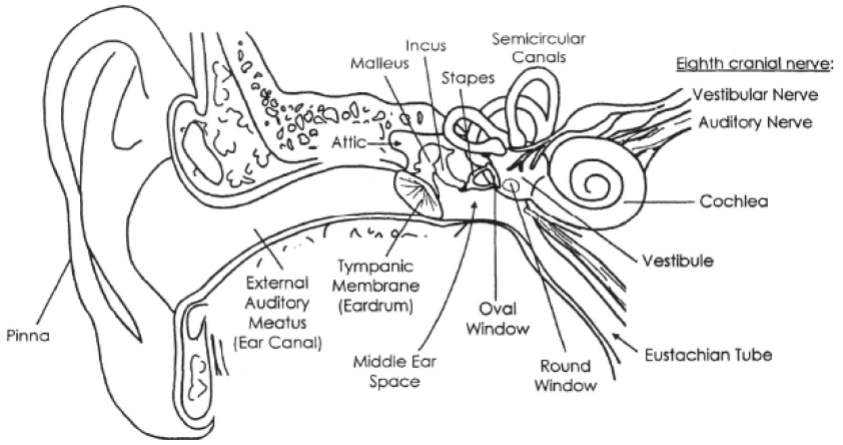

Figure 1.1: Human ear (Gelfand, 1998 [73]). The figure does not reproduce ear elements on a realistic scale in order to improve their graphic display.

1.1.1 Outer Ear

The outer ear consists of a cartilaginous flange, the *pinna*, incorporating a resonant cavity that connects to the *ear canal* (about 3 cm in length and 0.7 cm in diameter) and finally to the *tympanic membrane*, or *eardrum* (see Figure 1.1). The latter is an elastic thin diaphragm (with a thickness of about 0.1 mm) and represents the boundary between the outer ear and the middle ear. Sound pressure waves are conveyed by the pinna into the ear canal and vibrate the tympanic membrane.

The outer ear performs an initial filtering of the sound waves, increasing the sound pressure gain in the 2 to 4 kHz region. In particular, for the human hearing duct, the resonance frequency is well approximated by the standing wave condition for a tube closed at one end. Namely, resonance occurs at frequencies f_n when the tube length l is an odd multiple of a quarter of wavelength, that is

$$f_n = (2n-1)\frac{c}{4l} \qquad n \in \mathbb{N} \tag{1.1}$$

where c is the speed of sound in air. The first resonance frequency f_1 is about 2800 Hz. As a result, the human ear is most sensitive to sound frequencies ranging in [2000, 4000] Hz.

1.1.2 Middle Ear

The middle ear is a bony cavity filled with air, connected by the tympanic membrane with the outer ear and by the *oval window* and the *round window* with the inner ear (see Figure 1.1). The tympanic membrane connects to the oval window through the *ossicles* (three small bones), namely, *malleus*, *incus*, and *stapes*.

The middle ear transmits the sound vibrations from the outer ear to the *cochlea* in the inner ear, working as an impedance-matching device. The tympanic membrane has a much higher surface area than the oval window, and the latter vibrates in the cochlear fluid. If not for impedance matching, most of the energy of the sound waves in air would be reflected by the cochlear fluid. This impedance matching is carried out by the surface ratio and the ossicles. The latter act as levers that increase the force at the expense of velocity, resulting in the required concentration of energy at the oval window.

Moreover, the middle ear also functions as a pressure amplifier. High surface ratio between the tympanic membrane and the oval window, the curvature ratio of the tympanic membrane and the geometry of the levers system of the ossicles perform an amplification gain of about 25 dB.

The middle ear operates its functions efficiently in a certain frequencies range because it works as a band-pass filter. Its resonance frequency is about 1500 Hz and its passband is about [400, 4000] Hz. As a result, the human hearing sensibility reduces for sound frequencies outside the passband of the middle ear.

1.1.3 Inner Ear

The *vestibular apparatus* (the semicircular canals and the otolith organs) and the *cochlea* form the inner ear. The vestibular apparatus mainly operates the detection of movement and acceleration. On the contrary, the cochlea carries out the primary function of the auditory system, namely, the transduction of the mechanic signal into an electrical signal and the spectral analysis of the acoustic signal. Before we go into the details of the cochlear functioning (section 1.2), the cochlear anatomy will be now shown.

Human Cochlea

The cochlea is a tubular cavity filled with liquid and twisted into a spiral (in Figure 1.2 the uncoiled cochlea is shown). The human cochlea has a total length of 32-35 mm and a diameter of about 2 mm. It is divided in three chambers: the *scala vestibuli* (the upper chamber), the *scala tympani* (the

lower chamber) and the *scala media* (between the scala vestibuli and the scala timpani) (see Figure 1.3).

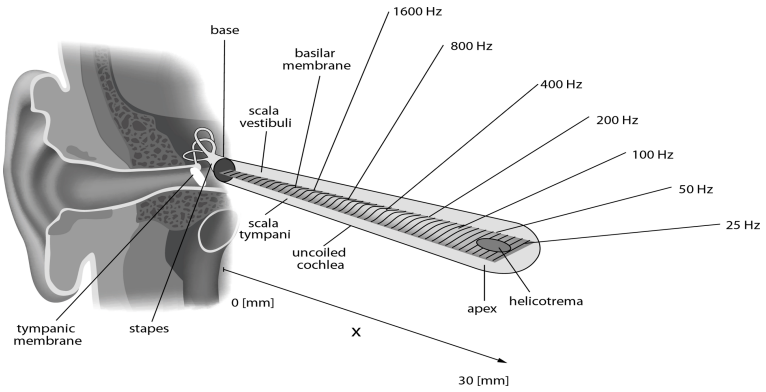

Figure 1.2: Human ear with the uncoiled cochlea.

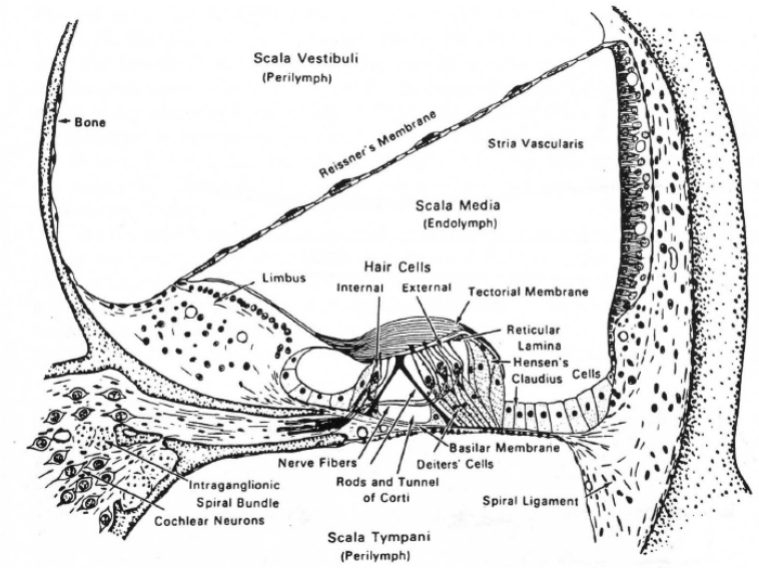

Figure 1.3: Cochlea cross section (Gelfand, 1998 [73]).

Reissner's membrane separates the scala vestibuli from the scala media, which in turn is separated from the scala tympani by the *spiral lamina* and the *basilar membrane* (BM). The BM is connected to the middle ear by the link between the stapes and the oval window. This region is called *base* of the BM. The scala vestibuli and the scala tympani are filled with perilimph, a fluid similar to extracellular fluid and essentially incompressible, while the

scala media is filled with endolymph, a fluid with a high K^+ concentration and a low Na^+ concentration.

At the end of the cochlea (the *apex*), the upper and lower chamber are connected by a small hole (*helicotrema*), which equalizes the local fluid pressure on the BM.

When a sound stimulus is supplied, a pressure wave is transmitted to the ear canal and makes the eardrum vibrate. Then the middle ear transmits the acoustic wave from the eardrum to the oval window (connected to the stapes) by the motion induced in the chain of the three ossicles malleus - incus - stapes. A resultant wave in the perilymph travels along the length of the scala vestibuli, creating complementary waves in the BM and the scala tympani. Because the perilymph is essentially incompressible, it is necessary for the scala tympani also to have a moving window, the round window, an elastic membrane analogous to the oval window; otherwise, conservation of mass would preclude movement of the stapes. The inward motion of the stapes at the oval window is compensated by the corresponding outward motion of fluid at the round window.

The primary transduction medium of sound into electrical signal is represented by the *organ of Corti*, which sits on the top of BM. This organ is composed by a row of *inner hair cells* (IHCs) and three rows of *outer hair cells* (OHCs). In the human ear there are about 3500 IHCs and 15000 OHCs. The hair cells have hairs projecting out the top, and these hairs are attached to a flap called the *tectorial membrane* (TM) that sits over the organ of Corti. Waves in the BM create a shear force on these hairs, which in turn causes a change in the membrane potential of the hair cell. In particular, this is transmitted to nerve cells by the IHCs, and from there to the brain.

1.2 Cochlear Mechanics

A sound wave is a mechanical wave that moves through a medium characterized by properties of elasticity and inertia. If a pure-tone (that is, a sinusoidal stimulus) is supplied, the particles in the medium oscillate around their equilibrium position as a mass in a harmonic oscillator if displaced from its equilibrium. The resulting sound wave moves by alternately compressing and rarefying regions in the medium. In the compressed regions the medium is denser and in the rarefied regions it is less dense. This implies that the pressure is higher in the compressed regions than in the rarefied regions. A series of pressure pulses will move through the medium as the sound wave travels.

Such a sound pressure wave propagates through the outer ear and the

middle ear in air when a sound stimulus is supplied in the ear canal. The stapes pressure on the oval window transmits the wave to the inner ear, where the third hearing stage is performed by the cochlea. Here, the pressure wave propagates in the cochlear liquid, which flows from the upper chamber, the scala vestibuli, to the lower one, the scala timpani, through the helicotrema. This flow generates a differential pressure in the liquid between the two chambers and, as a result, the BM and the TM oscillate transversely in a relative movement. The BM is more elastic than the TM, and, therefore, more affected by the oscillatory motion caused by the differential pressure in the cochlear fluid.

Although the width of the cochlea decreases from the base to the apex, the width of the basilar membrane increases in this direction (see Figure 1.4). Moreover, from the base to the apex the BM stiffness decreases exponentially, while the length of the hair bundles on the hair cells increases. Longer hair cell bundles respond to inputs of lower frequency, and shorter bundles are tuned to higher frequencies. Consequently, each position along the BM resonates at its own corresponding resonance frequency. Namely, the BM acts as a frequency analyzer. This implies that a *traveling wave* (TW) generates

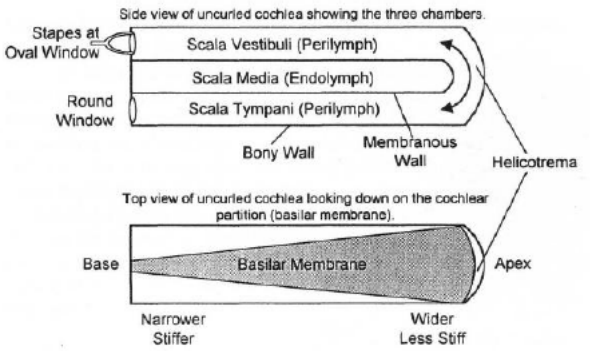

Figure 1.4: Uncoiled cochlea schematization (Gelfand, 1998 [73]).

along the BM because of the fluid differential pressure, showing maximal amplitude where the BM local transverse impedance minimizes. This is a resonance condition that depends on the stimulus frequency. It has been experimentally found that in the human cochlea the base is tuned to about 20 kHz and the apex to about 20 Hz, due to the different elasticity along the BM. This property is called *cochlear tonotopicity*, quantitatively expressed by the *Greenwood Map* (Greenwood, 1990 [78]) as a logarithmic relation between the position x along the BM and the corresponding resonance angular frequency

$\omega(x)$:

$$\omega(x) = \omega_1 + \omega_0 e^{-k_\omega x} \tag{1.2}$$

where human cochlear values for the constants are $\omega_1 = -2\pi\,145\,rad/s$, $\omega_0 = 2\pi\,20655\,rad/s$, $k_\omega = 1.382\,cm^{-1}$. Neglecting the constant ω_1 (which is significant only for frequencies less than 1 kHz), (1.2) implies that equal distances along the BM correspond to equal frequency logarithm ranges.

A transduction mechanism of mechanical oscillations into a neural signal occurs in the cochlea. Firstly, the BM oscillation in a tonotopic site $x(\omega)$ stimulates the overlying OHCs by contracting their cilia. This contraction modifies their permeability to ions, generating an electrical signal which stimulates the OHCs and contracts their cilia again. OHCs are inclined with respect to the BM longitudinal direction. For this reason when their cilia are contracted again, the generated signal is not transmitted to the point $x(\omega)$, but to the point $x(\omega)+\Delta$ (Δ is the projection of the OHCs along BM; Δ values are experimentally found of about 30-50 μm in the mammalian cochlea by Robles and Ruggero, 2001 [155]). This feedback cycle is an active nonlinear mechanism because the initial cilia contraction is amplified by a compressive gain function decreasing in amplitude. This preserves the cochlea from being damaged by loud sound stimuli. In particular, in normal hearing subjects, the input/output function is linear at low and high stimulus levels, while it becomes strongly compressive at intermediate stimulus levels. Therefore, OHCs represent the fundamental nonlinear amplification element of auditory system, and supply energy to a cochlear position if stimulated.

Finally, the IHCs perform their role in the cochlear mechanism. The BM amplified oscillation contracts the IHCs cilia, that convert the pressure variation of the cochlear fluid in electrical signal direct to the acoustic nerve. Each bundle of the acoustic nerve connects a tonotopic site along the BM with the corresponding cortex region. In this way, the cochlea identifies the constituent frequencies of a sound wave by means of the localization of the stimulated tonotopic site.

In the next section, some experimental studies will be shown in order to clarify some cochlear properties described here.

1.3 Some experimental studies

As already discussed in the previous section, a sound stimulus, supplied in the ear canal, generates a pressure wave which is transmitted to the cochlea in the inner ear after passing through the middle ear. A resulting motion is induced in the cochlear liquid which flows from the scala vestibuli to the scala timpani at the apex through the helicotrema.

For very low frequency stimuli, a fluid motion and a resulting traveling wave along the BM generate from the base to the apex. Contrary, for higher frequency stimuli (above 100 Hz) the fluid motion extends over only a limited length of the cochlea and does not reach the helicotrema at the apex. If two different pure-tones (that is, two sinusoidal tones of frequency $f_2 > f_1$) are supplied, a BM resonance condition occurs closer to the base for the stimulus with higher frequency, and moves towards the apex as the stimulus frequency decreases (von Békésy, 1960 [203]; de Boer, 1980 [49]). Figure 1.5 shows that the amplitude envelope of the traveling wave is first increasing, then decreasing, and the position of the peak of the envelope depends on the frequency of the stimulus. In particular, the TW moves along the BM towards the tonotopic site, with decreasing wave speed, as well as wavelength, and increasing wave amplitude. Approaching the resonant place, sharp variations of the local transverse impedance causes more intense speed reduction and consequent maximal amplitude. Note that this amplitude grows with increasing distance from the base.

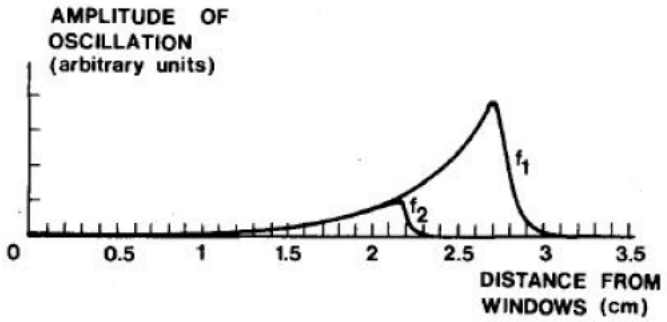

Figure 1.5: BM amplitude envelope generated by two different pure-tones of frequency $f_2 > f_1$ (de Boer, 1980 [49]).

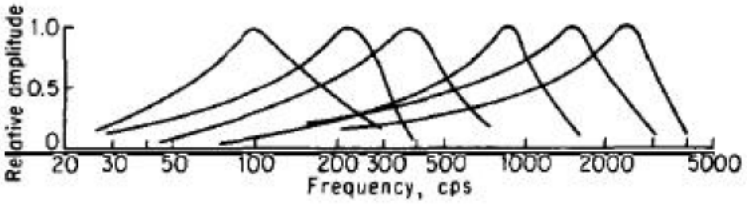

Figure 1.6: BM amplitude envelope for six BM positions in the human cochlea, as a function of stimulus frequency (von Békésy, 1960 [203]).

Measuring the cochlear vibration represents a direct technique for study-

ing cochlear mechanics. The BM is accessible to observation along its whole length, thus it could be studied at fixed frequency. Nevertheless, a more feasible way to evaluate experimentally the cochlear behavior considers the amplitude envelope for a fixed BM position as a function of frequency, that is the frequency response of the BM for that fixed place (see Figure 1.6). Each BM position resonates at a particular frequency, and the tonotopic site moves towards the cochlear base as the stimulus frequency increases. Figure 1.6 shows amplitude envelopes that are similar above 1 kHz, as expected in a *scale invariant* cochlea according to the Greenwood Map (1.2). This property is violated for frequencies which are less than 1 kHz because of the constant ω_1 in (1.2). This is noticeable in the amplitude envelopes at lower frequency in Figure 1.6.

Therefore, the cochlea acts as frequency analyzer by determining the stimulus frequency from the BM place with maximal displacement, and as bandpass filter if the BM response of a fixed position is considered.

As a function of the stimulus level, the cochlear response shows an increasing trend determined by a nonlinear amplification mechanism. Figure 1.7 shows the experimental frequency response of velocity of BM displacement at the tonotopic site of around 14 kHz, for stimulus level from 10 dB SPL to 100 dB SPL[1] in 10 dB steps (Ren and Nuttall, 2001 [149]). The measurement has been carried out by means of laser interferometry in the cochlear basal turn of gerbils before and after death, by supplying sine sweep tones. The latter are tones of continuously increasing frequency with a constant rate. Laser interferometry is a widely used technique in measurements of BM vibrations due to its high sensibility. Figure 1.7A and Figure 1.7B show BM velocity and derived iso-response curves, respectively, in a sensitive cochlea. Analogously, Figure 1.7D Figure 1.7E are referred to a post-mortem insensitive cochlea. The BM velocity is an increasing function of stimulus level with maximal amplitude around 14 kHz. Above the resonant frequency of the fixed position, a sharp reduction of amplitude velocity is observable, with a greater decreasing rate with respect to the low frequency trend. Moreover, while the stimulus level increases, in the sensitive cochlea the resonance bandwidth increases and a shift of the resonant frequency occurs towards lower frequencies (note the dashed line in Figure 1.7A-B-D-E and that the resonant frequency is less than 10 kHz at 100 dB SPL). Finally, whereas the BM velocity is a linear function of stimulus level for low and high levels, a compressive growth characterizes the frequency responses between 50 dB

[1]SPL is acronym of Standard Pressure Level. The unit of measurement of sound pressure level is expressed in decibel SPL (dB SPL) if it is referred to the standard pressure level $P_0 = 20\,\mu Pa$. P_0 corresponds to hearing threshold at 1 kHz. Specifically, $P(dB\,SPL) = 20\,log_{10}(P/P_0)$.

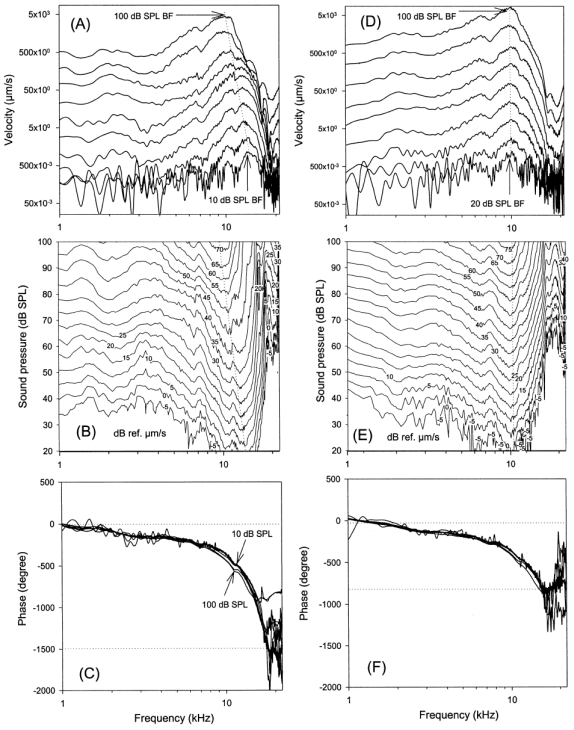

Figure 1.7: Amplitude and phase spectra of the BM velocity at different sound pressure levels in a sensitive (A and C) and a post-mortem insensitive (D and F) cochlea of gerbils. The iso-response curves (B and E) were derived from amplitude spectra (A and D). Reproduced from Ren and Nuttall (2001) [149].

SPL to 80 dB SPL stimulus level. Such an experimental evidence about the nonlinear dependence of the cochlear amplifier on stimulus level has also been observed by Kanis and de Boer (1993) [102] and Nobili and Mammano (1996) [140].

On the contrary, Figure 1.7C shows that in the post-mortem insensitive cochlea the growth of the frequency response is linear for each stimulus level with grater amplitudes at higher levels with respect to the sensitive cochlea. The resonance bandwidth does not change and the shift of the resonant frequency does not occur. These evidences prove the functioning of an active nonlinear feedback mechanism driven by sensitive OHCs (see section 1.2), which do not work in the post-mortem insensitive cochlea. On the other hand, phase spectra in the sensitive cochlea (Figure 1.7C) show a frequency slope which is smaller for lower stimuli and frequencies below the resonance frequency with respect to frequencies near the resonance. The slope value

decreases for post-mortem insensitive cochlea, and no significant dependence on stimulus level is more visible (Figure 1.7F).

The amplification gain of the cochlear feedback mechanism is shown in Figure 1.8. In case of insensitive cochlea (Figure 1.8C) the gain does not change over all frequencies, while it is a decreasing function of stimulus level around the resonant frequency of about 14 kHz on sensitive cochlea (Figure 1.7A). Therefore, both active amplification and a protection mechanism act in the cochlea in order to strongly amplify low-level sounds and avoid damage due to loud sounds. Finally, phase spectra of the gain function confirm the dependence on stimulus level and a greater slope for sensitive cochlea (Figure 1.7B) than for the insensitive case (Figure 1.7D). That is, deterioration of tuning, loss of compression and decrease of phase lag occur in a post-mortem cochlea.

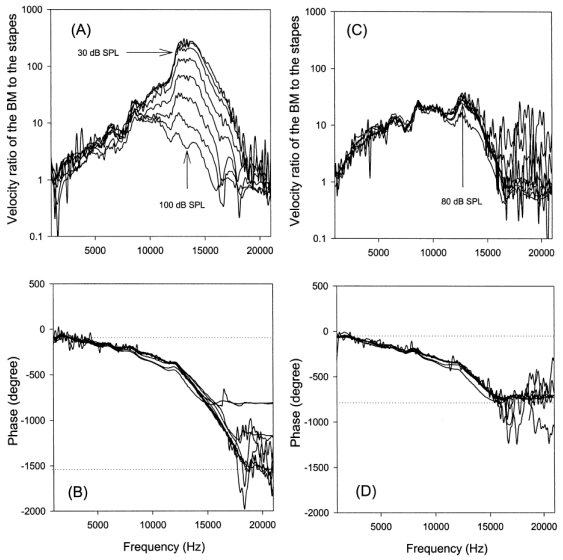

Figure 1.8: Gain spectra as velocity ratio of the BM to the stapes for sensitive cochlea (A-B) and post-mortem insensitive cochlea (C-D) of gerbils (Ren and Nuttall, 2001 [149]).

1.4 Otoacoustic Emissions: OAEs

The human ear functionality may be investigated by means of different auditory tests, for example pure-tone audiometry and middle-ear impedance audiometry (tympanometry). Another effective and objective auditory test employs *Otoacoustic Emissions* (OAEs). They are spontaneous or evoked

signals which come from the inner ear and can be measured in the ear canal. The formulation of cochlear models may support the study about the OAEs generation and, thus, improve the knowledge of human cochlea and the design of objective diagnostic techniques.

In 1948 Thomas Gold [75] was the first to predict the existence of an active cochlear mechanism which could produce self-sustained waves of the BM, and consequent OAEs. Nevertheless, such sound emissions were experimentally demonstrated by David Kemp only in 1978 [106] and were called *Spontaneous* OAEs (SOAEs).

In general, an OAE is a sound generated in the cochlea and measured as a variation in the pressure in the ear canal (Hall, 2000 [86]). If a sound stimulus is supplied in the ear canal, OAEs can be evoked. For this purpose, OAEs measurements are carried out by involving a probe composed by loudspeakers and a microphone and inserted in a subject's ear canal. In the literature, and for clinical purposes, OAEs are classified according to the stimulus supplied. In particular, *Transient Evoked* OAEs (TEOAEs) are generated by transient stimuli as a short click or a tone burst, *Stimulus Frequency* OAEs (SFOAEs) are generated by a single frequency tone, and *Distortion Product* OAEs (DPOAEs) are generated by two tones of nearby frequencies.

In 1999 Shera and Guinan [169] also proposed alternative OAEs classification, based on their generation mechanisms. Specifically, OAEs are generated either by coherent linear reflection or by nonlinear distortion. In the *linear reflection mechanism* the wave traveling on the BM is reflected back by micromechanical irregularities (called *roughness*) distributed along the BM. The largest contribution comes from the region close to the resonant tonotopic place corresponding to the stimulus frequency. This mechanism is identified as *place-fixed* (Kemp, 1986 [108]), because for small variations of the stimulus frequency the generation places do not change. As a result, the phase of an OAE generated by such a mechanism is a rapidly decreasing function of frequency (Talmadge et al., 1998 [189]; Shera et al., 2005 [170]). In the *nonlinear distortion mechanism* the cubic nonlinearity of cochlear amplifier comes into play. For a two-frequencies stimulus (as in DPOAEs), the cochlear nonlinearity generates a BM traveling wave containing linear combinations of the stimulus frequencies in their overlap region. This mechanism is identified as *wave-fixed* (Kemp, 1986 [108]) because the generation place depends on the stimulus frequencies. Thus, the OAE phase is a constant function of the frequency in a scale invariant cochlea (with deviations at low frequencies; Talmadge et al., 1998 [189]; Shera et al., 2005 [170]; Dhar et al., 2011 [55]). OAEs are the vector sum of the components generated by the two above mechanisms, their relative contributions varying according to the stimulus level. In general, the linear reflection mechanism predominates at low

stimulus levels, while the nonlinear distortion one is most relevant at higher levels, due to the nonlinearity of the cochlear response. The presence of both generation mechanisms produces the known *fine structure* of OAE spectra (Kalluri and Shera, 2007 [101]). The latter show oscillations in amplitude with minimum and maximum values respectively corresponding to destructive and constructive interference of the responses to the above discussed generation mechanisms. Fine structure is observable in DPOAEs and visible in Figure 1.12, which will be shown dealing with distortion products. There are also experimental evidences of fine structure in SFOAEs (as in Figure 1.10, which will be discussed further on). In the last years, some authors in literature suggests that the reflection contribution to SFOAE or TEOAE may also come from a region basal to the resonant site by a place-fixed mechanism but with a flatter phase-frequency relation (Choi et al., 2008 [36]; Moleti et al., 2013 [132]; Sisto et al., 2013 [182]). As a result, the different frequency behavior of the response phase from the peak region and a more basal region may generate fine structure without occurring nonlinear distortion.

OAEs are used in clinical applications due to the relationship between level or detectability of OAEs and the sensitivity of hearing (Zwicker and Schloth, 1984 [212]; McFadden and Mishra, 1993 [130]; Talmadge et al., 1998 [189]; Shera and Guinan, 1999 [169]). Indeed, cochlear damage can reduce or remove the presence of all kinds of OAEs. In particular, TEOAEs and DPOAEs are involved in tests aimed at detecting hearing defects (Hall, 2000 [86]). On the other hand, neonates and other children who are too young to cooperate in conventional hearing tests are tested for TEOAEs (Tognola et al., 2001 [196]).

Now a short overview about some typologies of OAEs will be shown.

SOAE

Spontaneous OAEs (SOAEs) generate in the inner ear without any sound stimulus. They demonstrate the existence of the active feedback mechanism of the cochlear amplifier, which supplies energy to the BM by OHCs.

SOAEs are low-amplitude narrow-band signals which are commonly found in a range of 33% to 70% of normally hearing subjects. Multiple SOAEs are also commonly measured. In general, measurements of SOAEs are carried out using click stimuli to synchronize the emission and improve the signal-noise ratio. In this case the emission is called Synchronized SOAE (SSOAE).

A typical SOAE spectrum (see Figure 1.9) shows spectral lines with very low amplitude (less than 20 dB) and narrow bandwidth (even less than 1 kHz). While the frequency of a SOAE remains constant (within 1%) for years (Hall, 2000 [86]), the amplitude may vary with time. There is evidence about

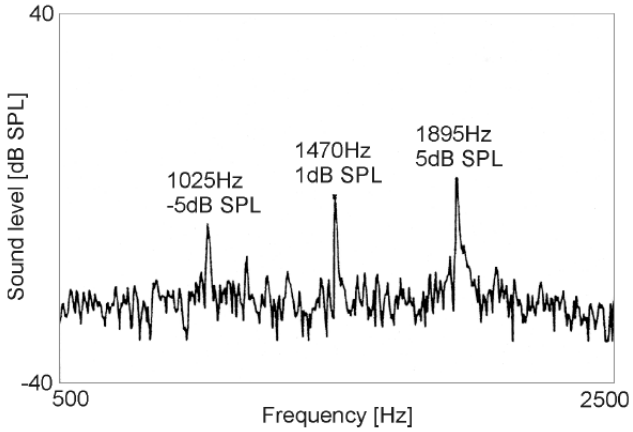

Figure 1.9: Time-averaged spectrum of SOAEs measured in a human ear (Probst et al., 1991 [145]).

the relation between the frequency of a SOAE and the hearing threshold (Schloth, 1983 [161]). SOAEs are absent in frequency bands with hearing losses greater than 20 dB (Sisto et al., 2001 [179]). However, the absence of SOAEs does not necessary imply a cochlear damage. They are not found in about 30% of normally hearing subjects and, thus, they are not widely employed in clinical applications.

SFOAE

Stimulus Frequency OAEs (SFOAEs) are generated by a sinusoidal tone. In this case the emission arises in addition to the stimulus at the same frequency. For this reason a differential technique is involved in measurements of SFOAEs (Kalluri and Shera, 2007 [101]). Specifically, it employs a *suppressor* tone, which is higher in level and nearby in frequency to the sinusoidal tone (the *probe*). The suppressor strongly affects the gain of the cochlear amplifier also at the probe frequency. The emission is thus given by the difference between the signal evoked by the probe and the suppressor supplied simultaneously, and the signal evoked by the probe only, which contains the unsuppressed OAE. This operation cancels the stimulus, and the resulting signal contains the OAE at the stimulus frequency and the suppressor tone. Nevertheless, the latter may be distinguished due to its different frequency. Figure 1.10 (upper) shows the spectrum of SFOAEs generated by a pure tone with continuously increasing frequency. The typical fine structure is observable, being due to the interference between two different generation mechanisms/places (discussed in the introduction of this section) which gen-

erate the emission.

On the other hand, Figure 1.10 (bottom) shows the phase of the emission. The phase slope of OAEs is a caracteristic time that represents the *phase gradient-delay*, that is, the group delay of the traveling wave. It can be interpreted as an estimate of the transmission delay (or latency) of the round-trip cochlear transmission (Sisto et al., 2007 [181]), for place-fixed OAE generation. Consequently, it is a decreasing function of frequency. This is because the distance from the cochlear base of the BM tonotopic sites, and thus their latency, decrease with increasing frequency, according to the Greenwood Map (1.2). A sequential single frequency analysis of the cochlear properties by means of successive SFOAE measurements at several frequencies involves a long time. Consequently, a SFOAE test is less suitable for clinical application. However, such a test allows to investigate the BM with finer spectral resolution. Moreover, it avoids nonlinear distortion components in the response because the cochlea is stimulated in each SFOAE measurement with a single frequency.

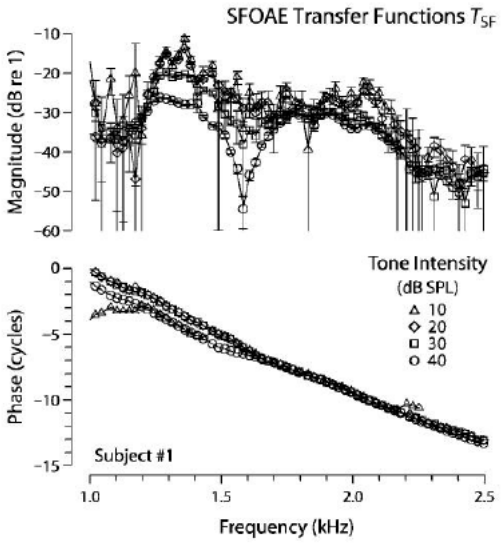

Figure 1.10: Spectral amplitude and phase of a SFOAE (Kalluri and Shera, 2007 [101])

TEOAE

Transient Evoked OAEs (TEOAEs) are generated by transient stimuli, that is, stimuli with wide spectral band. The clinical applications widely use

clicks, which are stimuli with duration of 100-200 μs and spectral band of 5-10 kHz. TEOAEs are found in about 98% of normally hearing subjects. For this reason, they are involved in clinical applications (Probst et al., 1991 [145]) as in screening tests on neonates (Tognola et al., 2001 [196]).

When a short-duration wide-band signal (such as a transient stimulus) is supplied in the ear canal, a broad cochlear range along the BM is stimulated. That is, many tonotopic places generate a response with different latency. In particular, the instantaneous frequency of a TEOAE varies inversely with latency according to the tonotopic mapping of Greenwood [78]. Indeed, increasing frequencies are tuned on positions decreasing towards the base of the BM (see section 1.2). In the panel "Response Waveform" of Figure 1.11 a typical time behavior of a TEOAE is shown. Several frequency components are observable at different latencies, which are shorter for higher frequencies and longer for lower frequencies. The resulting spectrum of a TEOAE is continuous (see the upper-right panel "Response FFT" in Figure 1.11) with amplitude that depends on the stimulus level (Zwicker and Schloth, 1984 [212]; Probst et al., 1991 [145]). Moreover, the latency of different frequency components of TEOAE varies inversely with stimulus level (Sisto and Moleti, 2007 [176]).

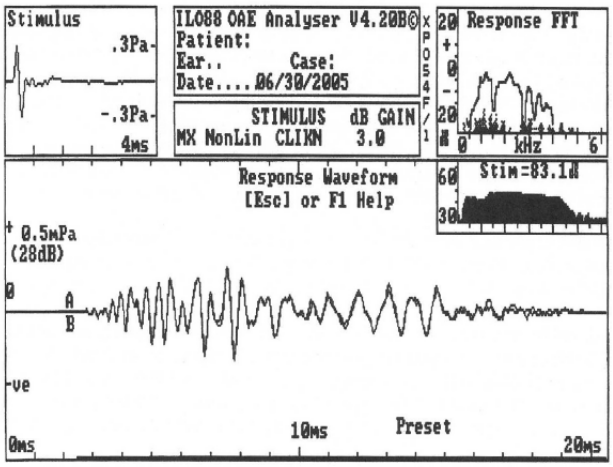

Figure 1.11: TEOAE measurement evoked by a click stimulus in a normal-hearing human subject, obtained with a commercially available equipment (Robinette and Glattke, 2007 [154]).

DPOAE

Distortion product OAEs (DPOAEs) are generated by the mechanical nonlinear intermodulation of two simultaneous sinusoidal tones which are nearby in frequency. In particular, overlapping of the traveling waves corresponding to the two stimulus frequencies (f_1 and f_2 such that $f_1 < f_2$) occurs near the f_2 resonant place, generating a distortion wave containing linear combination of f_1 and f_2. This wave travels both back towards the cochlear base generating the Zero-Latency (ZL) DP component, and to the corresponding resonant place. This last wave is known as Intracochlear DP (IDP) and is reflected back as a Long-Latency (LL) DP component. At the cochlear base, ZL and LL components add vectorially to generate the DPOAE recorded in the ear canal. The most intense DPOAEs are at $2f_1 - f_2$ and $2f_2 - f_1$ frequencies, and their intensity depends on the stimulus level and the primary frequency ratio $r = f_2/f_1$. The optimal ratio has been experimentally found to be about 1.22, with decreasing effects on DPOAE amplitude for lower and higher ratio values (Knight and Kemp, 2001 [116]; Rhode, 2007 [151]). Successive measurements of DPOAEs at different frequencies generate the spectrum shown in Figure 1.12 (Long et al., 2008 [128]) and characterized by the typical fine structure already discussed in the introduction of this section.

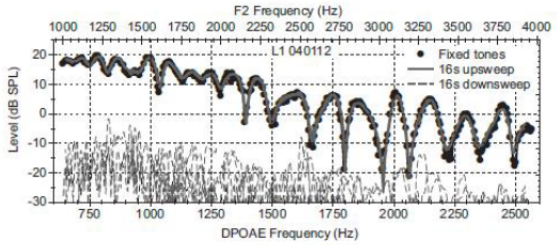

Figure 1.12: DPOAE measured by sweep tone (that is, a tone continuously increasing in frequency) on a human subject (Long et al., 2008 [128]).

In clinical applications *DP-gram* can be carried out graphing the DP level as a function of f_2. In this way, the generation tonotopic site of DPs can be analyzed by an objective test. However, DP-grams are not yet widely used in diagnostic tests. This is because of fine structure oscillations and inter-individual fluctuations in DP level among subjects which are equivalent with respect to the audiometric hearing threshold.

1.5 Time-domain cochlear models

The diagnostic power of OAEs may become more effectual if the knowledge of their generation mechanisms and measurement techniques are improved. In this context, the formulation of suitable and realistic cochlear models represents a strong valid instrument to also support the clinical prevention of cochlear damage.

Experimental studies, above discussed, have highlighted that the key feature of cochlear physiology is a strong nonlinear dependence on stimulus level. Therefore linear or quasi-linear cochlear models are not able to provide realistic predictions of cochlear response, unless low sound stimulus levels are considered as input to the model. A nonlinear model should be solved in time domain with high computational costs. However, a state-space model formulation and a customized numerical method may be used in order to obtain a fast and reliable numerical approximation of the model solution. This technique will be shown in Chapter 3 and Chapter 4. On this ground of this dissertation, time-domain active cochlear models will be introduced and the formulation of nonlinear active terms will be discussed.

1.5.1 Active cochlear models

The cochlea can be schematized as a box $\Omega = [0, L] \times [-H, H] \times [-W/2, W/2]$ of rectangular constant cross section[2], filled with homogeneous incompressible cochlear fluid and divided by the BM in an upper cavity and a lower cavity (v. Figure 1.13-Left).

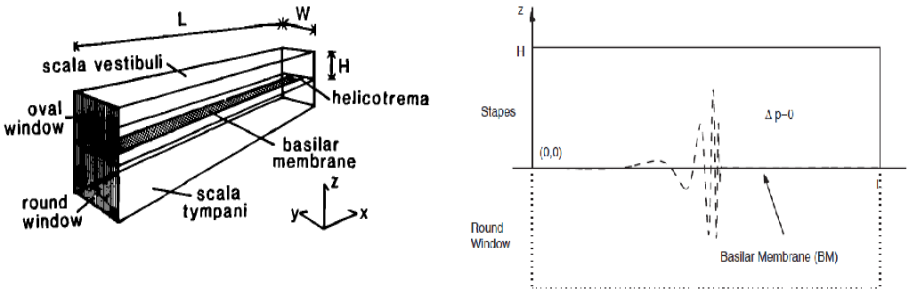

Figure 1.13: Left: Box schematization of the cochlea (Neely and Kim, 1986 [138]). Right: BM motion due to a pure tone (Kim and Xin, 2005 [114]).

[2]Dimensions of the cochlear box:
length of the BM: $L = 3.5\,cm$;
half-height of the cochlear duct: $H = 0.1\,cm$;
width of the cochlear duct: $W = 0.1\,cm$.

The BM vibrates transversely when a stimulus is given in the ear canal, as described in section 1.2. In particular, if the supplied stimulus is a pure tone (that is, it is a single frequency), the BM vibrates reaching maximal amplitude in the resonant site at the frequency of the pure tone, as in Figure 1.13-Right. Consequently, the cochlea can be treated as a bidimensional rectangle in which the propagation of the signal can be explained by an one-dimensional transmission line model along the BM direction (Furst and Lapid, 1988 [69]; Talmadge, 1998 [189]; Shera et al., 2005 [170]). In this class of models, the differential pressure across the BM and the transverse BM velocity act as the voltage and the current in an analog electrical transmission line, respectively.

The *first equation* of this model describes the propagation of the differential pressure (between the two cavities) along the BM through the helicotrema at the apex. Let p be the differential pressure, ρ the cochlear fluid density and $\xi(x,t)$ the transverse displacement of the BM at the longitudinal position x and time t. Let the BM direction be coincident with the x-axis of a Cartesian reference system centered in the base. Then the equation is the following:

$$\frac{\partial^2 p(x,t)}{\partial x^2} - \frac{2\rho}{H}\ddot{\xi}(x,t) = 0 \tag{1.3}$$

with boundary conditions:

- condition at the base ($x = 0$ - the oval window moves with the stapes and $\ddot{\xi}_{ow}$ is its longitudinal acceleration)

$$\frac{\partial p(0,t)}{\partial x} = 2\rho\ddot{\xi}_{ow}(t) \tag{1.4}$$

- condition at helicotrema ($x = L$)

$$p(L,t) = 0 \tag{1.5}$$

Finally, since the BM vibrates as a damped spring-mass system, it is described as a forced harmonic oscillator. So the *second equation* of the considered model is:

$$\ddot{\xi}(x,t) + \gamma_{bm}(x)\dot{\xi}(x,t) + \omega_{bm}^2(x)\xi(x,t) = \frac{p(x,t) + q(x,t)}{\sigma_{bm}} \tag{1.6}$$

where $\gamma_{bm}(x)$, $\omega_{bm}^2(x)$ and σ_{bm} are respectively the damping function, the stiffness function and the mass density of the BM.

The driving force of the harmonic oscillator (1.6) is the sum of the local differential fluid pressure $p(x,t)$ and an additional force $q(x,t)$ that represents the action of the active feedback mechanism driven by OHCs. There exist different formulations for such additional force $q(x,t)$. Some of them will be shown in the models of the next subsections. Namely, a term proportional to the BM transverse velocity (*Anti-damping model*) or the BM delayed transverse displacement (*Delayed stiffness model*) could be used. In particular, this thesis has been based on the model containing delayed terms, so that the numerical solution of delayed equations has been studied further on in the next chapters.

By (1.6) each tonotopic site along the BM is described as a single active oscillator. Namely, angular frequency and passive damping coefficient are functions of the position x according to the Greenwood Map (1.2):

$$\omega_{bm}(x) = \omega_1 + \omega_0 e^{-k_\omega x} \tag{1.7}$$

$$\gamma_{bm}(x) = \gamma_1 + \gamma_0 e^{-k_\gamma x} \tag{1.8}$$

($\gamma_1 = 100\ s^{-1}$ and $\gamma_0 = 5035\ s^{-1}$ from Talmadge et al., 1998 [189]) and the local passive quality factor is

$$Q(x) = \frac{\omega_{bm}(x)}{\gamma_{bm}(x)}. \tag{1.9}$$

In the limit $k_\omega = k_\gamma$ and $\omega_1 = \gamma_1 = 0$, the quality factor (1.9) does not depend on frequency because it assumes the following constant value

$$Q_0 = \frac{\omega_0}{\gamma_0}. \tag{1.10}$$

As a result, in this limit the Greenwood Maps (1.7)-(1.8) do not explicitly break the scale invariance symmetry and make the model solution easier to be analyzed.

An equation similar to (1.6) is also considered for the oval window, the first element of the model ($x = 0$), which encloses the middle ear and the oval window dynamics. Such an equation is the following:

$$\ddot{\xi}_{ow}(t) + \gamma_{ow}\dot{\xi}_{ow}(t) + \omega_{ow}^2 \xi_{ow}(t) = \frac{1}{\sigma_{ow}}[p(0,t) + G_{me}P_{dr}(t)] \tag{1.11}$$

where $G_{me}P_{dr}(t)$ is the pressure exerted on the oval window by the stimulus supplied in the ear canal, with mechanical gain of the ossicles $G_{me} = 21.4$, and P_{dr} the calibrated pressure in the ear canal. Moreover, $\gamma_{ow} = 500\ s^{-1}$ is the middle ear damping constant, $\omega_{ow} = 1500\ Hz \cdot 2\pi$ the middle ear frequency and $\sigma_{ow} = 1.85\, g/cm^2$ the effective oval window density, as quoted by Talmadge et al. (1998) [189]. A thorough analysis of (1.11) will be discussed in the next section.

1.5.2 Single-oscillator model for the middle ear

In this section a simple middle ear model will be shown, as formulated by Talmadge et al. (1998) [189]. In particular, the tympanic membrane is modeled as a single piston which acts on a fixed incudo-stapedial joint (see Figure 1.14). On the other hand, the ear canal is assumed to be capped by a probe

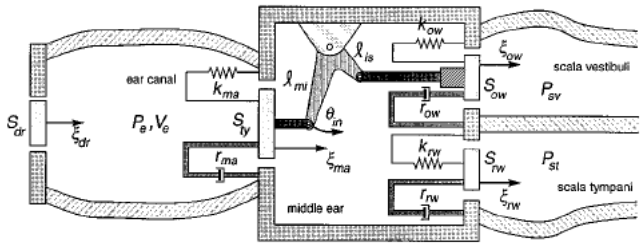

Figure 1.14: Middle ear model of Talmadge et al. (1998) [189].

which contains loudspeakers and a microphone. The length of the ear canal between the probe and the tympanic membrane is supposed to be small relative to the sound wavelength. In this way, the pressure $P_e(t)$ in the ear canal may be considered uniform. Finally, if all air pressure changes are considered to be adiabatic, then the mechanical model schematized in Figure 1.14 is formulated by a single oscillator equation, as follows

$$\ddot{\xi}_{ow}(t) + \gamma_{ow}\dot{\xi}_{ow}(t) + \omega_{ow,e}^2 \xi_{ow}(t) = \frac{1}{\sigma_{ow}}\left[p(0,t) + G_{me}P_e(t)\right] \tag{1.12}$$

where

$$G_{me} = \frac{S_{ty}}{S_{ow}}\Gamma_{mi}. \tag{1.13}$$

and where the parameters σ_{ow}, γ_{ow} and Γ_{mi} are phenomenological constants defined in Table I of Talmadge et al. (1998) [189], reproduced in Figure 1.15. The quantity $\omega_{ow,e}$ is the frequency of middle ear leading the contribution of the tympanic cavity only. It is given by the ratio of the effective mechanical stiffness of the middle ear to its effective mass. The following relationship holds between the middle ear frequency $\omega_{ow,e}$ and the mechanical frequency of the ossicles $\omega_{ow,mech}$,

$$\omega_{ow,e}^2 = \omega_{ow,mech}^2 + \frac{P_{tc}^a S_{ty}^2 \Gamma_{mi}^2}{m_{ow}V_{tc}} \tag{1.14}$$

where $P_{tc}^a S_{ty}^2 \Gamma_{mi}^2 / (m_{ow}V_{tc}) \approx (2\pi \times 945\ Hz)^2$ represents the contribution to the square of the middle ear frequency from the tympanic cavity. Moreover,

Parameter	Value/Definition	Description
a_d	$(S_{\text{avg}}P_0/2\rho V_e)G_{\text{me}} \approx 1.7\times10^5$ cm s^{-2}	parameter coupling P_e to $(1/\omega^2)\partial P_d/\partial x$
Γ_{mi}	1.4	lever ratio of incus
$\gamma_0(x)$	$\gamma_0 e^{-k_\gamma x}+\gamma_1$	passive linear damping
γ_0	5035 s^{-1}	damping exponential coefficient
γ_1	100 s^{-1}	damping additive constant
$\gamma_2(x)$	$\gamma_0(x)/b_{nl}^2$,	nonlinear damping
b_{nl}	1.4×10^{-7} cm	Scale for nonlinear saturation
γ_{ow}	500 s^{-1}	middle ear damping constant
G_{me}	$S_{\text{ty}}/S_{\text{ow}}\Gamma_{mi}=21.4$	mechanical gain of ossicles
$\kappa_f(x)$	$\rho_f\omega_0^2(x), \rho_f=0.16$	''fast feedback'' stiffness
$\kappa_s(x)$	$\rho_s\omega_0^2(x), \rho_s=0.1416$	''slow feedback'' stiffness
$\hat{k}$	$k(\hat{x},\omega)\cong 75$ cm^{-1}	wave number at activity pattern maximum
k_ω	1.382 cm^{-1}	frequency map exponential constant
k_0	$\sqrt{2\rho W_{\text{bm}}/\rho_{\text{bm}}S_{\text{avg}}}\cong 31$ cm^{-1}	geometrical wave number of cochlea
$k_{\text{ow},0}$	$2\rho S_{\text{ow}}/\sigma_{\text{bm}}S_{\text{avg}}\cong 1100$ cm^{-1}	coupling of oval window to perilymph
L_{bm}	3.5 cm	length of basilar membrane
m_{ow}	0.059 g	effective mass of oval window+ossicles
σ_{bm}	0.0055 g cm^{-2}	areal density of basilar membrane
σ_{ow}	$m_{\text{ow}}/S_{\text{ow}}\cong 1.85$ g cm^{-2}	areal density of oval window
P^a	$\rho_a c_a^2=1.42\times10^6$ dyn cm^{-2}	adiabatic bulk modulus of air
ρ	1.0 g cm^{-3}	density of perilymph
S_{avg}	0.011 cm^2	reciprocal average cross-sectional area of cochlear scalae
S_{ow}	0.032 cm^2	area of oval window
S_{ty}	0.49 cm^2	effective area of tympanic membrane
$\tau_f(x)$	$\psi_f/\omega_0(x), \psi_f=0.24\cdot 2\pi$	delay of ''fast feedback''
$\tau_s(x)$	$\psi_s/\omega_0(x), \psi_s=1.742\cdot 2\pi$	delay of ''slow feedback''
V_{tc}	2.0 cm^2	volume of tympanic cavity
$\omega_0(x)$	$\omega_0 e^{-k_\omega x}+\omega_1$	place-frequency map
ω_0	20 800 Hz$\times 2\pi$	frequency map exponential coefficient
ω_1	-145.5 Hz$\times 2\pi$	frequency map additive constant
ω_{ow}	1500 Hz$\times 2\pi$	middle ear frequency
W_{bm}	0.029 cm	average width of basilar membrane

Figure 1.15: Talmadge's cochlear parameters (Talmadge et al., 1998 [189]).

$P_{tc}^a = \gamma_{air} P_0^{tc}$, with $\gamma_{air} \cong 1.4$ the ratio of specific heats of air, and P_0^{tc} the ambient pressure in the tympanic cavity.

In (1.12) the displacement of the oval window ξ_{ow} is related to $P_e(t)$, a pressure fixed in the ear canal. However, in an experimental setup $P_e(t)$ is an observable, while the fixed experimental input is the calibrated ear canal pressure $P_{dr}(t)$, supposing rigid eardrum. If adiabatic compression or expansion is assumed, $P_e(t)$ and $P_{dr}(t)$ are related by the following relationship

$$P_{dr}(t) = P_e(t) + \frac{P_e^a S_{ty} \Gamma_{mi}}{V_e} \xi_{ow}(t) \tag{1.15}$$

where $P_e^a = \gamma_{air} P_e^0$, with P_e^0 the ambient pressure of the air in the ear canal.

Let ω_{ow} be the frequency of middle ear leading the contribution of tym-

panic and ear canal cavities, and expressed by the following relation

$$\omega_{ow}^2 \equiv \omega_{ow,dr}^2 = \omega_{ow,mech}^2 + \frac{S_{ty}^2 \Gamma_{mi}^2}{m_{ow}} \left[\frac{P_{tc}^a}{V_{tc}} + \frac{P_e^a}{V_e} \right] \tag{1.16}$$

where $P_e^a S_{ty}^2 \Gamma_{mi}^2 / (m_{ow} V_e) \approx (2\pi \times 1340\ Hz)^2$ is the ear canal volume contribution to ω_{ow}^2. By considering (1.14), (1.16) becomes

$$\omega_{ow}^2 = \omega_{ow,e}^2 + \frac{S_{ty}^2 \Gamma_{mi}^2 P_e^a}{m_{ow} V_e}. \tag{1.17}$$

By evaluating (1.17) experimentally, the value of ω_{ow} is around $1500\ Hz \times 2\pi$ in resonance condition on the forward transmission gain (Puria, 2003[146]; Voss and Shera, 2004 [204]). As a result, the middle ear may be considered as a broadband filter with resonance frequency $\omega_{ow} = 1500\ Hz \times 2\pi$. This value may be carried out by setting the value for the stiffness k_{ow} and the mass density σ_{ow}, since $\omega_{ow} = \sqrt{k_{ow}/\sigma_{ow}}$. In this way the middle ear and oval window dynamics is included in the cochlear model.

Finally, by using (1.13), (1.15) and (1.17), and since $\sigma_{ow} = m_{ow}/S_{ow}$, (1.12) becomes equal to (1.11)

$$\ddot{\xi}_{ow}(t) + \gamma_{ow} \dot{\xi}_{ow}(t) + \omega_{ow}^2 \xi_{ow}(t) = \frac{1}{\sigma_{ow}} \left[p(0,t) + G_{me} P_{dr}(t) \right].$$

The formulation (1.11) represents the model equation for the oval window coupled to the middle ear and the ear canal. The pressure $G_{me} P_{dr}$ on the oval window may be evaluated for a supplied stimulus level L. In the simple case of sinusoidal stimulus, let $P = P_{dr}$ be the stimulus amplitude and $L = P\,(dB\ SPL) = 20\, log_{10}(P/P_0)$ be the stimulus level. Then $P_{dr} = P_0\ 10^{L/20}$ and

$$P_{ow} = G_{me} P_{dr} = G_{me} P_0\ 10^{L/20} = 4.2 \cdot 10^{-4} 10^{L/20}\ Pa \tag{1.18}$$

where the values $G_{me} = 21.4$ and $P_0 = 20\ \mu Pa$ from Talmadge et al. (1998) [189] are involved.

1.5.3 The anti-damping model

The active cochlear model, discussed in section 1.5, is based on an one-dimensional linear transmission-line cochlear box-model. Here, a nonlinear term is introduced in order to describe the additional pressure $q(x,t)$ on the BM by OHCs in (1.6). Specifically, the OHCs force is considered to

be proportional to the local BM transverse velocity $\dot{\xi}(x,t)$ by a nonlinear function $\Gamma_{nl}(x,\dot{\xi})$ of the following form described in Moleti et al. (2013) [132]

$$\Gamma_{nl}(x,\dot{\xi})\dot{\xi} = (\gamma_{bm}(x) - \Gamma_a)\left[1 - tanh\left(\frac{\dot{\xi}^2}{\dot{\xi}_{sat}^2}\right)\right]\dot{\xi} \tag{1.19}$$

where Γ_a is a constant, and $1/\dot{\xi}_{sat}$ establishes a saturation velocity below which the OHCs gain is linear. The (1.19) acts as an anti-damping force, a sort of negative resistance. Consequently, since this term works as $q(x,t)/\sigma_{bm}$ in (1.6), the function $\Gamma_{nl}(x,\dot{\xi})$ adds to the passive damping coefficient γ_{bm}, yielding the following effective damping function

$$\Gamma_{eff}(x,\dot{\xi}) = \gamma_{bm}(x) - \Gamma_{nl}(x,\dot{\xi}) = \gamma_{bm}(x) - (\gamma_{bm}(x) - \Gamma_a)\left[1 - tanh\left(\frac{\dot{\xi}^2}{\dot{\xi}_{sat}^2}\right)\right] \tag{1.20}$$

This function shows two linear asymptotic regimes with constant damping: (1.20) becomes $\Gamma_{eff} = \Gamma_a$ (coefficient of active damping) for low $\dot{\xi}$ values and $\Gamma_{eff} = \gamma_{bm}(x)$ (coefficient of passive damping) for high $\dot{\xi}$ values. For intermediate $\dot{\xi}$ values an approximately quadratic damping is achieved.

Therefore, the formulation (1.19) can implement the compressive nonlinearity of the cochlear response for intermediate stimuli, and the cochlear linearity for low and high stimuli, as observed experimentally by Ren and Nuttall (2001) [149] and discussed in section 1.3. Moreover, a suitable tuning of the free parameters Γ_a, Γ_{eff} and $\dot{\xi}_{sat}$ allows to adjust the gain function of the cochlear amplifier.

Then, the oscillating equation (1.6) is modified as follows

$$\ddot{\xi}(x,t) + \gamma_{bm}(x)\dot{\xi}(x,t) + \omega_{bm}^2(x)\xi(x,t) = \frac{p(x,t)}{\sigma_{bm}} + \Gamma_{nl}(x,\dot{\xi})\dot{\xi}. \tag{1.21}$$

Let us define

$$\alpha(\dot{\xi}) = \alpha_0\left[1 - tanh\left(\frac{\dot{\xi}^2}{\dot{\xi}_{sat}^2}\right)\right] \tag{1.22}$$

with

$$\alpha_0 = \frac{\gamma_{bm}(x) - \Gamma_a}{\gamma_{bm}(x)}, \tag{1.23}$$

so(1.19) becomes

$$\Gamma_{nl}(x,\dot{\xi})\dot{\xi} = \gamma_{bm}(x)\alpha(\dot{\xi})\dot{\xi} \tag{1.24}$$

This formulation is useful in order to manage the variation of the cochlear gain by changing the value of α_0. In particular a value of α_0 close to unity

will give a large variation of the cochlear gain between the two asymptotic regimes. On the other side, a high value of the passive quality factor (1.9) implies moderate damping also at high stimulus levels.

Finally, variation of cochlear properties along the BM has to be included in the model. In humans, irregularities (namely, roughness) along the BM may cause reflections of the TW and, thus, are responsible for coherent linear reflection (see section 1.4). In order to introduce cochlear roughness in the model, a small random fluctuation of the local resonance frequency may be considered, of the form described in Moleti et al. (2013) [132]. Specifically, the squared angular frequency in (1.21) is substituted by the following expression (in the limit $\omega_1 = 0$ of scale invariance symmetry)

$$\omega_{bm}^2(x) = \omega_0^2 e^{-2k_\omega x}(1 + \epsilon R) \tag{1.25}$$

where R is a random number, normally distributed, with variance equal to unity, and ϵ represents the roughness relative amplitude. In this way, small randomly distributed inhomogeneities (that is, roughness) along the BM are included as random variations for a cochlear parameter, namely, the tonotopic resonance frequency. A forward TW will generate a coherent reflection from the TW peak, i.e. a backward wave directed towards the base. The fraction of this backward wave passing through the middle ear gives rise to OAEs in the ear canal. Further reflection at the base may give rise to standing waves at the frequencies matching a geometrical condition (integer number of wavelength between the resonant region and the base), resulting in the emission of SOAEs and hearing threshold fine structure (see section 1.4).

The nonlinear response of the model may be tested by means of single-tone numerical experiments. In Moleti et al. (2013) [132] stimuli of single frequency f_0=2 kHz with levels from 20 dB SPL to 80 dB SPL have been employed, and Figure 1.16 shows the cochlear response at frequency f_0 as function of the cochlear position x. The typical behavior of BM response is observable. In particular, at the resonance place $x(f_0) \cong$16 mm (according to the Greenwood Map (1.2)) the BM transverse velocity has maximal amplitude with a compressive growth rate as the stimulus level increases from 30 dB SPL to 60 dB SPL, while a linear growth rate occurs for low and high stimuli. On the other hand, an increasing bandwidth, a decreasing phase slope and a basal shift of the peak are also noticeable as the stimulus level increases, as already observed on animals (see Figure 1.7) by Ren and Nuttall (2001) [149] (see also Russell and Nielsen, 1997 [157] and Rhode, 2007 [151]). The scale invariance considered in the model allows to compare the frequency response of Figure 1.7 with the f_0 Fourier component of the response in x-domain of Figure 1.16.

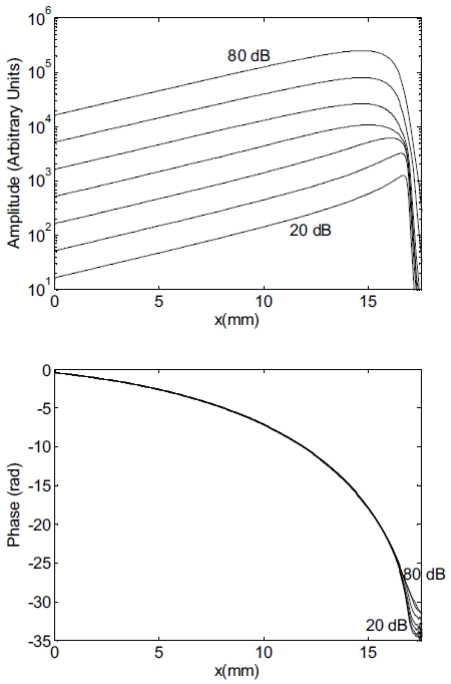

Figure 1.16: Numerical approximate solution of the anti-damping model for the BM response (amplitude in the top panel and phase in the bottom panel) to a 2 kHz tone as a function the cochlear position x (Moleti et al. (2013) [132]). The stimulus level varies in the range [20, 80] dB SPL in 10 dB steps. Other model parameters are: passive quality factor (1.10) $Q_0 = 12$, $\alpha_0 = 0.8$ in (1.22), roughness relative amplitude $\epsilon = 0.001$ in (1.25), saturation velocity $\dot{\xi}_{sat} = 14\, nm/ms$ in (1.19).

The OHCs mechanism represented by (1.22)-(1.24) may be also modeled in a slightly different form as in Sisto et al. (2010) [180]. Namely, the nonlinear term may be considered a function of either the BM transverse displacement or the BM transverse velocity.

1.5.4 The delayed stiffness model

In the anti-damping model the OHCs active mechanism is described by a term proportional to the transverse velocity of the BM. On the other side, Talmadge et al. (1998) [189] formulated a delayed stiffness model, first proposed by Zweig (1991) [210], Shera and Zweig (1993) [172], and Zweig and Shera (1995) [211]. These authors assumed that the spatial activity pattern of TW has to be tall, in order to produce significant reflection from a very small level

of cochlear inhomogeneities, and broad, in order to contain 1 to 2 wavelengths of TW and obtain coherence of the cochlear reflections. Experimental data on animals suggested such a property about tall and broad activity pattern in the cochlear response (Rhode, 1971 [150]). Kim et al. (1980) [113] formulated an active cochlear model with a distributed negative resistance on BM as an energy source which generates activity patterns that are tall but unphysiologically narrow. However, they argued that if the cochlear amplifier is assumed to be basal to the activity pattern peak, then tall and broad activity pattern of TW is generated. As suggested by experimental observations, the model of Zweig (1991) [210] performed tall-broad activity patterns by introducing time delayed stiffness. In this latter model each tonotopic place of the BM is considered as a negatively damped harmonic oscillator which is stabilized at time t by a cochlear amplifier force proportional to the BM velocity at the previous time $t-\tau$, with τ a constant delay. By following such assumptions, Talmadge et al. (1998) [189] proposed an one-dimensional macromechanical model which generates tall-broad activity patterns by means of the linear-active component of the cochlear mechanics, and a random inhomogeneity in cochlear properties. As discussed for the anti-damping model (section 1.5.3), by introducing cochlear roughness in place-frequency Greenwood Map (1.7), reflections of the forward TW may be generated. Talmadge et al. discuss that these reflections might be detected in the ear canal as otoacoustic emissions if they generate an activity pattern with a large tip-to-tail ratio and a broad peak. In this way, at least two wavelength of TW would be contained in the BM activity pattern and coherent reflection might occur. However, the tip-to-tail ratio of the activity pattern and the resulting TW reflections in the ear canal decrease with stimulus level. For this reason basal generators in the TW peak region may provide a significant cochlear response within the broad cochlear activity pattern at high stimulus levels.

Specifically, in the stiffness function, Talmadge et al. (1998) [189] introduce two additional forces proportional to the BM displacement delayed by characteristic times of the form suggested by Zweig (1991) [210], that is

$$\Omega(x,t) = \kappa_f(x)\xi(x, t-\tau_f(x)) + \kappa_s(x)\xi\left(x, t-\tau_s(x)\right) \tag{1.26}$$

where the quantities $\kappa_f(x)$, $\tau_f(x)$ and $\kappa_s(x)$, $\tau_s(x)$ are defined in Talmadge et al. (1998) [189] and represent a force proportional to delayed displacements. In particular $\kappa_f(x)$ and $\kappa_s(x)$ are called, respectively, *fast feedback stiffness* and *slow feedback stiffness*, and defined as

$$\kappa_f(x) = 0.16 \cdot \omega_{bm}^2(x) \qquad \kappa_s(x) = 0.1416 \cdot \omega_{bm}^2(x)\ , \tag{1.27}$$

$\tau_f(x)$ and $\tau_s(x)$ are called, respectively, *delay of fast feedback* and *delay of*

slow feedback, and defined as

$$\tau_f(x) = 0.24 \cdot 2\pi/\omega_{bm}(x) \qquad \tau_s(x) = 1.742 \cdot 2\pi/\omega_{bm}(x). \tag{1.28}$$

In (1.27)-(1.28) $\omega_{bm}(x)$ expresses the Greenwood Map (1.7). According to the above formulation, τ_f effects a phase shift of about 1/4 of a period ($0.24 \cdot 2\pi$), and τ_s of about $-1/4$ of a period ($1.742 \cdot 2\pi \cong 7/4 \cdot 2\pi$). As a result, in (1.26) the displacement ξ delayed by τ_f is out of phase with the velocity $\dot{\xi}$ and the *fast feedback time-delayed stiffness* expresses an anti-damping force. On the other hand, the displacement ξ delayed by τ_s performs a stabilizing effect. In particular, the *slow feedback time-delayed stiffness* works as anti-damping by creating broad BM profiles in a region which is basal to the resonant place. Actually, since the slow feedback term is proportional to the BM displacement (and not the BM velocity), OHCs energy is released basally to the tonotopic site because the delay corresponds to a constant fraction of period of its tonotopic frequency.

The effective stiffness function will be

$$\omega^2(x,\xi)\,\xi(x,t) = \omega_{bm}^2(x)\xi(x,t) + \kappa_f(x)\xi(x,t-\tau_f(x)) + \kappa_s(x)\xi(x,t-\tau_s(x)). \tag{1.29}$$

An additional damping force $\gamma_{nl}(x,\xi)\,\dot{\xi}$ is also introduced in the model to describe the cochlear nonlinearity as a quadratic function of nonlinear damping like a Van der Pol oscillator, where

$$\gamma_{nl}(x,\xi) = \gamma_2(x)\xi^2(x,t) \tag{1.30}$$

and $\gamma_2(x)$ is the *nonlinear damping* defined as

$$\gamma_2(x) = \gamma_{bm}(x)/b_{nl}^2. \tag{1.31}$$

In (1.31) $b_{nl} = 1.4 \cdot 10^{-7}$ cm is the scale for the nonlinear saturation, and $\gamma_{bm}(x)$ corresponds to the Greenwood Map (1.7). In this way the effective damping term will be

$$\gamma(x,\xi) = \gamma_{bm}(x) + \gamma_{bm}(x)\frac{\xi^2(x,t)}{b_{nl}^2} \tag{1.32}$$

Finally the oscillating equation (1.6) is modified as follows

$$\begin{aligned}\ddot{\xi}(x,t) + \gamma_{bm}(x)\dot{\xi}(x,t) + \omega_{bm}^2(x)\xi(x,t) = \frac{p(x,t)}{\sigma_{bm}} + \\ + \Big[-\gamma_{bm}(x)\frac{\xi^2(x,t)}{b_{nl}^2}\dot{\xi}(x,t) + \\ -\kappa_f(x)\xi(x,t-\tau_f(x)) - \kappa_s(x)\xi(x,t-\tau_s(x)) \Big].\end{aligned} \tag{1.33}$$

The time-dependent partial differential equation (PDE) model (1.3) and (1.33) has been analyzed in this thesis. A numerical technique to find its approximate solution will be proposed in Chapter 4, with numerical results in Chapter 5. Before this, next chapters will show the general theory of Delay Differential Equations (Chapter 2) and a numerical approach solving time-dependent PDEs (Chapter 3).

Chapter 2

Delay Differential Equations

In Chapter 1 the human auditory system has been described with special regard to the cochlea, the main organ of the inner ear. The cochlea acts as a transducer of acoustic mechanical signals into electrical signals transmitted to the brain (see section 1.2). During this process a spectral analysis of the incoming sound signal is also performed due to the cochlear tonotopicity property. Namely, different sound frequencies produce a resonance condition and a resulting mechanical oscillation in corresponding sites along the cochlea according to the Greenwood Map (1.2).

The cochlear response nonlinearly increases with the sound stimulus level due to the active mechanism driven by the outer hair cells (OHCs) (see section 1.2). The latter represent the primary component of the cochlear amplifier because they both operate the mechanical-electrical transduction of a sound signal, and supply energy to a cochlear position if stimulated.

In section 1.5 of Chapter 1, active cochlear models have been discussed, and two different formulations have been shown in order to explicit the nonlinear active mechanism performed by the OHCs. In this thesis a model with delayed terms (Zweig, 1991 [210]), of the form introduced by Talmadge et al. (1998) [189], will be analyzed. That is, the model oscillating equation (1.6) is considered in the formulation (1.33) for each tonotopic site of the cochlea. For this reason, the theory of delay differential equations (DDEs) will be considered. Greater focus will be on time dependent DDEs from which results on constant DDEs may be derived, this being the structure of the model at hand. In this chapter the main results about how to handle DDEs will be reported from Bellen and Zennaro (2003) [10]. Refer to [10] also for proof of the theorems which will be shown here in order to analyze existence and uniqueness of solution of time dependent DDEs (theorem 2.1 and theorem 2.2). The *method of steps* will be then discussed for approximating DDEs solution numerically. It represents a standard approach which

turns a DDE into a finite number of Initial Value Problems (IVPs) of Ordinary Differential Equations (ODEs). As a result, the DDE solution may be evaluated by carrying out the approximate solution of each IVP by means of any ODEs discrete method. The convergence of ODEs numerical methods will be discussed in theorem 2.3 and theorem 2.4 as in Bellen and Zennaro (2003) [10].

For reading this chapter, some notes about the differentiation notation will be useful. Here, temporal derivatives will be indicated by the dot notation. That is, for any function $f(t)$, $\dot{f}(t) = df/dt$. Moreover, $\dot{f}(t)^+$ and $\dot{f}(t)^-$ will indicate right derivative and left derivative, respectively. Let t_0 be a point in the domain of f. Then $f(t)$ will have a jump discontinuity in t_0 if there exist $f(t_0)^+$ and $f(t_0)^-$ and $f(t_0)^+ \neq f(t_0)^-$. This class of discontinuities will be a critical issue for DDEs, as will be shown in the next section.

2.1 DDEs: Delay Differential Equations

Many real-life phenomena can be modeled by IVPs of ODEs, formally expressed by the following relation

$$\begin{cases} \dot{y}(t) = g(t, y(t)) & t \geq t_0 \\ y(t_0) = y_0 \end{cases} \tag{2.1}$$

where $y(t)$ is the state variable describing a physical quantity which depends on time. In natural phenomena models the derivative $\dot{y}(t)$ of the state variable with respect to time variable may depend on past values of $y(t)$. In this way, (2.1) becomes an IVP of *Delay Differential Equations* (DDEs), as follows

$$\begin{cases} \dot{y}(t) = f(t, y(t-\tau_1), \ldots, y(t-\tau_n)) & t \geq t_0 \\ y(t) = \phi(t) & t \leq t_0 \end{cases} \tag{2.2}$$

where τ_i are the *delays* which are non-negative constants in the *constant delay case*, or functions of t in the *time dependent delay case*, $\tau_i = \tau_i(t)$, or functions of t and $y(t)$ in the *state dependent delay case*, $\tau_i = \tau_i(t, y(t))$. The function $\phi(t)$ is called *initial function* and is at least C^0-continuous. For the constant and time dependent delay cases, $\phi(t)$ is defined in $[\rho, t_0]$, where

$$\rho = \min_{1 \leq i \leq n} \left\{ \min_{t \geq t_0} (t - \tau_i) \right\}. \tag{2.3}$$

Note that for the state dependent delay case the bound ρ can be calculated when the dependence of τ on $y(t)$ is known.

In order to point out the difference between an ODE and a DDE, it is useful to consider (2.2) for $n = 2$ with a single delay τ, that is

$$\begin{cases} \dot{y}(t) = f(t, y(t), y(t-\tau)) & t \geq t_0 \\ y(t) = \phi(t) & t \leq t_0. \end{cases} \tag{2.4}$$

Compare (2.1) with (2.4). First, while the solution of ODEs is determined by an initial value $y(t_0)$, a DDE needs an initial function $\phi(t)$ for past values $t \leq t_0$. Second, the function $f(t, y(t), y(t-\tau))$ represents the right-hand derivative $\dot{y}(t)^+$, and in general $\dot{y}(t_0)^+ \neq \dot{\phi}(t_0)^-$, that is the solution $y(t)$ of (2.2) or (2.4) is not linked to the initial function $\phi(t)$ at t_0. Consequently, the continuity of $y(t_0)$ is not guaranteed for order higher than the C^0-continuity. Third, the derivative discontinuity in t_0 propagates along the integration interval. As a result, in general $y(t)$ is only C^1-continuous in an integration interval $[t_0, t_f]$, even if $f(t, y(t), y(t-\tau))$, $\tau(t, y(t))$ and $\phi(t)$ are C^∞-continuous.

Example 2.1. Consider the equation

$$\begin{cases} \dot{y}(t) = -y(t-1) & t \geq 0 \\ y(t) = 1 & t \leq 0. \end{cases} \tag{2.5}$$

Observe that the first derivative $\dot{y}(t)$ has a discontinuity in $t = 0$ because $\dot{y}(0)^- = 0$ and $\dot{y}(0)^+ = -y(-1) = -1$. The second derivative $\ddot{y}(t) = -\dot{y}(t-1)$ is discontinuous in $t = 1$ because $\ddot{y}(1)^- = -\dot{y}(0)^- = 0$ and $\ddot{y}(1)^+ = -\dot{y}(0)^+ = -1$. Analogously, all successive derivatives will be discontinuous at multiples of the delay $t = 2, 3, 4, \ldots$. The solution of (2.5) is shown in Figure 2.1. □

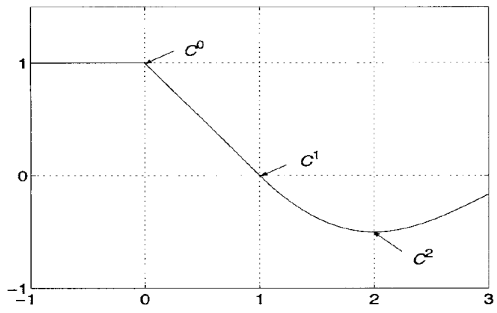

Figure 2.1: Graphical solution of (2.5).

Some physical problems are modeled by a type of DDEs in which the derivative $\dot{y}(t)$ depends on y and $\dot{y}$ at past values $t-\tau$. This type of equations

is called *Neutral Delay Differential Equations* (NDDEs) and is formulated as follows

$$\begin{cases} \dot{y}(t) = f(t, y(t), y(t-\tau), \dot{y}(t-\tau)) & t \geq t_0 \\ y(t) = \phi(t) & t \leq t_0 \end{cases} \tag{2.6}$$

where the initial function $\phi(t)$ is at least C^1-continuous, and, in general, is not linked to the solution $y(t)$ at t_0 for greater order than class C^0. This discontinuity propagates along the integration interval to points where $y(t)$ will be only C^0-continuous, while in the non-neutral case $y(t)$ may be of class C^1.

Example 2.2. Consider the equation

$$\begin{cases} \dot{y}(t) = -\dot{y}(t-1) & t \geq 0 \\ y(t) = t & t \leq 0. \end{cases} \tag{2.7}$$

Observe that the first derivative $\dot{y}(t)$ has a discontinuity in $t = 0$ because $\dot{y}(0)^- = 1$ and $\dot{y}(0)^+ = -\dot{y}(-1) = -1$. Analogously, all multiples of the delay $t = 1, 2, 3, 4, \ldots$ are discontinuity points for $\dot{y}(t)$. The solution of (2.7) is shown in Figure 2.2. □

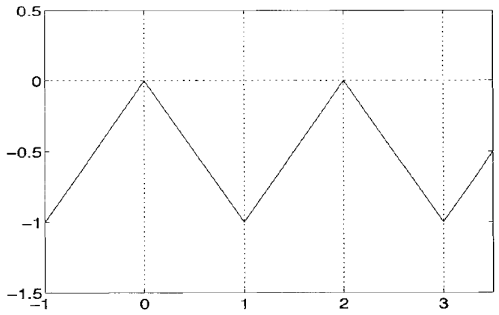

Figure 2.2: Graphical solution of (2.7).

For constant and time dependent delay cases, the theory of existence and uniqueness of solutions does not formally change with respect to the ODEs case if the delayed argument $t - \tau(t)$ is uniformly strictly positive (this latter condition is ensured in the constant delay case). However, the dynamical behavior of DDEs is different from those of ODEs. The latter may show oscillating solutions only if the system has at least two components, and chaotic behavior with at least three components (*Poincaré-Bendixon theorem*; Teschl, 2012 [195]). On the other hand, DDEs may present oscillatory or chaotic behavior in the scalar case.

On the other hand, the behavior of ODEs solution may radically change when delayed terms are included in the model. In particular, a delayed term might work with a regularizing effect, that is, stabilizing or destabilizing the behavior of the ODE solution. The following example will show this case.

Example 2.3. Consider the following linear scalar equation

$$\begin{cases} \dot{y}(t) = \lambda y(t) + \mu y(t-1) & t \geq 0 \\ y(t) = -t + 1 & t \leq 0 \end{cases} \tag{2.8}$$

where λ and μ are real constant coefficients.

If $\mu = 0$, (2.8) becomes an IVP of ODEs, namely

$$\begin{cases} \dot{y}(t) = \lambda y(t) & t \geq 0 \\ y(0) = 1 \end{cases} \tag{2.9}$$

The solution $y(t) = e^{\lambda t}$ of (2.9) vanishes asymptotically with upper bound fixed by the initial condition $y(0) = 1$ for any negative λ, and blows up for any positive λ.

If $\mu \neq 0$ the delayed term $\mu y(t-1)$ works as a forcing term. In particular, if $\mu > 0$ the solution of (2.8) vanishes asymptotically only for some negative λ values, and is not bounded by the initial value $y(0) = 1$. In Figure 2.3A and Figure 2.3B solutions of (2.8) for two negative values of λ and one positive value of μ are shown, while in Figure 2.3C the plotted solution shows that a negative μ works as stabilizer even if λ is positive. □

2.2 Regularity of solutions

In a first approach, the solution of DDEs can be found by using integration steps less than or equal to the delay τ. In this way, the delayed term $y(t-\tau)$ is substituted by a function $x(t-\tau)$ formulated, according to t values, as the initial function $\phi(t)$ or a continuous extension of the approximate solution previously computed. Specifically, the method applied to the IVP of DDEs (2.4) with constant τ is formulated as follows

$$\begin{cases} \dot{w}_{n+1}(t) = f(t, w_{n+1}(t), x(t-\tau)) & t_n \leq t \leq t_{n+1} \\ w_{n+1}(t_n) = y_n \end{cases} \tag{2.10}$$

with

$$x(s) = \begin{cases} \phi(s), & s \leq t_0 \\ \eta(s), & t_0 \leq s \leq t_n \end{cases} \tag{2.11}$$

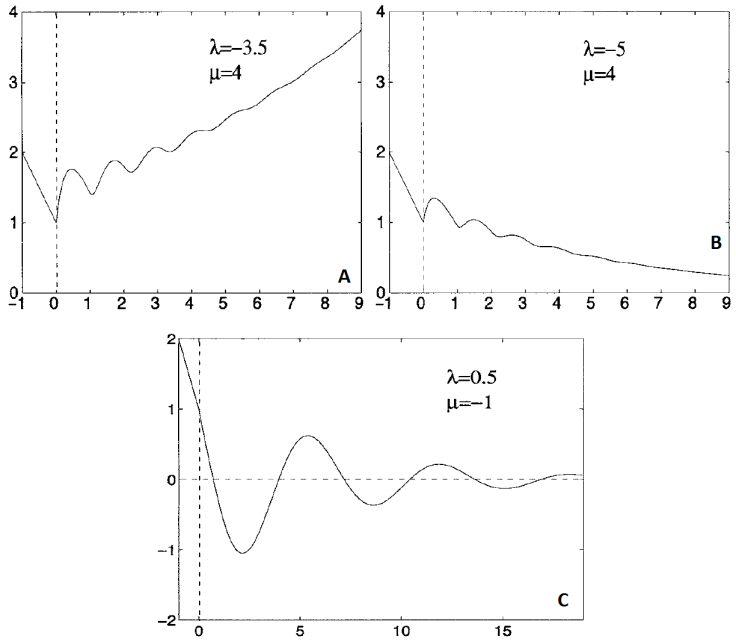

Figure 2.3: Graphical solution of (2.8).

The integration method (2.10)-(2.11) compute y_{n+1}, approximated by the value of w_{n+1}, and the function $\eta(t)$ on the interval $[t_n, t_{n+1}]$ such that $\eta(t_{n+1}) = y_{n+1}$.

For every step of the method (2.10)-(2.11), suppose to advance in time by means a finite difference method (see Chapter 3), as will be carried out for the delayed physical problem studied in this thesis. Then, a remarkable difference exists between ODEs and DDEs. In the case of ODEs, the step by step numerical method computes the approximation of the solution at mesh points only. On the other hand, in the case of a DDE, additional time points $t - \tau$ may be required other than the mesh points in order to compute the function $\eta(t)$. Consequently, numerical DDEs methods are derived as *continuous extensions* of numerical ODEs methods. Namely, the function $\eta(t)$ is generated by a posteriori interpolation of the values y_n computed with a discrete ODEs method, or by continuous ODEs methods, carrying out a continuous approximation of the solution.

However, in general DDEs solution cannot be numerically approximated by adapting the integration methods for ODEs. The choice of the method will be based on the analysis of the dynamical structure of DDEs. In particular, in this thesis, constant DDEs will be analyzed, this being the property of the physical model considered (see section 1.5.4 in Chapter 1).

As above discussed, in general, the dependence of y (constant or time dependent delay case) or $\dot{y}$ (state dependent delay case) on delayed arguments may generate discontinuity points which propagate from the discontinuity at t_0 to other discontinuities on $\dot{y}$ and successive derivatives. The number and the location of the discontinuities depends on the behavior of the delayed argument $\alpha(t) = t - \tau(t, y(t))$, called *deviated argument*. Since the delays are assumed always non-negative, the deviated arguments fulfill the condition $\alpha(t) \leq t$. Moreover if $\alpha(t) \geq t_0$, then additional time points $t^* < t_0$ are not required; consequently, no discontinuous points propagate along the integration interval $[t_0, t_f]$, and the regularity of the solution depends on the functions $f(t, y(t), y(t - \tau(t, y(t))))$ and $\alpha(t))$ only.

In Chapter 4 it will be shown that, for the delayed model analyzed in this thesis, the condition $\dot{y}(t_0 = 0)^+ = \dot{\phi}(t_0 = 0)^- = 0$ is fulfilled because, for the problem at hand, $\phi(t_0 = 0) = 0 \; \forall \, t \leq t_0 = 0$. In this way, discontinuity points are not generated in t_0.

However, in general, C^{p+1}-continuity is required for the solution $y(t)$ on each integration subinterval $[t_n, t_{n+1}]$ if method accuracy of order p is expected. For this purpose, the mesh points should include the discontinuity points of the solution at least for $t_0, t_1, \ldots, t_{p+1}$. This approach works even if DDEs enclose many deviated arguments, which might generate a more disordered behavior of the discontinuity points.

The number and the location of the discontinuities widely depends on the behavior of the deviated argument $\alpha(t)$. The jump discontinuities which originate in t_0 on the first derivative of $y(t)$ ($\dot{y}(t_0)^+ \neq \dot{\phi}(t_0)^-$), are defined *primary discontinuities* and propagate along the integration interval on successive derivatives. In this way, *1-level primary discontinuities* originate in $\ddot{y}$, *2-level primary discontinuities* originate in $\dddot{y}$ and so on.

Consider the IVP of DDEs (2.4) to be integrated in the time interval $[t_0, t_f]$ with the following assumptions: $\alpha(t) = t - \tau < t_0$ for some points $t \in [t_0, t_f]$; $\dot{\phi}(t_0)^- \neq \dot{y}(t_0)^+ = f(t_0, \phi(t_0), \phi(\alpha(t_0)))$. If the functions f, ϕ and α are continuous, then $\dot{y}(t)$ is continuous for any $t > t_0$. Moreover, if f, ϕ and α are differentiable, then $\ddot{y}(t)$ exists for any t except for the points $\xi_i > t_0$ such that

$$\alpha(\xi_i) = t_0 \qquad \text{and} \qquad \dot{\alpha}(\xi_i) \neq 0. \tag{2.12}$$

This is even deduced by finding the simple roots of the equation

$$\alpha(t) = t_0. \tag{2.13}$$

Consider the second derivative of the solution $y(t)$, that is

$$\ddot{y}(t)^{\pm} = \frac{\partial f}{\partial t}(t, y(t), y(\alpha(t))) + \frac{\partial f}{\partial y}(t, y(t), y(\alpha(t)))\dot{y}(t) + \frac{\partial f}{\partial x}(t, y(t), y(\alpha(t)))\dot{y}(\alpha(t))^{\pm}\dot{\alpha}(t) \tag{2.14}$$

and evaluate (2.14) in ξ_i, that is

$$\ddot{y}(\xi_i)^{+} = \frac{\partial f}{\partial t}(\xi_i, y(\xi_i), y(t_0)) + \frac{\partial f}{\partial y}(\xi_i, y(\xi_i), y(t_0))\dot{y}(\xi_i) + \frac{\partial f}{\partial x}(\xi_i, y(\xi_i), y(t_0))\dot{y}(t_0)^{+}\dot{\alpha}(x_i) \tag{2.15}$$

and

$$\ddot{y}(\xi_i)^{-} = \frac{\partial f}{\partial t}(\xi_i, y(\xi_i), y(t_0)) + \frac{\partial f}{\partial y}(\xi_i, y(\xi_i), y(t_0))\dot{y}(\xi_i) + \frac{\partial f}{\partial x}(\xi_i, y(\xi_i), y(t_0))\dot{\phi}(t_0)^{-}\dot{\alpha}(x_i). \tag{2.16}$$

In (2.15) and (2.16), the value t_0 of (2.13) in ξ_i has been used. Observe that $\ddot{y}(t)$ does not exist at ξ_i and its prolongation by $\ddot{y}(\xi_i) = \ddot{y}(\xi_i)^{+}$ has a jump discontinuity (1-level primary discontinuity) because $\dot{\alpha}(\xi_i) \neq 0$ and the solution $y(t)$ does not link smoothly to the initial function $\phi(t)$ at t_0 ($\dot{\phi}(t_0)^{-} \neq \dot{y}(t_0)^{+} = f(t_0, \phi(t_0), \phi(\alpha(t_0)))$). Each 1-level primary discontinuity ξ_i goes into a 2-level primary discontinuity in $\dddot{y}$ at any point $\zeta_j > \xi_i$. The latter is a simple root of the equation

$$\alpha(t) = \xi_i, \tag{2.17}$$

for some i. Hence, a *k-level primary discontinuity* point generates $(k+1)$-level primary discontinuities in $y^{(k+2)}$ at points where $y(t)$ becomes smoother and smoother as the primary discontinuity level increases (*property of smoothing of the solution*).

Definition 2.1. A discontinuity point ξ is said to be of order k if $y^{(s)}(\xi)$ exists for $s = 0, \ldots, k$ and $y^{(k)}$ is Lipschitz continuous at ξ. □

Consequently, a p-level primary discontinuity has order $k \geq p$. In general, the deviated argument $\alpha(t)$ may have a complicated behavior. However, for constant DDEs (as the physical model at hand, see section 1.5.4) the discontinuities, generating from t_0, are at the points $t_0 + k\tau$ with $k = 1, 2, \ldots$.

Let $\bar{\xi}_k$ be a k-level primary discontinuity point and $\bar{\xi}_0 = t_0$ the only 0-level primary discontinuity point. In general, the primary discontinuities propagate according to the following rule

$$\alpha(\bar{\xi}_k) = \bar{\xi}_{k-1}$$

For models with constant delay τ, the deviated argument $\alpha(t) = t - \tau$ is a strictly increasing function for all $t \in [t_0, t_f]$. Then, if $\alpha(t_0) < t_0$, the primary discontinuities form an increasing sequence $\xi_1 < \xi_2 < \ldots < \xi_j < \cdots$, where ξ_j is the sole j-level discontinuity point $\forall j$. The following definition holds:

Definition 2.2. The one-index subset of primary discontinuity points $\bar{\xi}_i$ defined inductively by $\bar{\xi}_0 = t_0$ and, for $i \geq 0$, by the minimum root $\bar{\xi}_{i+1}$ of

$$\alpha(t) = \bar{\xi}_i$$

with odd multiplicity, is called the set of *principal discontinuity points.* □

The principal discontinuities fulfill the following condition for any i,

$$\alpha(t) \leq \bar{\xi}_i \quad \forall\, t \in [\bar{\xi}_i, \bar{\xi}_{i+1}].$$

Consequently, since all the primary discontinuities are principal if $\alpha(t)$ is a strictly increasing function $\forall t \in [t_0, t_f]$, the knowledge of their location is sufficient to apply the method with success.

Discontinuities with respect to t can also originate on f, τ and ϕ in some of their derivatives. They are defined *secondary discontinuities* and propagate as the primary ones.

Finally, if DDEs depends on more than one deviated argument, a chaotic proliferation of the discontinuities might occur. This is because each discontinuity point might generate other discontinuities which may also coincide for different levels. Nevertheless, no additional conceptual difficulties arise when many delays are involved in a DDE with respect to one-delay case. Thus, a suitable programming in the implementation of the solving numerical method might be sufficient in many-delays case.

No further analysis on propagation and localization of the discontinuities of DDEs will be discussed here since it is not within the scope of this dissertation (more details can be found in Bellen and Zennaro (2003) [10]). As previously mentioned, the physical model explored does not present this issue because f is a continuous function and the solution $y(t)$ is smoothly linked to the initial function $\phi(t)$ at t_0.

2.3 Existence and uniqueness of solutions

Consider a time dependent DDE

$$\begin{cases} \dot{y}(t) = f(t, y(t), y(t - \tau(t))) & t \geq t_0 \\ y(t) = \phi(t) & t \leq t_0. \end{cases} \tag{2.18}$$

If the following condition is fulfilled

$$\inf_{[t_0, t_f] \times \mathbb{R}^d} \tau(t) = \tau_0 > 0 \tag{2.19}$$

then in the interval $[t_0, t_0 + \tau_0]$, (2.18) becomes the following ODE

$$\begin{cases} \dot{y}(t) = f(t, y(t), \phi(t - \tau(t))) & t \geq t_0 \\ y(t_0) = \phi(t_0) \end{cases} \tag{2.20}$$

which only requires continuity conditions on f, ϕ and τ to ensure the local existence and uniqueness of the solution $y(t)$ on $[t_0, t_0 + \tau_0]$. In order to guarantee the existence of the solution in a finite interval $[t_0, t_f]$, successive integrations of ODEs may be carried out on sub-intervals $[t_0 + i\tau_0, t_0 + (i+1)\tau_0]$ with $i = 0, 1, 2, \ldots$, employing the solution known in the interval $[t_0, t_0 + i\tau_0]$. This method is called *method of steps* (see also section 2.4) and provides the so-called *standard approach* to theoretically analyze or numerically approximate the solution of DDEs. Therefore, the following theorems hold.

Theorem 2.1. Local existence.
Consider the equation

$$\begin{cases} \dot{y}(t) = f(t, y(t), y(t - \tau(t))) & t_0 \leq t \leq t_f \\ y(t_0) = y_0 \end{cases} \tag{2.21}$$

and assume that the function $f(t, u, v)$ is continuous on $A \subseteq [t_0, t_f) \times \mathbb{R}^d \times \mathbb{R}^d$ and locally Lipschitz continuous with respect to u and v. Moreover, assume that the delay function $\tau(t) \geq 0$ is continuous in $[t_0, t_f)$, $\tau(t_0) = 0$ and, for some $\xi > 0$, $t - \tau(t) > t_0$ in the interval $(t_0, t_0 + \xi]$. The problem (2.21) has a unique solution in $[t_0, t_0 + \delta)$ for some $\delta > 0$ and this solution depends continuously on the initial data. □

Theorem 2.2. Global existence.
If, under the hypotheses of Theorem 2.1, the unique maximal solution of (2.21) is bounded, then it exists on the entire interval $[t_0, t_f)$. □

Corollary 2.1. Global uniqueness.
Besides the hypothesis of Theorem 2.1, assume that the function $f(t, u, v)$ satisfies the condition

$$\|f(t, u, v)\| \leq M(t) + N(t)\,(\|u\| + \|v\|) \tag{2.22}$$

in $[t_0, t_f) \times \mathbb{R}^d \times \mathbb{R}^d$, where $M(t)$ and $N(t)$ are continuous positive functions on $[t_0, t_f)$. Then the solution of (2.21) exists and is unique on the entire interval $[t_0, t_f)$. □

Finally, theorems can be discussed in order to guarantee the local and the global existence and uniqueness of the solution of state dependent DDEs and NDDEs. They will not be reported here but can be found in Bellen and Zennaro (2003) [10].

2.4 *Method of steps* for constant or non-vanishing time dependent DDEs

Consider the following IVP based on time dependent DDEs

$$\begin{cases} \dot{y}(t) = f(t, y(t), y(t - \tau(t))) & t_0 \leq t \leq t_f \\ y(t) = \phi(t) & t \leq t_0. \end{cases} \tag{2.23}$$

The problem (2.23) binds the derivative of the solution $y(t)$ with the solution itself, as occurs in ODEs, and also the solution at past time values. This condition complicates the theoretical and numerical solution of DDEs with respect to ODEs.

The *method of steps* represents a basic approach which numerically approximates the DDEs solution by means of any ODE discrete method. In particular, *Linear Multistep Methods* may be considered on a mesh Δ of points t_n including all deviated argument $t_n - \tau(t_n)$, that is

$$\begin{gathered} \Delta = \{t_0, t_1, \ldots, t_n, \ldots, t_N = t_f\} \quad \text{such that} \\ t_n - \tau(t_n) < t_0 \quad \text{or} \quad t_n - \tau(t_n) \in \Delta \quad \forall\, t_n \in \Delta \end{gathered} \tag{2.24}$$

As example, if the *forward Euler method* is applied to (2.23) with variable step size, the corresponding discrete problem is

$$y_{n+1} = y_n + h_{n+1} f(t_n, y_n, y_q) \tag{2.25}$$

with $q < n$.

In order to derive a general code for the *method of steps*, some results on continuous ODE methods will be useful, and thus shown in the next section.

2.4.1 Continuous ODE methods

Consider the following IVP of ODEs

$$\begin{cases} \dot{y}(t) = g(t, y(t)) \quad t_0 \le t \le t_f \\ y(t_0) = y_0 \end{cases} \tag{2.26}$$

where $g(t, y) \in C^0([t_0, t_f] \times \mathbb{R}^d, \mathbb{R}^d)$ is continuous with respect to t and globally Lipschitz continuous with respect to y in a given norm $\|\cdot\|$ of $\mathbb{R}^d$, that is

$$\|g(t, y_1) - g(t, y_2)\| \le L \|y_1 - y_2\| \quad \forall t \in [t_0, t_f] \quad \text{and} \quad \forall y_1, y_2 \in \mathbb{R}^d, \tag{2.27}$$

for some Lipschitz constant $L > 0$.

Let $\Delta = \{t_0, t_1, \ldots, t_n, \ldots, t_N = t_f\}$ be a given mesh and $h_{n+1} = t_{n+1} - t_n$, with $n = 0, \ldots, N-1$, be the corresponding step sizes. Then a general *k-step method* (which includes both one-step and linear multistep methods) on Δ will have the following form

$$y_{n+1} = \alpha_{n,1} y_n + \ldots + \alpha_{n,k} y_{n-k+1} + h_{n+1} \Phi(y_n, \ldots, y_{n-k+1}; g, \Delta_n) \tag{2.28}$$

where $n \ge k-1$, $\Delta_n = \{t_{n-k+1}, \ldots, t_n, t_{n+1}\}$, and the *increment function* Φ is globally Lipschitz continuous with respect to $y_n, \ldots, y_{n-k+1}$ with the Lipschitz constant which depends only on the constant L in (2.27). The initial values $y_0, \ldots, y_{k-1}$ are given and the coefficients $\alpha_{n,i}$ are uniformly bounded with respect to n. Finally, the increment function Φ satisfies the following condition with respect to the argument g: there exist a step size $h_g > 0$ and a constant $\gamma_g > 0$, continuously dependent on L, but independent of the nodal values $y_n, \ldots y_{n-k+1}$ and of the mesh points Δ_n, such that, for all step sizes $h_{n-k+2}, \ldots, h_{n+1} \le h_g$,

$$\begin{aligned} &\|\Phi(y_n, \ldots, y_{n-k+1}; \tilde{g}, \Delta_n) - \Phi(y_n, \ldots, y_{n-k+1}; g, \Delta_n)\| \\ &\qquad \le \gamma_g \sup_{t_{n-k+1} \le t \le t_{n+1},\, y \in \mathbb{R}^d} \|\tilde{g}(t, y) - g(t, y)\| \end{aligned} \tag{2.29}$$

that is, Φ is continuous with respect to g with a sublinear growth with respect to the increment $\tilde{g} - g$.

Consider a continuous extension $\eta(t)$ of the method (2.28) on $[t_n, t_{n+1}]$ obtained by means of a *multistep interpolation* or a *one-step interpolation*. The following definition holds.

Definition 2.3. Continuous extension of an ODE method.

We call *continuous extension* or *interpolant* of the ODE method (2.28) the piecewise polynomial function $\eta(t)$ given by the restrictions on each interval

$[t_n, t_{n+1}]$ of any interpolant based on values computed in a possibly larger interval $[t_{n-i_n}, t_{n+j_n+1}]$, i_n, $j_n \geq 0$, of the form

$$\begin{aligned}\eta(t_n + \theta h_{n+1}) = \beta_{n,1}(\theta) y_{n+j_n} + \ldots + \beta_{n,j_n+i_n+1}(\theta) y_{n-i_n} \\ + h_{n+1} \Psi(y_{n+j_n}, \ldots, y_{n-i_n}; \theta, g, \Delta_n'), \quad 0 \leq \theta \leq 1\end{aligned} \tag{2.30}$$

where $\Delta_n' = \{t_{n-i_n}, \ldots, t_{n+j_n}, t_{n+j_n+1}\}$, satisfying the continuity conditions

$$\eta(t_n) = y_n \qquad \text{and} \qquad \eta(t_{n+1}) = y_{n+1}. \tag{2.31}$$

If $i_n = j_n = 0$, then the interpolation procedure is based on values belonging to the sole interval $[t_n, t_{n+1}]$ and is referred to as *one-step interpolation*. Otherwise, the interpolation procedure is called *multistep interpolation*.

In short, any ODE method (2.28) endowed with its continuous extension (2.30) will be called a *continuous ODE method*. □

Therefore, the continuous extension (2.30) will be computed simultaneously to the ODE solution if $j_n = 0$, or after the computation of the solution $y(t_{n+j_n+1})$ if $j_n > 0$. Moreover, it will satisfy continuity conditions in the sense of the conditions discussed for (2.28).

In order to discuss the convergence of the numerical method (2.28), consistency and zero-stability are required. Specifically, if the local truncation error of the numerical method is $o(1)$ as the time step h_n vanishes (consistency) and the global error has the same asymptotic behavior of the truncation error as $h_n \to 0$ (zero-stability), then the convergence of the ODE method will be guaranteed as $h_n \to 0$ (LeVeque, 2007 [126]). Conditions of consistency, zero-stability and therefore, convergence, will be now given.

Definition 2.4. Consistency of the ODE method.

We say the ODE method (2.28) is *consistent of order* p if $p \geq 1$ is the largest integer such that, for all C^p-continuous right-hand-side functions g in (2.26) and for all mesh points, we have that

$$\|z_{n+1}(t_{n+1}) - \tilde{y}_{n+1}\| = O\left(h_{n+1}^{p+1}\right) \tag{2.32}$$

uniformly with respect to y_n^* in any bounded subset of $\mathbb{R}^d$ and to $n = 0, \ldots, N-1$, where $z_{n+1}(t)$ is the local solution to the local problem

$$\begin{cases} \dot{z}_{n+1}(t) = g(t, z_{n+1}(t)) \quad t_n \leq t \leq t_{n+1} \\ z_{n+1}(t_n) = y_n^* \end{cases} \tag{2.33}$$

and

$$\begin{aligned}\tilde{y}_{n+1} = \alpha_{n,1} z_{n+1}(t_n) + \ldots + \alpha_{n,k} z_{n+1}(t_{n-k+1}) \\ + h_{n+1} \Phi(z_{n+1}(t_n), \ldots, z_{n+1}(t_{n-k+1}); g; \Delta_n).\end{aligned} \tag{2.34}$$

We say that the interpolant (2.30) of the ODE method (2.28) is *consistent of uniform order* q if $q \geq 1$ is the largest integer such that, for all C^q-continuous right-hand-side functions g and for all mesh points, we have that

$$\max_{t_n \leq t \leq t_{n+1}} \|z_{n+1}(t) - \tilde{\eta}(t)\| = O\left(h_{n+1}^{q+1}\right) \tag{2.35}$$

where

$$\begin{aligned}\tilde{\eta}(t_n + \theta h_{n+1}) = \beta_{n,1}(\theta) z_{n+1}(t_{n+j_n}) + \ldots + \beta_{n,j_n+i_n+1}(\theta) z_{n+1}(t_{n-i_n}) \\ + h_{n+1} \Psi(z_{n+1}(t_{n+j_n}), \ldots, z_{n+1}(t_{n-i_n}); \theta, g, \Delta'_n).\end{aligned} \tag{2.36}$$

Because of the continuity condition (2.31), it is clear that the uniform order q of the interpolant (2.30) and the order p of the method (2.28) satisfy the inequality

$$1 \leq q \leq p. \tag{2.37}$$

□

Theorem 2.3. Convergence of the ODE method.

Let the ODE method (2.28) be consistent of order $p \geq 1$ and, for each n, let

$$C_n = \begin{pmatrix} \alpha_{n,1} & \alpha_{n,2} & \ldots & \alpha_{n,k-1} & \alpha_{n,k} \\ 1 & 0 & \ldots & 0 & 0 \\ 0 & 1 & \ldots & 0 & 0 \\ \vdots & \vdots & & \vdots & \vdots \\ 0 & 0 & \ldots & 1 & 0 \end{pmatrix} \tag{2.38}$$

be the companion matrix of the polynomial

$$p_n(\lambda) = \lambda^k - \sum_{i=1}^{k} \alpha_{n,i} \lambda^{k-i}. \tag{2.39}$$

If

- there exists a norm $\|\cdot\|_*$ on $\mathbb{R}^k$, independent of both n and Δ, such that, for the corresponding induced matrix norm, the *zero-stability* condition

$$\|C_n\|_* \leq 1 \tag{2.40}$$

  holds;

- the right-hand-side function $g(t, y)$ in (2.26) is C^p-continuous;

- the set of starting values $y_0, \ldots, y_{k-1}$ approximate the exact solution to the order p;

then the ODE method (2.28) is convergent of global order p on any bounded interval $[t_0, t_f]$, that is

$$\max_{1\leq n\leq N} \|y(t_n) - y_n\| = O(h^p) \tag{2.41}$$

where $h = \max_{1\leq n\leq N} h_n$.

Moreover, if the interpolant (2.30) is consistent of uniform order q, then the continuous ODE method (2.28)-(2.30) is uniformly convergent of global order $q' = \min\{p, q+1\}$, that is

$$\max_{t_0\leq t\leq t_f} \|y(t) - \eta(t)\| = O(h^{q'}). \tag{2.42}$$

□

Remark 2.1. If the ODE method (2.28) is implemented with constant step size h, then the coefficients $\alpha_{n,i}$ are independent of the mesh Δ and, hence, all the polynomials $p_n(\lambda)$ (2.39) are equal to the same polynomial $p(\lambda)$ and their companion matrices C_n (2.38) are equal to the same matrix C. It is well known (LeVeque, 2007 [126]) that, in this case, the zero-stability condition (2.40) is equivalent to the following root condition

$$p(\lambda) = 0 \qquad \Rightarrow \qquad \{|\lambda| \leq 1 \; with \, \lambda \, simple \; if \;\; |\lambda| = 1\}. \tag{2.43}$$

□

The zero-stability of a consistent numerical method ensures its stability and convergence. Rather, at each iterative step the global error is bounded in terms of the local truncation error, which can be involved to evaluate the time step to be used. However, the zero-stability does not guarantee that the numerical method will compute a reasonable solution of the equation to be solved on the mesh chosen. In particular, time steps are required as large as possible consistent with accuracy restrictions in order to reduce the time of numeric integration. For this reason another form of stability has to be considered in order to establish if the global error is well behaved with the time step used. The *absolute stability* (Lambert, 1993 [124]) is sometimes involved and the eigenvalues λ_i of the Jacobian matrix of the numeric method might be considered to evaluate it. Specifically, the ODE method (2.28) is said to have *region of absolute stability* $\mathscr{R}_A$, where $\mathscr{R}_A$ is a region of the complex z-plane and $z = h\lambda_i$ for a given time step h at n^{th} iterative step, if it is *absolutely stable* for all $z \in \mathscr{R}_A$, that is the global error is bounded for the given h. Refer to Lambert (1993) [124] and LeVeque (2007) [126] for more details about zero-stability and absolute stability, while the following example will clarify this topic.

Example 2.4. Consider the test model problem

$$\begin{cases} \dot{y}(t) = \lambda y(t) \quad t > 0 \\ y(0) = 0 \end{cases} \tag{2.44}$$

and apply the forward Euler method (2.25) with constant step size h (and without delayed terms, that is, $y_q = 0 \; \forall q < n$) to solve (2.44), which becomes

$$y_{n+1} = y_n + h\lambda y_n \tag{2.45}$$

with y_0 the initial guess. For an one-step method with constant step size, (2.38) is the scalar value $\alpha_{n,1}$, and for the method (2.45) $\alpha_{n,1} = 1 \; \forall n$. Therefore (2.40), that is also (2.43), is fulfilled and the Euler method is zero-stable. In order to investigate the absolute stability, the behavior of (2.45) will be evaluated as $t \to \infty$ fixed h. Consider that

$$y_{n+1} = y_n + h\lambda y_n = (1 + h\lambda)^{n+1} y_0. \tag{2.46}$$

Then, since the solution of (2.44) is the function $y(t) = e^{\lambda t}$ (which vanishes as $t \to \infty$ only if $\lambda < 0$), the Euler method is absolutely stable if $|1 + h\lambda| \leq 1$, and the its region of absolute stability is defined as follows

$$\mathscr{R}_A = \{z \equiv h\lambda \in \mathbb{C} : -2 \leq z \leq 0\}. \tag{2.47}$$

This is represented by the complex disk of radius 1 and centered at the point -1, see Figure 2.4a (observe also the region of absolute stability of other numerical methods in Figure 2.4b-c-d). □

2.4.2 An Algorithm for the *method of steps*

According to the main results pointed out in the previous sections and this section about continuous ODE methods, the ODE method (2.28) may be employed in order to solve DDEs. In particular, given the IVP of time dependent DDEs (2.23), let us choose the mesh (2.24) including the principal discontinuities $\xi_0 = t_0 < \xi_1 < \ldots < \xi_s < \xi_{s+1} = t_f$, and assume the hypothesis (2.19) and step size $h_{n+1} = t_{n+1} - t_n \leq \tau_0$. A step size greater than τ_0 would generate overlapping between sub-intervals of integration, and this event is here avoided. Then, the method (2.28)-(2.31) generates the approximation y_n at time t_n of the solution $y(t)$ step by step by means of solving the following sequence of ODEs

$$\begin{cases} \dot{z}(t) = f(t, z(t), x(t - \tau(t))) \quad \xi_i \leq t \leq \xi_{i+1} \\ z(\xi_i) = x(\xi_i) \end{cases} \tag{2.48}$$

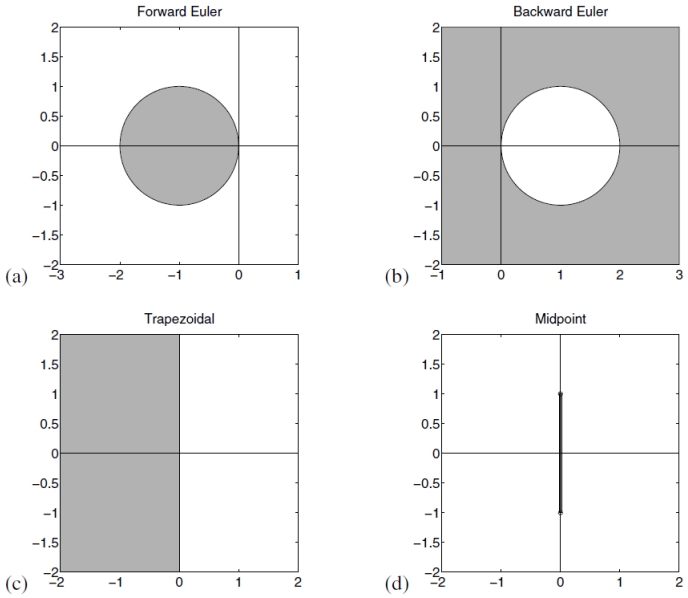

Figure 2.4: Absolute stability region (pointed out by shaded space) for (a) forward Euler, (b) backward Euler, (c) trapezoidal, (d) midpoint method (LeVeque, 2007 [126]).

with

$$x(u) = \begin{cases} \phi(u), & u \leq t_0 \\ \eta(u), & t_0 \leq u \leq t_f \end{cases} \tag{2.49}$$

and $\eta(t)$ the continuous extension (2.30).

Summing up, the *method of steps* is described by the following pseudo-code.

Algorithm (*method of steps*)

1. Locate all the principal discontinuity points and the discontinuity points of order $\leq p$, namely, $\xi_1, \ldots, \xi_s (< t_f)$, and set $\xi_0 = t_0$, $\xi_{s+1} = t_f$.

2. Solve the equation

$$\begin{cases} \dot{z}(t) = f(t, z(t), \phi(t - \tau(t))) & \xi_0 \leq t \leq \xi_1 \\ z(\xi_0) = \phi(\xi_0) \end{cases}$$

   by any discrete ODE method.

3. For $i = 1$ to s:

- compute and store the continuous extension $\eta(t)$ for $t \in [\xi_{i-1}, \xi_i]$ by interpolating data from the same interval $[\xi_{i-1}, \xi_i]$ only;
- solve the equation

$$\begin{cases} \dot{z}(t) = f(t, z(t), \eta(t - \tau(t))) & \xi_i \leq t \leq \xi_{i+1} \\ z(\xi_i) = \eta(\xi_i) \end{cases}$$

by the discrete ODE method.

4. Plot the approximate solution $\eta(t)$ in $[\xi_0, \xi_{s+1}]$.
5. End.

The convergence of the *method of steps* is given by the following theorem (for the proof refer to Bellen and Zennaro, 2003 [10]).

Theorem 2.4. Convergence of the *method of steps*.
Consider the delay differential equations (2.18) where $f(t, y, x)$ is C^p-continuous in $[t_0, t_f] \times \mathbb{R}^d \times \mathbb{R}^d$, the delay $\tau(t)$ is C^p-continuous in $[t_0, t_f]$ and fulfills hypothesis $\tau(t) \geq \tau_0$, and the initial function $\phi(t)$ is C^p-continuous. Moreover, assume that:

- the mesh $\Delta = \{t_0, t_1, \ldots, t_n, \ldots, t_N = t_f\}$ includes all the principal discontinuity points and the discontinuity points of order $\leq p$ lying in $[t_0, t_f]$, denoted by $\xi_1, \ldots, \xi_s (< t_f)$;
- the discrete ODE method is consistent of order p, is zero-stable (see section 2.4.1) and, for $k > 1$, is restarted after each discontinuity point ξ_i, $i = 0, 1, \ldots, s$, by a method of order $\geq p - 1$;
- the continuous extension $\eta(t)$ of the method is consistent of uniform order q;
- for each n, the interval $[t_{n-i_n}, t_{n+j_n+1}]$ where the interpolation takes place is included in $[\xi_i, \xi_{i+1}]$ for some index $0 \leq i \leq s$.

Then the resulting *method of steps* has discrete global order and uniform global order $q' = \min\{p, q + 1\}$; that is

$$\max_{1 \leq n \leq N} \|y(t_n) - y_n\| = O(h^{q'})$$

and

$$\max_{t_0 \leq t \leq t_f} \|y(t) - \eta(t)\| = O(h^{q'})$$

where $h = \max_{1 \leq n \leq N} h_n$. □

In Chapter 5 it will be discussed that the constant delayed physical model of section 1.5.4 (in Chapter 1) does not manifest discontinuity points if suitable conditions on the stimulus function are fulfilled. Therefore, the localization of discontinuities will not be included in the algorithm implemented here.

Chapter 3

Numerical solution of time-dependent PDEs

As in Elliott et al. (2007) [61], Moleti et al. (2009) [135] and Sisto et al. (2010) [180], a representation of the cochlear models, described in section 1.5 of Chapter 1, in the *State Space* may be considered, based on the spatial discretization of the equations by means of the method of lines (MOL - section 3.1). In this way, the continuous PDE model (1.4)-(1.6), described in Chapter 1, may be converted into a sequence of N Initial Value Problems (IVPs) of Ordinary Differential Equations (ODEs) for the *anti-damping model*, or constant Delay Differential Equations (DDEs) for the *delayed stiffness model* (the two cochlear models have been respectively described in section 1.5.3 and section 1.5.4 of Chapter 1). Such a sequence of IVPs will be discrete in space and continuous in time, and may be numerically integrated in time. The IVPs are stiff (phenomenon which will be described in section 3.2) with a non trivial mass matrix (as will be shown in Chapter 4). This is why, on this ground, we use a time integrator based on the Matlab `ode15s` package (section 3.3). In particular, a faster time-step integration technique has been employed for the anti-damping model in Sisto et al. (2010) [180] or Moleti et al. (2013) [132], as highlighted by Bertaccini and Sisto (2011) [20]. Specifically, a customized `ode15s` package has been developed as a hybrid direct-iterative solver which exploits Krylov subspace methods. This technique might be also effective for the delayed stiffness model. In particular, a step by step integration method for DDEs will be proposed and discussed in Chapter 4. Shampine and Thompson (2001) [168] wrote a code, *dd23*, to solve constant DDEs in Matlab. However, this code seems to be not appropriate in our framework because of stiffness of the DDE model. For this reason an approach based on the customized `ode15s` (see section 3.3.2) package may be involved in order to numerically integrate the considered stiff constant DDE model in Matlab.

Therefore, this chapter will discuss all the main tools which will be involved in order to develop the semidiscrete formulation and, then, yield a numerical approximate solution of the cochlear models analyzed in Chapter 4 and Chapter 5.

3.1 Semidiscretization in space

The numerical solution of differential equations depending on spatial variables may be studied discretizing the continuous equation. The *finite difference method* (LeVeque, 2007 [126]; Bertaccini, 2011 [13]) replaces the spatial derivatives with corresponding finite difference approximations. In particular, if $u(x)$ is the continuous solution of the differential equation, the first derivative $u_x(\bar{x})$ may be approximated at point $\bar{x}$ by the *one-sided approximations*

$$D_+u(\bar{x}) \equiv \frac{u(\bar{x}+\Delta x)-u(\bar{x})}{\Delta x} \tag{3.1}$$

or

$$D_-u(\bar{x}) \equiv \frac{u(\bar{x})-u(\bar{x}-\Delta x)}{\Delta x} \tag{3.2}$$

where Δx is the mesh spacing on the x-axis. The (3.1) evaluates the approximation of $u_x(\bar{x})$ only at values of $x \geq \bar{x}$, while (3.2) only at values of $x \leq \bar{x}$. Both approximations are *first order accurate*, that is the truncation error in the approximation $u_x(\bar{x}) \approx D_\pm u(\bar{x})$ is proportional to Δx. This is estimated if $u(\bar{x}+\Delta x)$ and $u(\bar{x}-\Delta x)$ are evaluated by Taylor Series expansions about the point $\bar{x}$

$$u(\bar{x}+\Delta x) = u(\bar{x}) + (\Delta x)u_x(\bar{x}) + \frac{1}{2}(\Delta x)^2 u_{xx}(\bar{x}) + \frac{1}{6}(\Delta x)^3 u_{xxx}(\bar{x}) + O((\Delta x)^4) \tag{3.3}$$

$$u(\bar{x}-\Delta x) = u(\bar{x}) - (\Delta x)u_x(\bar{x}) + \frac{1}{2}(\Delta x)^2 u_{xx}(\bar{x}) - \frac{1}{6}(\Delta x)^3 u_{xxx}(\bar{x}) + O((\Delta x)^4) \tag{3.4}$$

which give the following truncation errors

$$D_+u(\bar{x}) - u_x(\bar{x}) = \frac{1}{2}(\Delta x)u_{xx}(\bar{x}) + \frac{1}{6}(\Delta x)^2 u_{xxx}(\bar{x}) + O((\Delta x)^3) \tag{3.5}$$

$$D_-u(\bar{x}) - u_x(\bar{x}) = -\frac{1}{2}(\Delta x)u_{xx}(\bar{x}) + \frac{1}{6}(\Delta x)^2 u_{xxx}(\bar{x}) + O((\Delta x)^3). \tag{3.6}$$

For sufficiently small Δx, the errors (3.5)-(3.6) are dominated by the first term $\frac{1}{2}(\Delta x)u_{xx}(\bar{x})$, which will behave like a constant times Δx (note that $u_{xx}(\bar{x})$, $u_{xxx}(\bar{x})$, etc., are constant values fixed by $\bar{x}$).

The average of the one-sided approximations gives the following *centered approximation*

$$D_0 u(\bar{x}) \equiv \frac{u(\bar{x}+\Delta x) - u(\bar{x}-\Delta x)}{2\,\Delta x} \tag{3.7}$$

which is a *second order accurate* approximation, that is the error is proportional to $(\Delta x)^2$ and, thus, smaller than the error of one-sided approximations. Namely, by substituting (3.3)-(3.4) in (3.7), the truncation error is

$$D_0 u(\bar{x}) - u_x(\bar{x}) = \frac{1}{6}(\Delta x)^2 u_{xxx}(\bar{x}) + O((\Delta x)^4). \tag{3.8}$$

and dominated by the first term $\frac{1}{6}(\Delta x)^2 u_{xxx}(\bar{x})$, which will behave like a constant times $(\Delta x)^2$.

Analogously, the second derivative $u_{xx}(x)$ may be approximated at point $\bar{x}$ by the *second order centered* approximation

$$\begin{aligned} D^2 u(\bar{x}) &= \frac{1}{(\Delta x)^2}[u(\bar{x}-\Delta x) - 2u(\bar{x}) + u(\bar{x}+\Delta x)] = \\ &= u_{xx}(\bar{x}) + \frac{1}{12}(\Delta x)^2 u_{xxxx}(\bar{x}) + O((\Delta x)^4) \end{aligned} \tag{3.9}$$

In order to integrate time-dependent partial differential equations (PDEs) numerically, the discretization of partial derivatives with respect to the spatial variable may be performed separately from the partial derivatives with respect to the time variable. This approach is called *Method of Lines* (MOL) (LeVeque, 2007 [126]).

Consider a time dependent PDE with $u(x,t)$ continuous solution, which is a function of the spatial variable x and the temporal variable t. The spatial derivative may be discretized by the finite difference method, carrying out the following approximation

$$u(x_i, t) \approx U_i(t) \tag{3.10}$$

where $U_i(t)$ is the numerical approximation function at the grid points $x_i = i\Delta x$. In this way, the time dependent PDE is turned into a system of coupled ordinary differential equations (ODEs), discrete in space and continuous in time. At every grid point x_i the variable $U_i(t)$ varies continuously in time, like along a time-line (see Fig.3.1). Namely, in the (x,t) domain the couples (x_i, t) represent a line along which the approximate solutions of the PDE will be analyzed. Then, the system of ODEs can be temporally integrated by a suitable software package for ODEs.

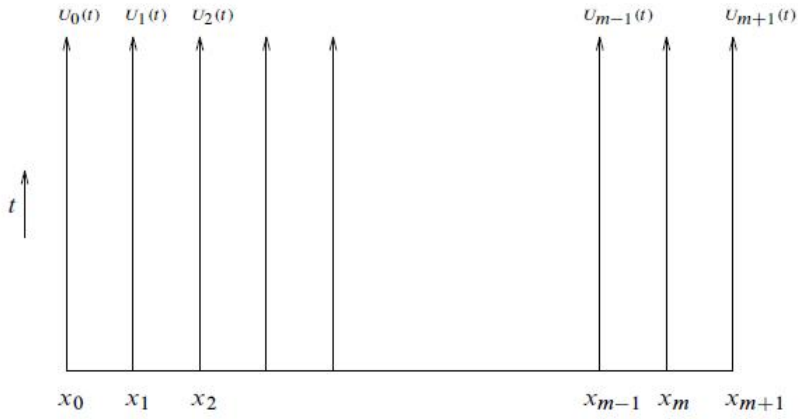

Figure 3.1: Graphical representation of the method of lines (MOL) (LeVeque, 2007 [126]).

3.2 Stiff problems

Consider the linear constant coefficient inhomogeneous system

$$\dot{y}(t) = Ay(t) + \varphi(t) \tag{3.11}$$

with $A \in \mathbb{R}^{d\times d}$ the Jacobian matrix, $\varphi(t) \in \mathbb{R}^d$ and t the time variable. If A has d distinct eigenvalues $\lambda_j \in \mathbb{C}$, with $\{v_j\}_{j=1,\dots,d}$ the corresponding eigenvectors, the solution $y(t)$ of (3.11) may be written as follows (Lambert, 1993 [124]):

$$y(t) = \sum_{j=1}^{d} C_j e^{\lambda_j t} v_j + \psi(t) = y_{hom} + \psi(t) \tag{3.12}$$

where C_j are constant and $\psi(t)$ is a particular integral.

If $\Re(\lambda_j) < 0 \; \forall j = 1, \dots d$, then the solution $y(t)$ approaches the particular integral $\psi(t)$ asympotically as $t \to \infty$ because the term y_{hom} vanishes as $t \to \infty$. In particular, y_{hom} will decay monotonically if λ_j is real or oscillating if λ_j is complex.

Therefore, t being a time variable, y_{hom} may be considered as the *transient solution* and $\psi(t)$ as the *steady-state solution* for $t \to \infty$. In particular, y_{hom} will be a *fast transient* for large $|\Re(\lambda_j)|$ and a *slow transient* for small $|\Re(\lambda_j)|$. Let $\lambda_f, \lambda_s \in \{\lambda_j, j = 1, \dots, d\}$ be the eigenvalues corresponding to the fast and slow decay of y_{hom}, respectively, and defined as follows

$$|\Re(\lambda_s)| \leq |\Re(\lambda_j)| \leq |\Re(\lambda_f)| \tag{3.13}$$

If the steady-state solution is the required solution, then the time integration of (3.11) advances until the slowest transient is negligible. Namely, the smaller $|\Re(\lambda_s)|$, or rather $|\Re(\lambda_f)|$, is, the longer time integration is. Moreover, if the employed numerical method has a finite region of absolute stability $\mathscr{R}_A$, then the time step h has to be sufficiently small in order to fulfill the stability condition $h\lambda_j \in \mathscr{R}_A$ (see section 2.4.1 in Chapter 2). As a result, very large $|\Re(\lambda_f)|$ and very small $|\Re(\lambda_s)|$ introduce difficulties in advancing in time because excessively small step sizes have to be involved, taking a long time of integration. This phenomenon is called *stiffness* of the system to be solved, and a precise mathematical definition cannot be formulated. Since the stiffness arises when $|\Re(\lambda_f)|$ is very large and $|\Re(\lambda_s)|$ is very small, it is convenient to evaluate the ratio $r_{stiff} = |\Re(\lambda_f)| \,/\, |\Re(\lambda_s)|$. The latter is the *stiffness ratio*, which gives a measure of the stiffness of the system. In particular, a linear constant coefficient system is stiff if its eigenvalues have negative real part and the stiffness ratio is large ($r_{stiff} \gg 1$).

However, stiff systems might have stiffness ratio of 1, as in the case of a unique eigenvalue. On the other side, systems with large stiffness ratio are not necessarily stiff, as for eigenvalues close to the imaginary axis which give oscillatory and not damped solutions. In the latter case, small time steps would be required for accuracy reasons, so that stability tolerance may be of accuracy order.

Quote the description of LeVeque (2007) [126] about the phenomenon of stiffness.

> In general a problem is called *stiff* if, roughly speaking, we are attempting to compute a particular solution that is smooth and slowly varying (relative to the time interval of the computation), but in a context where the nearby solution curves are much more rapidly varying. In other word, if we perturb the solution slightly at any time, the resulting solution curve through the perturbed data has rapid variation. Typically this takes the form a short-lived *transient* response that moves the solution back toward a smooth solution (LeVeque, 2007 [126]).

Example 3.1. Consider the following scalar ODE

$$\dot{u}(t) = \lambda(u - \cos t) - \sin t \tag{3.14}$$

where λ is a scalar parameter.

If the initial data is $u(0) = 1$, the solution of (3.14) is the function $u(t) = \cos t$ for any λ.

Contrary, if the initial data has the general form $u(t_0) = \eta$ that does not lie on the curve $u(t) = \cos t$, the solution of (3.14) changes. However, if $\Re(\lambda) < 0$ the solution of (3.14) is the function

$$u(t) = e^{\lambda(t-t_0)}(\eta - \cos(t_0)) + \cos t \tag{3.15}$$

which approaches the steady-state solution, $\cos t$, exponentially quickly with decay rate λ. In particular, if λ increases on the negative axis, then the time scale of the transient component of (3.15) is much smaller than the time scale of the steady-state component. In this example the stiffness of (3.14) seems to be advantageous. This is because a greater λ yields a quicker relaxation of (3.15) towards the solution of (3.14) with the non-perturbed initial data $u(0) = 1$. Note the solution curves of (3.14) for different t_0 and η and for $\lambda = -1$ and $\lambda = -10$ in Figure 3.1. With respect to the case $\lambda = -1$ (left panel), in the case $\lambda = -10$ the equation solution actually more quickly approaches the steady-state solution $\cos t$ (right panel). This is because, for a greater λ value, the stiffness of (3.14) increases. However, in general, in stiff problems, the value of the parameter λ might affect the behavior of the solution generating a different function. □

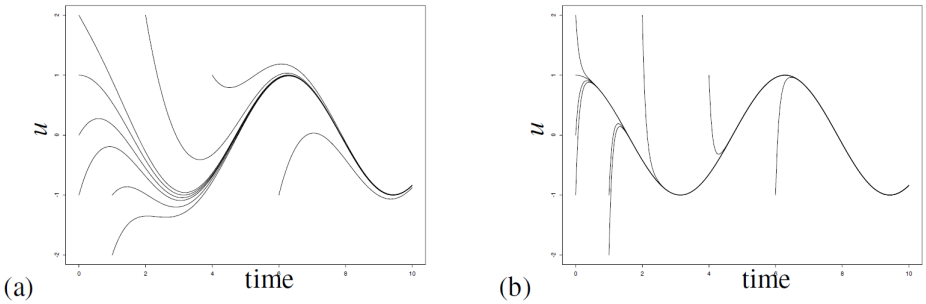

Figure 3.2: Solution curves of (3.14) for various initial values and $\lambda = -1$ (a) or $\lambda = -10$ (b). Reproduced from LeVeque (2007) [126].

When a differential equation is numerically integrated, an error is introduced, that is the numerical solution is perturbed with respect to the exact solution. Consequently, when the problem at hand is stiff, a rapid variation of the solution occurs through data with error. In Example 3.1, the solution $u(t) = \cos t$ of (3.14) with $u(0) = 1$ is almost insensitive to the numeric error. Actually, this solution is achieved although the initial data is perturbed, because any error introduced decays exponentially.

In the sense of absolute stability, many numerical methods are unstable unless the time step is small relative to the time scale of the transient. In a

stiff problem this time is smaller than the time scale of the smooth solution to be computed. In this case, a numerical method with a large region of absolute stability has to be involved, with the region extending far into the left half-plane. The stability regions of explicit methods are bounded, so they would not be suitable for stiff problems because they do not guarantee the numerical absolute stability. Instead, implicit methods might be more appropriate. In particular, numerical methods which have the entire half-plane in their region of absolute stability would represent the optimal choice. In this sense, the following definitions hold (LeVeque, 2007 [126]; Bertaccini, 2011 [13]).

Definition 3.1. An ODE method is said to be *A-stable* if its region of absolute stability $\mathscr{R}_A$ contains the entire left half-plane $\{z \in \mathbb{C} : \Re(z) \leq 0\}$.

Moreover, let $arg(z)$ be the argument of z with $arg(z) = \pi$ on the negative real axis. Then the ODE method is said to be *A(α)-stable* if the wedge $\pi - \alpha \leq arg(z) \leq \pi + \alpha$ is contained in the stability region □

Note that a A-stable method is A($\pi/2$)-stable, while a A(0)-stable method has the negative real axis in the absolute stability region.

Consider the test equation (2.44) of Chapter 2, $\dot{y}(t) = \lambda y(t)$, for which one-step methods give

$$y_{n+1} = R(z)y_n \tag{3.16}$$

where $R(z)$ is a function of $z = k\lambda$ and is called *stability function*. That is because, in terms of $R(z)$, the region of absolute stability can be so defined

$$\mathscr{R}_A = \{z \in \mathbb{C} : |R(z)| \leq 1\} \tag{3.17}$$

Then the following definition holds.

Definition 3.2. An ODE method is said to be L-stable if it is A-stable and $\lim_{z\to\infty} |R(z)| = 0$. □

The L-stability is useful when the equation to be solved has a very fast transient which we want to damp in a single time step because we are not interested in solving it with very small step size. In this case stability region in the right half-plane will improve the stability of the numerical method which approximates the solution.

In the next section, a potentially effective family of schemes for stiff problems will be briefly recalled. In particular, we will focus on the BDF (Backward Differential Formula) methods, which are implemented in a Matlab solver package.

3.3 Some Matlab ODE integrator packages

An IVP of ODEs discretized in space to be solved in time, is formally expressed as follows

$$\begin{cases} \dot{y} = F(t, y) \quad t_0 \leq t \leq t_f \\ y(t_0) = y_0 \end{cases} \tag{3.18}$$

or, if the mass matrix $M(t, y)$ is non-trivial (non-singular and, usually, sparse),

$$\begin{cases} M(t, y)\dot{y} = f(t, y) \quad t_0 \leq t \leq t_f \\ y(t_0) = y_0. \end{cases} \tag{3.19}$$

In order to integrate numerically various IVPs of ODEs, Matlab ODE Suite (Shampine and Reichelt, 1997 [167]) offers a widely used environment for scientific computing. In particular, stiff problems with mass matrix depending on time (as in the physical problem at hand, see section 4.2 in Chapter 4), can be handled by the `ode15s` package.

3.3.1 `ode15s`: Stiff Problems

The `ode15s` package is a variable step size and order code in backward differences of the Klopfeinstein-Shampine family of *Numerical Differentiation Formulas* (NDFs; Klopfenstein, 1971 [115]; Reiher, 1978 [148]; Shampine and Reichelt, 1997 [167]). The latter are similar to the *Backward Differentiation Formulas* (BDFs), which largely solve stiff problems.

If constant step size $h = t_{n+1} - t_n$ and backward differences are considered, a BDF of order k, carrying out the approximation y_{n+1} of solution, has the following expression (Shampine and Reichelt, 1997 [167])

$$\sum_{m=1}^{k} \frac{1}{m} \nabla^m y_{n+1} - hF(t_{n+1}, y_{n+1}) = 0. \tag{3.20}$$

The (3.20) is an implicit formula generally solved by a Newton method with the following initial guess

$$y_{n+1}^{(0)} = \sum_{m=0}^{k} \nabla^m y_n. \tag{3.21}$$

The leading term in the truncation error of a BDF of order k is

$$\frac{1}{(k+1)} \left[h^{k+1} y^{(k+1)} \right] \approx \frac{1}{k+1} \nabla^{k+1} y_{n+1}. \tag{3.22}$$

BDF codes vary both the step size and the order of the formula, but while the first and the second order of BDFs are A-stable and L-stable (see Figure 3.3), BDFs of greater order than 6 are not even zero-stable.

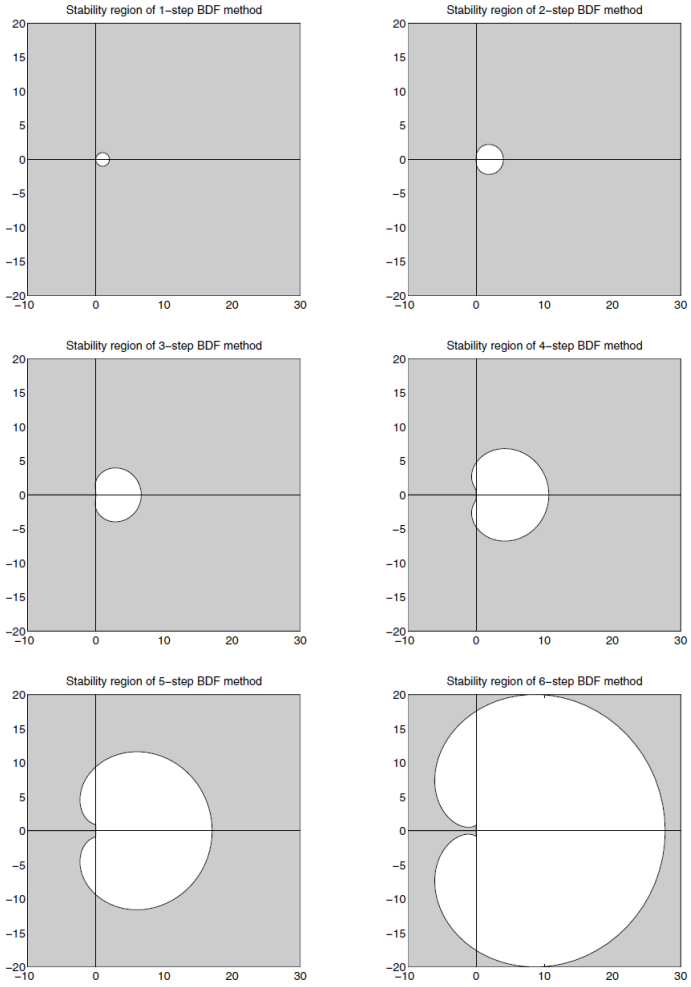

Figure 3.3: Region of absolute stability (pointed out by shaded space) of BDFs (LeVeque, 2007 [126]).

In order to improve the computation efficiency of BDFs, NDFs have been considered, where the dependence of the initial condition (3.21) on past values of y_n is exploited and inserted in (3.20), that is

$$\sum_{m=1}^{k} \frac{1}{m} \nabla^m y_{n+1} - hF(t_{n+1}, y_{n+1}) - \kappa\gamma_k(y_{n+1} - y_{n+1}^{(0)}) = 0. \tag{3.23}$$

The (3.23) expresses a general NDF, where κ is a scalar parameter and $\gamma_k = \sum_{j=1}^{k} 1/j$ are coefficients. For $\kappa = 0$, the NDF (3.23) reduces to the BDF (3.20).

The leading term in the truncation error for the NDF (3.23) has the following form

$$\left(\kappa\gamma_k + \frac{1}{k+1}\right) h^{k+1} y^{(k+1)} \tag{3.24}$$

During the implementation of NDFs or BDFs, the code chooses the largest step size such that the truncation error is less than or equal to a given tolerance. For the same order k and with suitable κ (in particular, negative values), the NDF truncation error (3.24) is less than the BDF one (3.22) (Shampine and Reichelt, 1997 [167]). Consequently, grater step sizes may be employed with NDFs (that is, the efficiency of the method is improved) achieving the same accuracy as BDFs and advancing in time in fewer steps. However, while NDFs stability is the same for BDFs at order 1 and 2, it decreases from order 3 up, particularly for k=5 (see Table in Figure 3.4 reported from Shampine and Reichelt (1997) [167]). For this reason, at order 5 NDF has been set as BDF [167].

order	NDF coeff	step ratio	stability angle		percent
k	κ	percent	BDF	NDF	change
1	-0.1850	26%	90°	90°	0%
2	-1/9	26%	90°	90°	0%
3	-0.0823	26%	86°	80°	-7%
4	-0.0415	12%	73°	66°	-10%
5	0	0%	51°	51°	0%

Figure 3.4: Efficiency (measured in percentage increase in step size) and A(α)-stability (measured in percentage increase in α) of NDFs with respect to BDFs (Shampine and Reichelt, 1997 [167]).

NDFs of order 5 are set as default in `ode15s` package, but the user can choose the maximum order and BDFs to be used to compute the solution according to stability evaluations.

NDFs would solve the general stiff problem (3.19) in the equivalent form

$$\dot{y} = F(t, y) = M^{-1}(t, y) f(t, y). \tag{3.25}$$

This procedure is not convenient because of the non-constant structure of M. For this reasons the equivalent system (3.25) is avoided by considering $M(t_n)$ as an approximation of $M(t_{n+1})$ at current time step t_{n+1}.

The Matalb `ode15s` syntax for a sequence of IVPs, in the form (3.19), is the following

```
[tout, yout] = ode15s(f(t,y),tspan,y0,options)        (3.26)
```

where `f(t,y)` evaluates the right-hand of the equation in (3.19), `tspan` is a vector which specifies the interval of integration $[t_0, t_f]$, `y0` is the vector of initial conditions; the structure `options` is built by `odeset` function and changes the default integration properties (for example, Jacobian or mass matrix properties); `yout` is the matrix in which each row is the solution at the time in the corresponding row of the time vector `tout`. The solver `ode15s` imposes the initial condition `y0` at `tspan(1)` and integrates from `tspan(1)` to `tspan(end)`[1]. If the solution is requested at specific time points $[t_0, t_1, \ldots, t_f]$, then you can set `tspan=[t0,t1,...,tf]`.

For a complete description of the Matlab Ode Suite, refer to Shampine and Reichelt (1997) [167]. Moreover, look up also the `Help` function of Matlab for a quick and detailed overview about `ode15s` package.

Some solver properties can be set by means of the `odeset` function. The general Matlab syntax for `odeset` is the following

```
options = odeset('name1',value1,'name2',value2,...)        (3.27)
```

where the named integration properties `'name1'`, `'name2'`, ... take the corresponding specified values `value1`, `value2`, ..., instead of default values. Specifically, for the use of the solver `ode15s` employed in this thesis, it is useful to discuss the following categories of properties (as one can also find in the `Help` function of Matlab).

Error Control Properties. For every i-th component y_i of the solution, the error control fulfills the following mixed relative and absolute error (e_r and e_{a_i}, respectively) test on maximum norm estimating the local error e_i, that is

$$|e_i| \leq e_r \, |y_i| + e_{a_i}. \tag{3.28}$$

The condition (3.28) is yielded by the solver by means of the following control

$$|e_i| \leq max(\texttt{RelTol} * abs(y_i), \texttt{AbsTol(i)}), \tag{3.29}$$

that is, the local error e_i must be less than or equal to the max-function of the relative tolerance, `RelTol`, and the absolute tolerance, `AbsTol`. The scalar

[1] A Matlab row or column vector has the first element identified by the index `1` and the last element by the indexing function `end`.

tolerance `RelTol` represents a measure of the error relative to the size of each solution component y_i, because it controls the number of correct digits in all solution components, except those smaller than thresholds `AbsTol(i)`. `RelTol` has a default value of 10^{-3}, thus corresponds to 0.1% accuracy. On the other hand, the absolute error tollerance `AbsTol(i)` is a threshold below which the value of the i-th solution component y_i is unimportant. Therefore `AbsTol` is a vector which determines the accuracy when the solution approaches zero. It is 10^{-6} for all solution components, by default. The values of `RelTol` and `AbsTol(i)` can be modified in `options` according to the scale of the equation to be solved.

Jacobian Matrix Properties. The stiff ODE solvers often execute faster if additional information about the Jacobian matrix $\partial f/\partial y$ is provided. The Jacobian matrix is the matrix of partial derivatives of the function $f(t, y)$ in (3.19), and represents a critical issue to reliability and efficiency of stiff problems. It is approximated numerically using finite differences if any Jacobian function is not provided to calculate it.

Mass Matrix Properties. For a large sparse mass matrix $M(t, y)$ of the problem (3.19), solving the equation $M(t, y)\dot{y} = f(t, y)$ directly reduces the storage and run-time needed to solve the problem. By means of the `odeset` function, the mass matrix, or the function which evaluates it, can be provided. Moreover, the property `MStateDependence` allows to set `weak` or `strong` in order to specify the dependece of $M(t, y)$ on y.

`ode15s`-*Specific Properties.* As above discussed, `ode15s` is a variable-order solver for stiff problems, and uses NDFs by default. If the property `BDF` is set `on`, then BDFs are employed. Moreover, by the property `MaxOrder`, the maximum order formula (from 1 to 5) can be set. This is useful for some stiff problems that are solved more efficiently if `MaxOrder` is reduced, so that only the most stable formulas are used.

The cochlear models shown in section 1.5 of Chapter 1 have been analyzed by yielding the numerical approximate solution in Matlab environment. In particular, the solver `ode15s` of Matlab has been involved to integrate numerically the stiff problems at hand. However, a customized routine `ode15s` might allow to take some computational advantages, as will be shortly described in the next section, and specifically analyzed with the matrix formulation of the cochlear models considered in Chapter 4.

3.3.2 Customized `ode15s`

The cochlear model studied in this dissertation (the delayed stiffness model) is represented by a PDE model based on a constant DDE. It will be compared with a PDE model based on an ODE (the anti-damping model). The continuous representation of such models has been described in Chapter 1, while Chapter 4 will show the models discretized in space. Both problems describe the same physical phenomenon by means of two different formulations. Moreover, both problems are stiff. While the ODE model has been solved in Matlab by Moleti et al., 2009 [135], and Bertaccini and Sisto, 2011 [20], the DDE model of Talmadge et al. (1998) [189] will be numerically integrated in this dissertation in the time domain.

Since `ode15s` is a variable-step, variable-order implicit solver with an infinite region of absolute stability, it can efficiently solve stiff ODEs which have a Jacobian matrix with negative real eigenvalues and need very small and adaptive time step size, in order to guarantee the numerical stability (as for the problem at hand; see Chapter 4 and Moleti et al., 2009 [135]). When implicit methods are involved, each time step builds a system of nonlinear algebraic equations, whose size is determined by the number N of spatial mesh points. In cochlea modeling, N represents the number of OHCs which is intrinsically finite and very large. For this reason, in order to adopt a realistic cochlear model, high N should be employed (at least 500).

Bertaccini and Sisto (2011) [20] propose a modification of Matlab `ode15s` package involving Krylov space projection iterative methods for the solution of large and sparse linearized systems, building at each step of the time integration, instead of sparse direct solvers built in `ode15s` (Bertaccini and Calvetti, 2007 [15]; Bertaccini and Fanelli, 2009 [17]). This technique results faster by reducing the computational complexity in the case of differential equations with multiple banded Jacobian matrix, as in the physical models considered in this thesis. Moreover, projection methods may converge faster if Jacobian matrix is clustered in one half of the complex plane (Bertaccini and Ng, 2003 [19]). Here this approach will be applied by involving GMRES (Generalized Minimum Residual) method as Krylov space projection iterative method built in `ode15s`.

Chapter 4 will discuss in detail the advantages of a customized `ode15s` for the problem at hand. Before this, it will be useful to recall the main properties of Krylov subspace methods, and, in particular, the GMRES method, with reference to Bertaccini, 2011 [14]. Further details can be found in Saad, 1995 [159].

Projection methods

Consider the following linear system

$$Ax = b \tag{3.30}$$

with $A \in \mathbb{R}^{n\times n}$. A *projection method* seeks an approximate solution $\tilde{x}$ of (3.30) from an m-dimensional subspace $\mathscr{K}_m$ of $\mathbb{R}^n$ by imposing m independent orthogonality constraints (Saad, 1995 [159]). In particular, the residual vector $R(x) = b - Ax$ (for the current approximation x) is constrained to be orthogonal to m linearly independent vectors of an m-dimensional subspace $\mathscr{L}_m$ called the *subspace of constraints*. If an initial approximate solution x_0 is given, then the projection method into the affine subspace $x_0 + \mathscr{K}_m$ and orthogonal to $\mathscr{L}_m$ advances in the following way:

$$\text{find } \tilde{x} \in x_0 + \mathscr{K}_m \qquad \text{such that} \qquad R(\tilde{x}) = b - A\tilde{x} \perp \mathscr{L}_m \tag{3.31}$$

The orthogonality condition is called condition of Petrov-Galerkin and is applied at each iterative step, in which the initial guess x_0 is equal to the approximation found in the previous step. A projection method is called *orthogonal* if $\mathscr{L}_m$ coincides with $\mathscr{K}_m$ and (3.31) performs the minimum on the A-norm of the solution error[2] over $x_0 + \mathscr{K}_m$, while it is called *oblique* if $\mathscr{L}_m$ is different from $\mathscr{K}_m$ and (3.31) performs the minimum on the 2-norm of the residual vector over $x_0 + \mathscr{K}_m$. In general, such a method uses a succession of projection steps, and $\mathscr{K}_m$ and $\mathscr{L}_m$ change at each iterative step.

Krylov subspace methods

A class of projection methods is represented by *Krylov subspace methods* (Saad, 1995 [159]) in which $\mathscr{K}_m$ is the Krylov subspace

$$\mathscr{K}_m = span\{R_0, AR_0, A^2R_0, \ldots, A^{m-1}R_0\} \tag{3.32}$$

where R_0 is the initial residual vector $R(x_0) = b - Ax_0$.

Specifically, the approximate solution x_m of (3.30) at the step m of the approximation process in the Krylov subspace, will have the following form

$$A^{-1}b \approx x_m = x_0 + q_{m-1}(A)R_0 \tag{3.33}$$

where q_{m-1} is a polynomial of the matrix A of degree $m-1$. Note that the dimension m of $\mathscr{K}_m$ increases at each iterative step.

[2]For the linear system (3.30), the A-norm of the solution error is given by $(A(\bar{x}-x), \bar{x}-x)$, where $\bar{x}$ is the true solution of (3.30).

As already discussed above, in a projection method the constraints subspace $\mathscr{L}_m$ can be coincident with $\mathscr{K}_m$ (orthogonal case) or different from $\mathscr{K}_m$ (oblique case). In the first case, the Full Orthogonalization method, based on the Arnoldi's method, will be discussed. In the second case, the minimum-residual variation $\mathscr{L}_m = A\mathscr{K}_m$ is the best known choice for oblique projection methods, as will be shown with the GMRES method.

The *Arnoldi's method* is an orthogonal projection method onto $\mathscr{K}_m = \mathscr{L}_m$ for general non-Hermitian matrices. It is used for approximating eigenvalues of large sparse matrices by building up an orthogonal basis of the Krylov subspace K_m. A basic algorithm of Arnoldi has the following form in exact arithmetic (refer to Saad, 1995 [159] for further details about Arnoldi's Algorithm).

Algorithm 3.1. (Basic Arnoldi)

1. Choose a vector v_1 of norm 1.
2. For $j = 1, 2, \ldots, m$ Do:
3. Compute $h_{ij} := (Av_j, v_i)$ for $i = 1, 2, \ldots, j$
4. Compute $w_j := Av_j - \sum_{i=1}^{j} h_{ij} v_i$
5. $h_{j+1,j} = \|w_j\|_2$.
6. If $h_{j+1,j} = 0$ then Stop
7. $v_{j+1} = w_j / h_{j+1,j}$
8. End Do

At each step $j + 1$, a standard Gram-Schmidt procedure is applied to orthonormalize the vector Av_j. Some properties of Arnoldi's Algorithm 3.1 will be shown in the next propositions (their proofs can be found in Saad, 1995 [159]).

Proposition 3.1. Assume that Algorithm 3.1 does not stop before the m-th step. Then the vectors $v_1, v_2, \ldots, v_m$ form an orthonormal basis of the Krylov subspace

$$\mathscr{K}_m = span\{v_1, Av_1, \ldots, A^{m-1}v_1\}.$$

□

Proposition 3.2. Denote by V_m, the $n \times m$ matrix with column vectors $v_1, \ldots, v_m$, by $\bar{H}_m$, the $(m+1) \times m$ Hessenberg matrix whose nonzero entries h_{ij} are defined by Algorithm 3.1, and by H_m the matrix obtained from $\bar{H}_m$ by deleting its last row. Then the following relation holds:

$$AV_m = V_m H_m + w_m e_m^T \tag{3.34}$$

$$= V_{m+1} \bar{H}_m, \tag{3.35}$$

$$V_m^T A V_m = H_m. \tag{3.36}$$

□

The Arnoldi's basic Algorithm 3.1 breaks down at the step j if the norm of w_j vanishes. That is, the vector v_{j+1} cannot be computed and the algorithm stops. Then, the following proposition holds.

Proposition 3.3. Algorithm 3.1 breaks down at step j(i.e., $h_{j+1} = 0$ in line 5 of Algorithm 3.1), if and only if the minimal polynomial of v_1 is of degree j. Moreover, in this case the subspace $\mathscr{K}_j$ is invariant under the matrix A. □

Arnoldi's Algorithm 3.1 shows a basic version which might be used in exact arithmetic. In practice, modified algorithms are employed to take more advantage by implementations of the Gram-Schmidt procedure. Further details can be found in Saad (1995) [159].

The Arnoldi's method may be used in order to approximate the solution of linear systems numerically. This approach is called *Full Orthogonalization Method* (FOM) and belongs to the class of orthogonal projection methods. Specifically, $\mathscr{L}_m = \mathscr{K}_m$, where $\mathscr{K}_m$ is defined by (3.32), or also the following convenient formulation

$$\mathscr{K}_m = span\{v_1, Av_1, A^2 v_1, \ldots, A^{m-1} v_1\} \tag{3.37}$$

where

$$v_1 = \frac{R_0}{\|R_0\|_2} = \frac{b - Ax_0}{\|b - Ax_0\|_2}. \tag{3.38}$$

Any vector x_m in $x_0 + \mathscr{K}_m$ can be written as

$$x_m = x_0 + V_m y_m \tag{3.39}$$

where V_m is the $n \times m$ matrix with column vectors $v_1, \ldots, v_m$ which forms a basis of the Kryolov subspace $\mathscr{K}_m$, and y_m is an m-vector.

In general, if W is the $n \times m$ matrix with column vectors forming a basis of $\mathscr{L}_m$, the orthogonality condition (3.31) yields the following system of equations for y_m

$$W_m^T A V_m y_m = W_m^T R_0. \tag{3.40}$$

For an orthogonal projection method ($\mathscr{L}_m = \mathscr{K}_m$), (3.40) becomes

$$V_m^T A V_m y_m = V_m^T R_0, \tag{3.41}$$

that is

$$y_m = (AV_m)^{-1} R_0 = H_m^{-1} V_m^T R_0 \tag{3.42}$$

where (3.36) has been exploited. Moreover, if set $\beta = \|R_0\|_2$, by (3.38) we have

$$V_m^T R_0 = V_m^T (\beta v_1) = \beta e_1. \tag{3.43}$$

Consequently, the approximate solution (3.39) is satisfied if

$$y_m = H_m^{-1}(\beta e_1). \tag{3.44}$$

FOM is based on the above formulations and a modified Gram-Schmidt for the Arnoldi step.

Algorithm 3.2. Algorithm (Full Orthogonalization Method - FOM)

1. Compute $R_0 = b - Ax_0$, $\beta := \|R_0\|_2$, and $v_1 := R_0/\beta$.
2. Define the $m \times m$ matrix $H_m = \{h_{ij}\}_{i,j=1,\ldots,m}$. Set $H_m = 0$.
3. For $j = 1, 2, \ldots, m$ Do:
4. Compute $w_j := Av_j$
5. For $i = 1, \ldots, j$ Do
6. $h_{ij} := (w_j, v_i)$
7. $w_j = w_j - h_{ij} v_i$
8. End Do
9. Compute $h_{j+1,j} = \|w_j\|_2$. If $h_{j+1,j} = 0$ set $m := j$ and go to 12
10. Compute $v_{j+1} = w_j / h_{j+1,j}$
11. End Do
12. Compute $y_m = H_m^{-1}(\beta e_1)$ and $x_m = x_0 + V_m y_m$.

In literature there exist variations of FOM algorithm, designed to take more advantage in its practical implementation. Refer to Saad (1995) [159] for this.

Another class of Krylov subspace methods can be considered choosing $\mathscr{L}_m = A\mathscr{K}_m$ (oblique projection methods) with $\mathscr{K}_m$ defined in (3.37)-(3.38). In this case the approximation process minimizes the residual norm over all vectors in $x_0+\mathscr{K}_m$. For this reason the method is called *Generalized Minimum Residual* (GMRES) method, and it is based on an approach similar to those of the FOM algorithm.

Defining

$$E(y) = \|b - Ax\|_2 = \|b - A(x_0 + V_m y)\|_2 , \tag{3.45}$$

the relation (3.35) results in

$$\begin{aligned} b - Ax &= b - A(x_0 + V_m y) \\ &= r_0 - AV_m y \\ &= \beta v_1 - V_{m+1}\bar{H}_m y \\ &= V_{m+1}(\beta e_1 - \bar{H}_m y). \end{aligned} \tag{3.46}$$

Since the column-vectors of V_{m+1} are orthonormal, then

$$E(y) = \|b - A(x_0 + V_m y)\|_2 = \left\|\beta e_1 - \bar{H}_m y\right\|_2 . \tag{3.47}$$

The GMRES approximation is the unique vector (3.39) of $x_0 + \mathscr{K}_m$ which minimizes (3.45). This approximation can be yielded as $x_m = x_0 + V_m y_m$ with y_m which minimizes the function (3.47) $E(y) = \left\|\beta e_1 - \bar{H}_m y\right\|_2$, that is

$$x_m = x_0 + V_m y_m \tag{3.48}$$

where

$$y_m = argmin_y \left\|\beta e_1 - \bar{H}_m y\right\|_2 . \tag{3.49}$$

The minimizer y_m (3.49) is yielded by an $(m+1) \times m$ least-squares problem solution. In general, m is small, so that y_m requires a low computational cost.

A basic algorithm GMRES is here shown (Saad, 1995 [159]).

Algorithm 3.3. Algorithm (Basic GMRES)

1. Compute $r_0 = b - Ax_0$, $\beta := \|r_0\|_2$, and $v_1 := r_0/\beta$.
2. Define the $(m+1) \times m$ matrix $\bar{H}_m = \{h_{ij}\}_{1 \le i \le m+1,\, 1 \le j \le m}$. Set $\bar{H}_m = 0$.
3. For $j = 1, 2, \ldots, m$ Do:

4. Compute $w_j := Av_j$
5. For $i = 1, \ldots, j$ Do
6. $h_{ij} := (w_j, v_i)$
7. $w_j = w_j - h_{ij}v_i$
8. End Do
9. $h_{j+1,j} = \|w_j\|_2$. If $h_{j+1,j} = 0$ set $m := j$ and go to 12
10. $v_{j+1} = w_j/h_{j+1,j}$
11. End Do
12. Compute y_m the minimizer of $\left\|\beta e_1 - \bar{H}_m y\right\|_2$ and $x_m = x_0 + V_m y_m$.

This Algorithm involves a modified Gram-Schmidt orthogonalization of the Arnoldi's Algorithm. As discussed above, more robust algorithms can be formulated in order to improve their practical implementation (see Saad, 1995 [159]).

Algorithm 3.3 contains the Arnoldi loop (lines from 3 to 11). Therefore, it stops at the step j if $v_{j+1} = 0$, that is $h_{j+1} = 0$ because the next vector cannot be generated. In this case, the residual vector is zero and the algorithm yields the exact solution at the step j. Then, the following proposition holds.

Proposition 3.4. Let A be a nonsingular matrix. Then, the GMRES algorithm breaks down at step j, i.e., $h_{j+1,j} = 0$, if and only if the approximate solution x_j is exact. □

In Bertaccini and Sisto (2011) [20] the GMRES method has been shown to be strategic to build a faster hybrid direct-iterative method into the `ode15s` package. This customized solver has been convenient for the time integration of a cochlear model similar to the anti-damping model, described in Chapter 1. Actually, the application of the GMRES method to the semidiscrete model of such problem shows computational advantages, which might be suitable also for the delayed model studied in this thesis. These advantages will be described in detail in Chapter 4, where the matrix formulation of the model to be integrated, will be built.

A convergence analysis of the GMRES Algorithm might be considered, based on Chebyshev polynomials, as discussed in Saad (1995) [159]. On the other hand, eigenvalues behavior of the iteration matrices gives useful information about the convergence of GMRES, as analyzed by Bertaccini and

Ng (2003) [19] and Bertaccini et al. (2007) [18], and evaluated by Bertaccini and Sisto (2011) [20] for a cochlear model (without delay) similar to the problems at hand. Chapter 4 also will give some details about this.

Chapter 4

The discrete model

The cochlear physiology has a strongly nonlinear behavior, and related theoretical models have to preserve this feature for performing realistic and reliable numerical simulations. The cochlear nonlinearity cannot be considered as a small perturbation of the linear model. This treatment might be a feasible way at very low sound levels, close to the auditory threshold. In general, nonlinear models should be solved in the time domain and high computational costs would be involved.

In Chapter 1 two cochlear models have been discussed: the anti-damping model (section 1.5.3) and the delayed stiffness model (section 1.5.4), which will be here recalled in section 4.1. They describe the nonlinear active feedback mechanism driven by the outer hair cells (OHCs; see section 1.2 for cochlear mechanics) by means of two different formulations. In particular, in the anti-damping model a non linear additional force, function of the basilar membrane (BM) transverse velocity, has been formulated as in Moleti et al. (2013) [132]. On the other side, in the delayed stiffness model, two additional forces, functions of the delayed BM transverse displacement, have been introduced in the stiffness function. Moreover, a nonlinear function of the BM displacement is introduced in the damping term to account for the nonlinear properties of the cochlear amplifier. The delayed stiffness model was formulated by Talmadge et al. (1998) [189], based on the assumptions of Zweig (1991) [210].

Both the anti-damping model and the delayed stiffness model are strongly nonlinear, thus a numerical approximation of the solution has to be carried out in the time domain. Performing numerical simulations in the time domain may be not convenient because of high computational cost. Nevertheless, the state-space formalism (proposed by Elliott et al., 2007 [61]), and a numerical technique based on the Matlab customized package `ode15s` (developed by Bertaccini and Sisto, 2011 [20], as discussed in section 3.3.2, Chapter 3),

may perform a faster numerical approximation of the model solution, as also discussed in Moleti et al. (2009) [135] and Sisto et al. (2010) [174] for the anti-damping model.

The state-space formalism uses finite differences for approximating spatial partial derivatives of the model equations. As a result, a matrix formulation will express the cochlear model with respect to the spatial variable, and the semidiscrete model will be thus obtained (section 4.2). The latter will be discrete in space and continuous in time. Then, the Matlab customized package `ode15s` may be employed in order to advance in time and find the approximate solution (section 4.3). This procedure has been effective with the anti-damping model, as will be discussed in section 4.3.1 (refer to [135]-[174]-[20] for some numerical results). By using a suitable method for solving constant delay differential equations (DDEs), as the *method of steps* (see Chapter 2, in particular section 2.4), the customized package `ode15s` might be alike convenient to perform numerical simulations of the delayed stiffness model (section 4.3.2). In this Chapter the semidiscrete model (section 4.2) and the fully discretized model (section 4.3) will be discussed for both models. Before this, it is useful recall the cochlear models analyzed, as will be shown in the next section.

4.1 The continuous model

The active cochlear models, shown in section 1.5.1 of Chapter 1, describe the stage of the hearing function performed in the inner ear. They represent the cochlea (rectified) as a two-dimensional rectangular box of length L and half-height H. Refer to Table 4.2 for the value of all parameters of the model equations which will be shown. The cochlea is divided by the BM in two

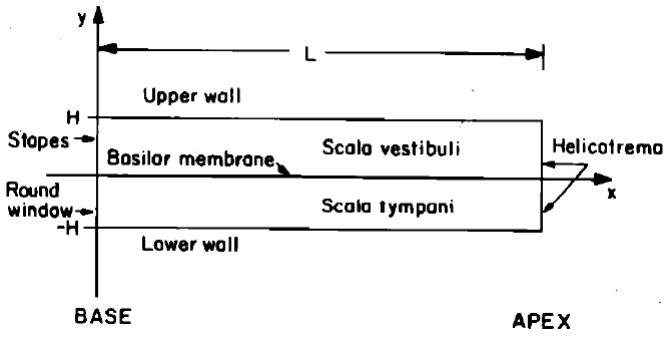

Figure 4.1: Two-dimensional schematization of the cochlea. Reported from Neely (1981) [137].

symmetric cavities (see Figure 4.1) and filled with an incompressible fluid of density ρ. When a sound stimulus is supplied in the ear canal, a pressure stimulus acts on the oval window. The latter is connected to the stapes at the base of the BM (at $x = 0$). This causes the movement of the cochlear fluid from the upper chamber (the scala vestibuli) to the lower chamber (the scala tympani) through the helicotrema at the apex of the BM (at $x = L$). An one dimensional transmission line equation describes the propagation of the differential pressure $p(x, t)$ between the two cavities, that is

$$\frac{\partial^2 p(x,t)}{\partial x^2} - \frac{2\rho}{H}\ddot{\xi}(x,t) = 0 \tag{4.1}$$

where $\ddot{\xi}$ is the BM transverse acceleration. Two boundary conditions hold for the PDE problem (4.1):

- condition at the base (at $x = 0$; $\ddot{\xi}_{ow}$ is the longitudinal acceleration of the oval window)
$$\frac{\partial p(0,t)}{\partial x} = 2\rho\ddot{\xi}_{ow}(t) \tag{4.2}$$
- short-circuit condition at the helicotrema (at $x = L$)
$$p(L,t) = 0. \tag{4.3}$$

The propagation of the cochlear fluid also causes an oscillating movement of the BM. Specifically, each BM tonotopic site may be described as a single forced damped harmonic oscillator. As shown in section 1.5.2 in Chapter 1, the forcing term associated with the sound stimulus, supplied in the ear canal, is included in the dynamic equation for the first oscillator-element at $x = 0$, that is

$$\ddot{\xi}_{ow}(t) + \gamma_{ow}\dot{\xi}_{ow}(t) + \omega_{ow}^2\xi_{ow}(t) = \frac{1}{\sigma_{ow}}[p(0,t) + P_{ow}(t)] \tag{4.4}$$

where ξ_{ow} is the displacement of the oval window. The relation (4.4) encloses the dynamics of the oval window and the middle ear coupled to the ear canal, described by the effective middle ear-oval window density σ_{ow}, damping γ_{ow} and resonance frequency ω_{ow}. The term $P_{ow}(t)$ in (4.4) represents the pressure performed by the stapes on the oval window because of the stimulus supplied in the ear canal. It is explicitly expressed as $G_{me}P_{dr}(t)$ in (1.11) in Chapter 1, with G_{me} the mechanical gain of the ossicles, and P_{dr} the calibrated pressure in the ear canal. Namely,

$$P_{ow}(t) = G_{me}P_{dr}(t) = \left(4.2 \cdot 10^{-4} 10^{L[dB]/20}\ [Pa]\right) s(t) \tag{4.5}$$

where $s(t)$ represents the time function of the sound stimulus[1]. The quantity enclosed in brackets in the third member of (4.5) turns the stimulus level $L[dB]$ from decibel units into Pascal units, according to (1.18) in Chapter 1.

On the other hand, each tonotopic site x along the BM is described by the dynamics of a single harmonic oscillator with angular frequency $\omega_{bm}(x)$ and passive linear damping $\gamma_{bm}(x)$. Namely, as expressed in (1.6) in Chapter 1,

$$\ddot{\xi}(x,t) + \gamma_{bm}(x)\dot{\xi}(x,t) + \omega_{bm}^2(x)(1+\epsilon R)\xi(x,t) = \frac{p(x,t)+q(x,t)}{\sigma_{bm}}. \quad (4.6)$$

The BM displacement ξ performs a resonance condition depending on the sound frequencies supplied in the ear canal. This property is called cochlear tonotopicity, and satisfies a logarithmic relationship between the stimulus frequency and the resonance position along the BM according to the Greenwood Map (1.7). In order to generate backward reflections from the resonant sites along the BM, a roughness parameter R [2] may be included in the stiffness, as described in section 1.5.3. Consequently, in the hypothesis of scale invariance, the place-frequency map (1.7) becomes

$$\omega_{bm}(x) \cong \omega_0 e^{-k_\omega x} \quad (4.7)$$

and, including R as in (1.25), we have

$$\omega_{bm}^2(x)(1+\epsilon R) \cong \omega_0^2 e^{-2k_\omega x}(1+\epsilon R). \quad (4.8)$$

Moreover, the passive damping $\gamma_{bm}(x)$ is defined by the Greenwood Map (1.7) (or (4.7) in the assumption of scale invariance) and the passive quality factor (1.10), that is

$$\gamma_{bm}(x) = \frac{\omega_{bm}(x)}{Q_0}. \quad (4.9)$$

According to (4.6), each tonotopic site is a single harmonic oscillator forced by the local differential pressure $p(x,t)$ of the cochlear fluid. An adding pressure $q(x,t)$ expresses the active nonlinear mechanism driven by the OHCs (see section 1.2 in Chapter 1). Suitable terms acting as damping and/or anti-damping forces, may be formulated and included in $q(x,t)$. In Chapter 1 two different formulations have been considered, and they will be here recalled briefly.

[1] In Chapter 5 different stimulus time functions will be shown. For example, if a stimulus with a single frequency f_0 is supplied, then $s(t) = sin(2\pi f_0 t)$.

[2] R is generated as random number from the normal distribution with mean 0 and variance 1.

In the anti-damping model (see section 1.5.3 in Chapter 1) a nonlinear anti-damping force in $q(x,t)$ is formulated as follows

$$q(x,t) = \sigma_{bm}\left[\gamma_{bm}(x)\alpha_0\left(1 - tanh\left(\frac{\dot{\xi}^2(x,t)}{\dot{\xi}^2_{sat}}\right)\right)\right]\dot{\xi}(x,t), \tag{4.10}$$

where α_0 gives a measure of the variation of the cochlear gain, while $\dot{\xi}_{sat}$ represents the BM velocity saturation length scale.

On the other hand, the delayed stiffness model (see section 1.5.4 in Chapter 1) introduces two additional forces proportional to the BM displacement delayed by, respectively, a time lag $\tau_f(x)$ and a time lag $\tau_s(x)$. These delays are defined in (1.28), and also reported here

$$\tau_f(x) = 2\pi\psi_f/\omega_{bm}(x) \qquad \tau_s(x) = 2\pi\psi_s/\omega_{bm}(x), \tag{4.11}$$

and their value has been carried out for some tonotopic sites in Table 4.1.

Table 4.1: Values of the fast delay τ_f and the slow delay τ_s according to (4.11) for some tonotopic sites $x(f)$. The frequency f and the corresponding resonance place $x(f)$ are connected by the relationship (4.7).

f (kHz)	$x(f)$ (mm)	$\tau_f(x)$ (ms)	$\tau_s(x)$ (ms)
20	0.23	0.012	0.087
15	2.31	0.016	0.116
10	5.25	0.024	0.174
7	7.83	0.034	0.249
5	10.26	0.048	0.348
3	13.96	0.080	0.581
2	16.89	0.120	0.871
1	21.91	0.240	1.742

Moreover, a nonlinear term is also included as quadratic function of the BM displacement in order to model the saturation of the cochlear response at high stimulus levels. Specifically, active nonlinear terms are so formulated in the function $q(x,t)$ of the delayed stiffness model

$$\begin{aligned} q(x,t) = -\sigma_{bm}\left[\rho_f\xi\left(x,t-\tau_f(x)\right) + \rho_s\xi\left(x,t-\tau_s(x)\right)\right]\omega^2_{bm}(x) + \\ -\sigma_{bm}\left[\gamma_{bm}(x)\alpha_0\left(\frac{\xi^2(x,t)}{\xi^2_{sat}}\right)\right]\dot{\xi}(x,t). \end{aligned} \tag{4.12}$$

In (4.12) the level of the cochlear nonlinearity is not fixed as in (1.31) by means of the constant b_{nl}. The latter is here considered as a free parameter,

namely, ξ_{sat}. In this way the nonlinear region of the cochlear response varies with the saturation amplitude ξ_{sat} and the number α_0, as in (4.10) for the anti-damping model.

Table 4.2 shows the values which have been considered for all the model parameters in the numerical simulations of this chapter and Chapter 5.

Table 4.2: Value and description of the parameters in the anti-damping (AD) model and the delayed stiffness (DS) model shown in this section.

Parameter	Value	Description
L	0.035 m	Length of the cochlea
H	0.01 m	Height of the cochlea
ρ	10^6 g/m^3	Fluid density of the cochlea
ω_0	20655 Hz $\times$ 2π	Greenwood Map frequency coefficient
k_ω	138.2 m^{-1}	Greenwood Map exponential constant
ϵ	$0 \div 1$	Roughness relative amplitude
R	Random number	Roughness along the BM
γ_{ow}	375 s^{-1}	Effective middle ear-oval window damping
ω_{ow}	5033 Hz $\times$ 2π	Effective middle ear-oval window frequency
σ_{ow}	2000 g/m^2	Effective middle ear-oval window density
G_{me}	21.4	Mechanical gain of ossicles
$L[dB]$	$10 \div 100$ dB	Sound stimulus level
σ_{bm}	55 g/m^2	BM density
ξ_{sat}	$(0.33 \div 1)\, 10^{-9}$ m	BM saturation displacement (in DS model)
$\dot{\xi}_{sat}$	$(1.4 \div 2)\, 10^{-5}$ m/s	BM saturation velocity (in AD model)
Q_0	$2 \div 8$	Passive quality factor
α_0	$0 \div 1$	OHC gain parameter
ρ_f	0.16	Fast feedback stiffness coefficient
ρ_s	0.1416	Slow feedback stiffness coefficient
ψ_f	0.24	Fast feedback delay coefficient
ψ_s	1.742	Slow feedback delay coefficient

4.2 The semidiscrete model: spatial discretization

An approximate solution of the cochlear models seen in Chapter 1, and recalled in the previous section, can be found by means of the numerical approach shown in section 3.1 in Chapter 3, that is, the method of lines. Specifically, the spatial partial derivatives of (4.1) will be approximated by

means of finite differences. For this purpose, the BM is divided in N uniform partitions of length $\Delta x = L/(N-1)$. In this way, the *state-space formalism* may be employed as suggested by Elliott et al. (2007) [61] and also used by Moleti et al. (2009) [135] and Sisto et al. (2010) [174]. Such a formalism describes the dynamics of a generic physical system in the time domain by means of a set of first-order differential equations, which are coupled and formulated in a vector-matrix form.

Let $P(t)$ be the N-dimensional vector of the differential pressures $p(x,t)$ and $\ddot{\Xi}(t)$ the N-dimensional vector of the accelerations $\ddot{\xi}(x,t)$ for each of N micro-mechanical elements. In this way, the fluid-dynamics equation (4.1) becomes the following matrix equation

$$F\,P(t) = \ddot{\Xi}(t) \tag{4.13}$$

where F is the $N \times N$ matrix of the standard second order centered finite differences (3.9) with step Δx:

$$F = \frac{H}{2\rho(\Delta x)^2} \begin{pmatrix} -\frac{3\Delta x}{2H} & \frac{2\Delta x}{H} & -\frac{\Delta x}{2H} & 0 & 0 & \dots & 0 \\ 1 & -2 & 1 & 0 & 0 & \dots & 0 \\ 0 & 1 & -2 & 1 & 0 & \dots & 0 \\ \vdots & \ddots & \ddots & \ddots & \ddots & \ddots & \vdots \\ 0 & \dots & 0 & 1 & -2 & 1 & 0 \\ 0 & \dots & 0 & 0 & 1 & -2 & 1 \\ 0 & \dots & 0 & 0 & 0 & 0 & -\frac{2\rho(\Delta x)^2}{H} \end{pmatrix} \tag{4.14}$$

The first and last row of F represent the boundary conditions at the base (4.2) and at the apex (4.3), respectively. For the first condition, a second order one-sided discretization has been used. Note that F without the first and the last row, is a Toeplitz matrix with a $O(\Delta_x^{-2})$ condition number[3] in Euclidean norm (LeVeque, 2007 [126]). Contrary, F condition number increases only slightly more with N (see the table reproduced in Figure 4.2 from Bertaccini and Sisto, 2011 [20]), and F eigenvalues are in the right half plane. These properties of F are crucial issues for solving the continuous model numerically. The formulation (4.14) of F defines (4.13) as a second order discretization with respect to the space variable x of the continuous problem (4.1)-(4.2)-(4.3).

[3]The condition number of a matrix A is a measure of the sensitivity to changes or errors occurring while you are solving the linear system $Ax = b$. It is defined by $\kappa(A) = \|A\| \left\|A^{-1}\right\|$ and the 1-norm, 2-norm, or ∞-norm are widely used (Trefethen and Bau, 1997 [198]). For such norms $\|A\| \left\|A^{-1}\right\| \geq \left\|AA^{-1}\right\| = \|I\| = 1$, then a condition number increases as $\kappa(A) \geq 1$. A low κ characterizes a well-conditioned system, while a high κ characterizes an ill-conditioned system.

Condition number and minimum and maximum eigenvalues of matrix F.

N	$\kappa_2(F)$	$\lambda_{\min}(F)$	$\lambda_{\max}(F)$
100	$3{\cdot}10^4$	-61.7	$-3.05{\cdot}10^{-3}$
200	$1.6{\cdot}10^5$	-247.1	$-3.08{\cdot}10^{-3}$
400	$8.4{\cdot}10^5$	-988.4	$-3.09{\cdot}10^{-3}$
800	$4.6{\cdot}10^6$	-3953.8	$-3.10{\cdot}10^{-3}$

Figure 4.2: Condition number in 2-norm and minimum and maximum eigenvalues of matrix F. The Table is reproduced from Bertaccini and Sisto, 2011 [20].

Similarly to Elliott et al. (2007) [61], let $U(t)$ be the $2N$-dimensional *vector of the state variables*. In the model of Elliott et al. an oscillator model with two masses is considered, because the dynamics of a single micromechanical element includes the relative movement between the tectorial membrane and the BM (see section 1.2 in Chapter 1 for greater details on the cochlear anatomy). Consequently, the state space system is formulated with two states for each of the two degree of freedom. In this thesis, a single oscillator model is analyzed as in Moleti et al. (2009) [135] and Sisto et al. (2010) [174]. Then a second-order system is formulated with one degree of freedom described by two states, namely, BM displacement and velocity. Specifically, the n^{th}-component of the vector $U(t)$ of the states is

$$U_n(t) = \begin{pmatrix} \dot{\xi}(x_n, t) \\ \xi(x_n, t) \end{pmatrix} \tag{4.15}$$

In this way, the oscillating equations (4.6) for the BM and (4.4) for the oval window become the following matrix equation

$$\dot{U}(t) = A_E U(t) + B_E[P(t) + S(t)] + B_E Q(t) \tag{4.16}$$

$$\dot{\Xi}(t) = C_E U(t) \tag{4.17}$$

where $S(t)$ is the N-dimensional vector that represents the stimulus given to the base. This vector has null components except the first one, which is equal to the forcing term $P_{ow}(t)$ expressed by (4.5) and applied to the oval window (the first discrete element $n = 1$). The matrix A_E is a $2N \times 2N$ block diagonal matrix, while B_E, C_E are $2N \times N$ and $N \times 2N$ block diagonal matrices, whose blocks are defined as follows

$$A_n = \begin{pmatrix} -\gamma_{bm}(x_n) & -\omega_{bm}^2(x_n) \\ 1 & 0 \end{pmatrix}, \quad B_n = \begin{pmatrix} \frac{1}{\sigma_{bm}} \\ 0 \end{pmatrix} \quad \text{for } n = 2, \dots, N-1$$

$$C_n = \begin{pmatrix} 1 & 0 \end{pmatrix} \qquad \text{for } n = 1, \dots, N$$

$$A_1 = \begin{pmatrix} -\gamma_{ow} & -\omega_{ow}^2 \\ 1 & 0 \end{pmatrix}, \qquad B_1 = \begin{pmatrix} \frac{1}{\sigma_{ow}} \\ 0 \end{pmatrix},$$

$$A_N = 0, \qquad B_N = 0. \quad (4.18)$$

Therefore, (4.16) describes the micromechanics for each of N cochlear micromechanical elements. The mechanics of the model is contained in the *system matrix* A_E, while B_E represents the *input matrix* which scales the *inputs vectors* $P(t)$, $S(t)$ and $Q(t)$ to the system. On the other hand, (4.17) provides the *output vector* $\dot{\Xi}(t)$ by means of the *output matrix* C_E, which selects the odd components of the vector to which it is applied, that is the output states of the model.

Finally, in (4.16), $Q(t)$ is the N-dimensional vector of the additional pressure $q(x,t)$ in (4.6) driven by OHCs. It is expressed by different formulations according to the cochlear models discussed in the sections 1.5.3-1.5.4 of Chapter 1, and recalled in the previous section.

If the *anti-damping model* (refer to Moleti et al., 2013 [132]) is considered, the additional pressure $q(x,t)$ (4.10) turns into the following expression in the state space

$$q(x_n,t) = \sigma_{bm}\left[\gamma_{bm}(x_n)\alpha_0\left(1 - tanh\left(\frac{\dot{\xi}^2(x_n,t)}{\dot{\xi}_{sat}^2}\right)\right)\right]\dot{\xi}(x_n,t) \qquad (4.19)$$

which corresponds to the matrix equation

$$Q_{AD}(t) = C_{AD}(t) D_E \dot{U}(t). \qquad (4.20)$$

In (4.20) C_{AD} is a $N \times N$ diagonal matrix whose components are so defined

$$C_{AD}(n,n) = \sigma_{bm}\left[\gamma_{bm}(x_n)\alpha_0\left(1 - tanh\left(\frac{\dot{\xi}^2(x_n,t)}{\dot{\xi}_{sat}^2}\right)\right)\right] \qquad (4.21)$$

and D_E is the $N \times 2N$ block diagonal matrix which selects the even components of the vector to which it is applied. In particular, D_E is defined as C_E but with the position of 0 and 1 inverted. In this way, in (4.20) D_E selects the BM transverse velocity $\dot{\xi}$ in the vector $\dot{U}(t)$.

The matrix F is invertible (Saad, 1995 [159]; Bertaccini and Sisto, 2011 [20]); as a result, (4.13), (4.16), (4.17) can be combined together into the following sequence of N initial value problems, each one parametrized with step Δx:

$$\begin{cases} M_{AD}(t)\,\dot{U}(t) = A_E U(t) + B_E S(t) \quad t \geq 0 \\ U(0) = 0 \end{cases} \tag{4.22}$$

where M_{AD} is the $2N \times 2N$ *nonlinear mass matrix* for the anti-damping model

$$M_{AD}(t) = I - B_E(F^{-1}C_E + C_{AD}(t)D_E) \tag{4.23}$$

which is not constant and nonlinear. The Jacobian matrix J of the sequence (or system matrix) of N IVPs is constant

$$J = A_E \tag{4.24}$$

and thus, the code will compute it once in the whole integration.

The mass matrix (4.23) changes if different cochlear models are considered.

If the *delayed-stiffness model* is considered, the adding delayed pressure $q(x,t)$ (4.12) turns into the following expression in the state space

$$\begin{aligned} q(x_n,t) = -\sigma_{bm}\left[\rho_f \xi\left(x_n, t-\tau_f(x_n)\right) + \rho_s \xi\left(x_n, t-\tau_s(x_n)\right)\right]\omega_{bm}^2(x_n) + \\ -\sigma_{bm}\left[\gamma_{bm}(x_n)\alpha_0\left(\frac{\xi^2(x_n,t)}{\xi_{sat}^2}\right)\right]\dot{\xi}(x_n,t) \end{aligned} \tag{4.25}$$

where

$$\tau_f(x_n) = 2\pi\psi_f/\omega_{bm}(x_n) \qquad \tau_s(x_n) = 2\pi\psi_s/\omega_{bm}(x_n). \tag{4.26}$$

The relation (4.25) becomes the following matrix equation

$$Q_{DS}(t) = -C_{DS}(t)D_E\dot{U}(t) - \left[U_{\tau_s}(t-\tau_s) + U_{\tau_f}(t-\tau_f)\right] \tag{4.27}$$

where C_{DS} is a $N \times N$ diagonal matrix whose components are so defined

$$C_{DS}(n,n) = \sigma_{bm}\left[\gamma_{bm}(x_n)\alpha_0\left(\frac{\xi^2(x_n,t)}{\xi_{sat}^2}\right)\right], \tag{4.28}$$

and D_E is the block diagonal matrix which selects the BM transverse velocity $\dot{\xi}$ in the vector $\dot{U}(t)$, as in (4.20). Moreover the N-dimensional vectors U_{τ_s} and U_{τ_f} are so defined

$$\begin{aligned} (U_{\tau_s})_n(t-\tau_s) &= \sigma_{bm}\rho_s\,\xi(x_n, t-\tau_s)\,\omega_{bm}^2(x_n) \\ (U_{\tau_f})_n(t-\tau_f) &= \sigma_{bm}\rho_f\,\xi(x_n, t-\tau_f)\,\omega_{bm}^2(x_n). \end{aligned} \tag{4.29}$$

By this formulation, (4.22) becomes

$$\begin{cases} M_{DS}(t)\,\dot{U}(t) = A_E U(t) + B_E\left[S(t) - U_{\tau_s}(t-\tau_s) - U_{\tau_f}(t-\tau_f)\right] & t \geq 0 \\ U(t) = 0 & t \leq 0 \end{cases} \tag{4.30}$$

with M_{DS} the following $2N \times 2N$ *nonlinear mass matrix* in the delayed stiffness model

$$M_{DS}(t) = I - B_E(F^{-1}C_E - C_{DS}(t)D_E). \tag{4.31}$$

The next section will show why this formulation can be strategic to time integrate the delayed stiffness model.

The formulation (4.22) or (4.30) can also be turned into the passive model, that is, the model which would describe a non sensitive cochlea. In this case the active nonlinear mechanism of the OHCs is not performed, that is the additional pressure Q_{AD} (4.20) or Q_{DS} (4.27) would be null. Consequently, the formulation of the passive model is so expressed

$$\begin{cases} M_{passive}\,\dot{U}(t) = A_E U(t) + B_E S(t) & t \geq 0 \\ U(0) = 0 \end{cases} \tag{4.32}$$

with $M_{passive}$ the following *passive mass matrix*

$$M_{passive} = I - B_E F^{-1} C_E. \tag{4.33}$$

4.3 The fully discretized model: time integration

4.3.1 Null delay case: the anti-damping model

The system of differential equations (4.22) represents the discretization in space of the PDE model described in Chapter 1 and section 4.1. Therefore, in order to get the numerical approximation of the model solution, we can integrate (4.22) with respect to the time variable. Firstly, it is important to evaluate the algebraic characteristics of the above equation in order to choose the integrator.

The state space form of a physical model gives a great advantage in the study of the model stability, a crucial issue for its time integration. In particular, the eigenvalues of the system matrix A_E in (4.22) represent the *poles* of the transfer function of the system, that is, the BM local admittance (Elliott et al., 2007 [61]). Let p_n be the pole of the n^{th} cochlear element.

Then, each pole generates a transient response proportional to $e^{\sigma_n t} sin(\omega_n t)$, where $\sigma_n = \Re\{p_n\}$ and represents the divergence rate of the transient, while $\omega_n = \Im\{p_n\}$ and defines the local resonant frequency $\omega_n = 2\pi f_n$. Specifically, if σ_n is negative, the transient convergences and the system is stable. On the other hand, if σ_n is positive, the transient diverges and the system is unstable.

In Bertaccini and Sisto (2011) [20] a variant of the anti-damping model has been studied by means of the same matrix formulation employed in this thesis. The authors showed that the Jacobian J of the problem analyzed, as well as the transfer matrices $M^{-1}J$ (with M the mass matrix of the system), have eigenvalues with large negative real part and nonzero imaginary part. As a consequence, small time steps and adaptivity with respect to the time discretization are necessary for time integration of the model equation. The anti-damping model (4.22) is also characterized by such properties, as shown by the spectrum of the Jacobian A_E in Figure 4.3, and the spectrum of the transfer matrix $M_{AD}^{-1} \cdot A_E$, where M_{AD} is the mass matrix (4.23). The latter depends on time through the matrix C_{AD} (4.21). For this reason, the spectrum of $M_{AD}^{-1} \cdot A_E$ has been computed by evaluating M_{AD} at a fixed time point. No unstable modes characterize the model, and the poles appear in complex conjugate pairs. In particular, since the model (4.22) has one degree of freedom, a couple of conjugate poles corresponds to each micromechanical element of the cochlea. Therefore the poles with negative imaginary part do not give additional information. Moreover, if we observe the poles in the second quadrant of the complex plane of Figure 4.3, we observe a magnitude of the divergence rate increasing with the frequency.

A fundamental issue of the time integration of (4.22) is also the algebraic structure of the matrices that define the state space form of the model. In particular, the model (4.22) has a nontrivial mass matrix, namely, M_{AD} (4.23). For this reason, explicit methods would not be appropriate here. This is because an explicit solver would require to solve a linear system at each time step. Moreover, (4.22) is stiff and its stiffness increases with the nonlinear function (4.10) (Bertaccini and Sisto, 2011 [20]). Consequently, implicit methods should be involved in order to advance in time. Matlab Ode Suite offers different packages to integrate stiff problems, as the `ode15s` solver described in section 3.3.1 of Chapter 3. However, the customized package `ode15s`, described in section 3.3.2, may be more effective for the problem at hand, as will be below highlighted.

Numerical methods for time-steps integration, based on implicit formulas as `ode15s`, require the solution of algebraic nonlinear systems, of the form

$$\mathcal{M}\, v = b, \tag{4.34}$$

at each step. This is the most time consuming operation of those packages.

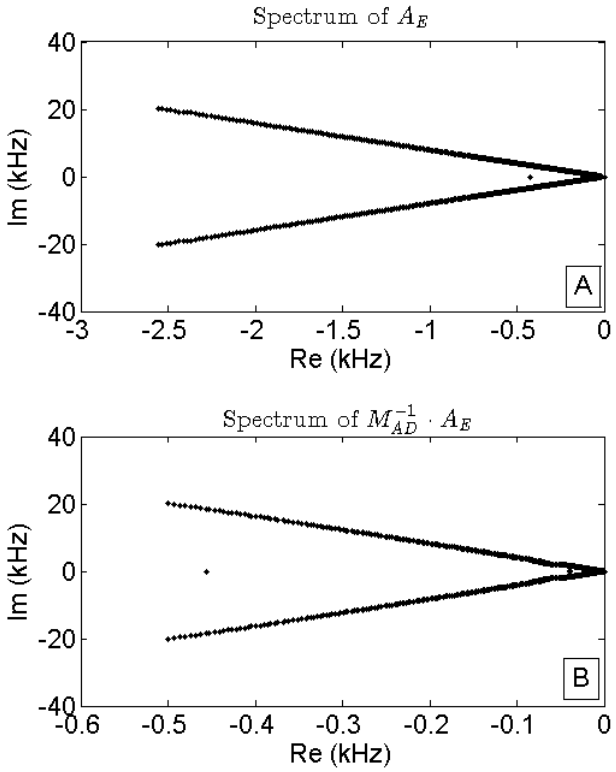

Figure 4.3: Eigenvalues of (A) the system matrix A_E defined in (4.18) and (B) the transfer matrix $M_{AD}^{-1} \cdot A_E$ of the problem (4.22) parametrized with $N = 500$. The mass matrix M_{AD} is a time function defined in (4.23) and, thus, has been evaluated at the time point $t^* = 20$ ms. The spectrum of A_E or $M_{AD}^{-1} \cdot A_E$ does not change for different N or t^*. For a better display of the spectrum, the first eigenvalue ($p_1 = -59.26$ kHz for A_E and $p_1 = -42.57$ kHz for $M_{AD}^{-1} \cdot A_E$) has not been shown.

In our case $\mathcal{M} = M_{AD} - a\,\Delta_t A_E$, with a constant and Δ_t the time step. For the sake of illustration, let us consider backward Euler method (in general, $y_{n+1} = y_n + h_{n+1} f(y_{n+1})$) applied to solve (4.22), namely

$$M_{AD}\frac{U^{i+1} - U^i}{\Delta_t} = A_E U^{i+1} + B_E S(t_{i+1}) \tag{4.35}$$

or

$$(M_{AD} - \Delta_t A_E)U^{i+1} = M_{AD}U^i + \Delta_t B_E S(t_{i+1}). \tag{4.36}$$

The equation (4.36) contains $\mathcal{M} = M_{AD} - a\,\Delta_t A_E$ with $a = 1$. If multi-steps formula (namely, backward differential formula, BDF, described in section 3.3.1 in Chapter 3) is applied, a will be a constant. Therefore (4.36) is

formally (4.34), with b corresponding to the second member of (4.36), and containing products between the matrices contained in M_{AD} (that is, B_E, C_E, D_E, C_{AD}, F^{-1}) and U^i.

F is a band matrix but its inverse, and therefore M_{AD} and $\mathcal{M}$, is full (that is, all of its entries are different from zero). Therefore the problems (4.22) are fully coupled. In order to perform realistic numerical simulations, N has to be large (at least 500) requiring a computationally expensive inversion of F (number of flops equals to the cubic power of F size). For this reason, it is convenient to avoid the inversion of F by decoupling our system. Consider also that C_{AD} changes, and thus is updated, at each step, because it depends on time through the BM displacement ξ. However, since C_{AD} is diagonal, its inversion would be linear with its size at each step.

Bertaccini and Sisto [20] propose to use a modified Matlab's package, i.e. the `ode15s` package (see section 3.3.1 in Chapter 3) with an adaptive hybrid iterative solver, instead of the usual built in direct solver based on Gaussian elimination. Some properties of this customized package `ode15s` have been already discussed in section 3.3.2. In particular, the GMRES method (see section 3.3.2) can be a good choice to solve (4.34). That is because it does not need to build the matrix $\mathcal{M}$ explicitly, but it performs matrix to vector products of the form $\mathcal{M}\,v$. That is, in order to get such products, products with B_E, C_E, D_E, C_{AD} matrices are performed, while a banded linear system with F matrix is solved through a direct method as Gaussian elimination (that has a computational cost which is linear with the size of the matrix rows).

Moreover the sequence of matrices $\mathcal{M}$ has a clustered spectrum (as shown in Bertaccini and Sisto, 2011 [20]), and GMRES method is particularly fast in these cases (Bertaccini and Ng, 2003 [19]), with a convergence almost insensitive to the nonlinear function (4.10).

For all the reasons discussed, the modified package `ode15s` seems to be more suitable to integrate (4.22).

4.3.2 Delayed case: the delayed stiffness model

The problem (4.30) is a sequence of N stiff Delay Differential Equations (DDEs, see Chapter 2), characterized by algebraic properties already discussed for the anti-damping model in the previous subsection. For this reason, also in this case an implicit multistep solver is required to integrate the model (4.30). Consequently, Matlab `ode15s` package customized as described in section 3.3.2 of Chapter 3, can be a good solver to apply in a numerical method for DDEs.

Firstly, let us evaluate the effect of the physical lags (4.26) on the delayed system (4.30), with respect to the anti-damping model (4.22). For this purpose, an analytical approximation of the delayed displacements $\xi(x_n, t - \tau_f(x_n))$ and $\xi(x_n, t - \tau_s(x_n))$ of (4.25) might be useful. Let $\xi(t-\tau)$ be the displacement depending on a generic delay τ. If small delays are involved, then a linear approximation of $\xi(t-\tau)$ can be considered. This is the case of tonotopic sites with high resonance frequency (higher than 2 kHz, at least), namely, cochlear places which are in the first half of the overall length of the rectified cochlea. In this way, in the limit of high frequencies, the following approximation holds

$$\xi(t-\tau) \approx \xi(t) - \tau\dot{\xi}(t). \tag{4.37}$$

The value of the coefficients ψ_f and ψ_s in (4.26) (see Table 4.2) generates a phase lag of the delayed displacements $\xi(x_n, t - \tau_f(x_n))$ and $\xi(x_n, t - \tau_s(x_n))$ with respect to the velocity $\dot{\xi}(x_n, t)$. In particular, ψ_f produces a delay of $1/4$ of period and causes a phase shift of π between $\xi(x_n, t - \tau_f(x_n))$ and $\dot{\xi}(x_n, t)$, that is, $\xi(x_n, t - \tau_f(x_n))$ behaves as $-\dot{\xi}(x_n, t)$. On the other hand, ψ_s produces a delay of -1/4 of period so that $\xi(x_n, t - \tau_s(x_n))$ introduces a stabilizing effect with respect to $\xi(x_n, t - \tau_f(x_n))$. As a consequence, this phase shift has to be considered in the approximation (4.37). Namely, the following approximations hold

$$\xi(x_n, t - \tau_f(x_n)) \approx \xi(x_n, t) - \tau_f(x_n)\dot{\xi}(x_n, t) \approx \xi(x_n, t) - \frac{1}{4}\frac{2\pi}{\omega_{bm}(x_n)}\dot{\xi}(x_n, t) \tag{4.38}$$

$$\xi(x_n, t - \tau_s(x_n)) \approx \xi(x_n, t) - \tau_s(x_n)\dot{\xi}(x_n, t) \approx \xi(x_n, t) + \frac{1}{4}\frac{2\pi}{\omega_{bm}(x_n)}\dot{\xi}(x_n, t) \tag{4.39}$$

for $t > \tau_f(x_n)$ and $t > \tau_s(x_n)$, respectively, for every $1 < n < N$. By means of (4.38)-(4.39), (4.25) becomes the following function $\tilde{q}(x_n, t)$

$$\begin{aligned}\tilde{q}(x_n, t) \approx -\sigma_{bm} \Bigg[\rho_f \left(\xi(x_n, t) - \frac{1}{4}\frac{2\pi}{\omega_{bm}(x_n)}\dot{\xi}(x_n, t) \right) + \\ + \rho_s \left(\xi(x_n, t) + \frac{1}{4}\frac{2\pi}{\omega_{bm}(x_n)}\dot{\xi}(x_n, t) \right) \Bigg] \omega_{bm}^2(x_n) + \\ -\sigma_{bm} \left[\gamma_{bm}(x_n)\alpha_0 \left(\frac{\xi^2(x_n, t)}{\xi_{sat}^2} \right) \right] \dot{\xi}(x_n, t)\end{aligned} \tag{4.40}$$

and the formulation (4.30) becomes

$$\begin{cases} M_{DS}(t)\,\dot{U}(t) = \tilde{A}_E U(t) + B_E S(t) & t \geq 0 \\ U(t) = 0 & t \leq 0. \end{cases} \tag{4.41}$$

In (4.41) the Jacobian (or system matrix) $\tilde{A}_E$ is so defined

$$\tilde{A}_E = A_E + A_{E_{lag}} \tag{4.42}$$

with A_E the same matrix defined in (4.18) and $A_{E_{lag}}$ a $2N \times 2N$ block diagonal matrix. The blocks of $A_{E_{lag}}$ are updated while advancing in time because the history $U(t) = 0$ for $t \leq 0$ has to be satisfied. After a time interval greater than the maximum delay, the n^{th} block of $A_{E_{lag}}$ will be defined as follows

$$\left(A_{E_{lag}}\right)_n = \begin{pmatrix} \frac{2\pi(\rho_f - \rho_s)}{4}\omega_{bm}^2(x_n) & -(\rho_f + \rho_s)\omega_{bm}^2(x_n) \\ 1 & 0 \end{pmatrix} \tag{4.43}$$

The formulation (4.41) could be useful to study the stability of the delayed problem (4.30), at least in the limit of frequencies higher than 2 kHz. Actually, in the numerical simulation of our cochlear models, the cochlea will be investigated in that frequency range.

The spectrum of the Jacobian $\tilde{A}_E$ and the transfer matrix $M_{DS}^{-1} \cdot \tilde{A}_E$ (at a fixed time greater than the maximum delay) of the problem (4.41) is shown in Figure 4.4. The behavior is similar to that observed in the anti-damping model in Figure 4.3. In particular, the delayed model (4.41) shows no unstable modes, and poles with large negative real part. As a consequence, the same issues discussed in the previous subsection have to be considered in order to integrate the delayed system (4.30). So, also in this case, the customized `ode15s` could be strategic for the problem at hand.

The model (4.30)-(4.31) represents a system of DDEs, then the *method of steps* discussed in section 2.4 of Chapter 2 has been considered in order to find an approximate solution. For equations with constant delay the method is formulated as follows.

Consider the following one-dimensional constant DDE:

$$\begin{cases} \dot{y}(t) = f(t, y(t), y(t-\tau)) & t_0 \leq t \leq t_f \\ y(t) = \phi(t) & t \leq t_0 \end{cases} \tag{4.44}$$

where f is continuous and Lipschitz with respect to $y(t)$ and $y(t-\tau)$, τ is a non negative constant delay, $\phi(t)$ is the continuous Lipschitz initial function. The solution of the DDE (4.44) exists and is unique (see section 2.3 in Chapter 2, and Bellen and Zennaro, 2003 [10]), and can be investigated turning (4.44) into T Initial Value Problems (IVPs), with T constant.

Namely, in order to obtain $y(t)$ in the interval $[t_0, t_0 + T\tau]$ (where T is a positive constant such that $T\tau \leq t_f$), T IVPs can be solved dividing the integration interval in T subintervals. Let m be the m^{th} subinterval, with

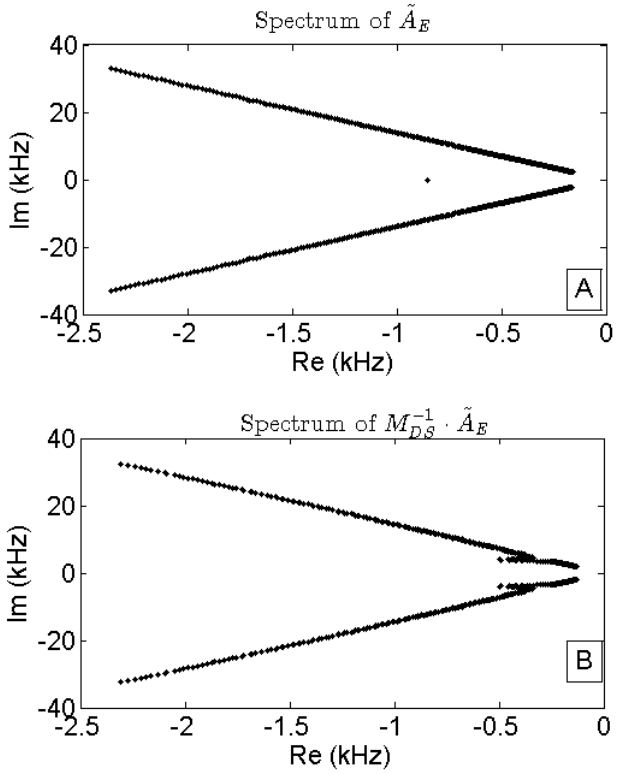

Figure 4.4: Eigenvalues of (A) the system matrix $\tilde{A}_E$ defined in (4.42) and (B) the transfer matrix $M_{DS}^{-1} \cdot \tilde{A}_E$ of the problem (4.41) parametrized with $N = 500$ and in the limit of frequencies higher than 2 kHz. The matrix M_{DS} is a time function defined in (4.31) and, thus, has been evaluated at the time point $t^* = 20$ ms. The spectrum of $\tilde{A}_E$ or $M_{DS}^{-1} \cdot \tilde{A}_E$ does not change for different N or $t^* > \tau^* \cong 10$ ms, where $\tau^* = \max_{1<n<N}\{\tau_s(x_n), \tau_f(x_n)\} = \tau_f(x_N)$. For a better display of the spectrum, the first eigenvalue ($p_1 = -118.51$ kHz for $\tilde{A}_E$ and $p_1 = -86.18$ kHz for $M_{DS}^{-1} \cdot \tilde{A}_E$) has not been shown.

$m \in \{1, \ldots, T\}$. Therefore, the m^{th} IVP will be the following system

$$\begin{cases} \dot{y}_m(t) = f(t, y_m(t), y_{m-1}(t-\tau)) & t \in [t_0 + (m-1)\tau, t_0 + m\tau] \\ y_m(t_0 + (m-1)\tau) = y_{m-1}(t_0 + (m-1)\tau), \end{cases} \tag{4.45}$$

with initial condition $y_m(t_0 + (m-1)\tau)$ fixed by the solution $y_{m-1}(t_0 + (m-1)\tau)$ computed at the last mesh point of the previous interval.

Finally, $y(t)$ will be defined by the following condition

$$y(t) = y_m(t) \qquad if\ (m-1)\tau \leq t \leq m\tau \quad \forall m \in \{1, \ldots, T\} \tag{4.46}$$

In the problem at hand, each of the N cochlear partitions is characterized

by the corresponding delays τ_s and τ_f according to (4.26). Consequently, for each of the N cochlear partitions an IVP similar to (4.45), but with two delays depending on $n = 1, \ldots, N$, has to be solved. For this reason, the time interval $[t_0, T\tau]$ to be integrated has to be divided in T subintervals of length given by the minimum value on the components of the vectors τ_s and τ_f. According to (4.26) and the Greenwood Map (1.2) or (4.7), we have

$$\tau \equiv \min_{1 \leq n \leq N} \{\tau_s(x_n), \tau_f(x_n)\} = \tau_f(x_1) \tag{4.47}$$

and, as shown in Table 4.1,

$$\tau_f(x_1) \cong 0.012 \text{ ms.} \tag{4.48}$$

In this way, according to the method (4.45) applied to the IVP (4.30) of DDEs with two delays, the vectors U_{τ_s} and U_{τ_f} (4.29) will be fixed at the initial mesh point of each m^{th} subinterval, and updated only when the corresponding solutions $\xi(t - \tau_s)$ and $\xi(t - \tau_f)$ are available by the time integration of the previous subintervals. Since the length (4.48) of an integration subinterval is small in the problem time scale (a realistic simulation time has a value of 10-20 ms), the time points will be computed with a resolution which might be sufficient to evaluate the delayed solutions. For example, if a subinterval is spanned in 3 points, the first and the last mesh point will be the initial and the final time, respectively. Then the time distance between two points will be 0.006 ms on the time length $\tau_f(x_1)$ (4.48), that is 0.012 ms. However, in the m^{th} interval an interpolation of the solution $y(t)$ computed until the $m^{th} - 1$ interval will be considered in order to improve the update of the delayed functions, since the lags are not multiple of $\tau_f(x_1)$.

Finally, in order to advance in time, in each m^{th} subinterval the time integration method (the customized `ode15s` package) discussed for the null delay case (section 4.3.1) has been applied. This approach does not allow to update the delayed terms while advancing in time. For this reason each subinterval has been integrated at 3 mesh points, with the delayed terms fixed at the second and third point with the same value. This is because all solvers in the ODE suite of Matlab impose the initial condition at the first mesh point of the integration interval, and integrate from this time point to the last one (see also section 3.3.1 in Chapter 3). If the integration interval is set only by two elements (that is, the initial and the final mesh point), then the solver returns the solution evaluated in each integration step. On the other hand, the Matlab user can choose specific times for computing the approximate solution. In this last case, the minimum number of mesh points will be three, with the first fixed by the initial condition.

Chapter 5

Numerical results

This chapter will show the results of the numerical experiments of the semidiscrete delayed stiffness model. The latter has been integrated with the technique of the *method of steps*, discussed in Chapter 2 for a generic Delay Differential Equation (DDE) and in Chapter 4 for the problem at hand. Moreover, some results about the anti-damping model will also be produced in order to compare the delayed model, analyzed in this thesis, with a variant of the cochlear models without delay. The equations of both models, formulated by means of spatial finite differences in the state space, will be recalled in section 5.1.

The time integration of the semidiscrete equations of both models requires some numerical considerations (section 5.2). In particular, a spatial Gaussian average of the nonlinear term is a crucial issue in order to obtain the convergence of the numerical solver used to advance in time, as evaluated in the anti-damping model by Moleti et al. (2013) [132]. Moreover, the delayed stiffness model would require that the model solution is smoothly linked to the history function to avoid primary discontinuities at the initial integration point. For this reason, the time function of the sound stimulus, supplied at the first discrete element, has to fulfill this request.

The anti-damping model has been integrated by means of the Matlab `ode15s` package, customized as discussed in Chapter 3. On the other hand, a numerical technique has been proposed for the delayed stiffness model, as discussed in Chapter 4, and based on the *method of steps* and the customized `ode15s` package. Here, a simplification of the code implemented in Matlab will be shown in section 5.3.

Then, numerical experiments of the delayed stiffness model will be discussed in section 5.4, section 5.5 and section 5.6, and compared with some numerical results of the anti-damping model. In such experiments the main free parameters will be varied in order to test their effect on the model so-

lution. Refer to Table 4.2 of Chapter 4 for the definition and the range of values used for the free model parameters. The following table may also help for a quick recall of the symbols used to show the results of the numerical simulations of this chapter.

Table 5.1: Description of the free parameters involved in the anti-damping (AD) model and the delayed stiffness (DS) model in this chapter.

Parameter	Description
L	Length of the cochlea
N	Number of the discrete elements along the cochlea
ϵ	Roughness relative amplitude
f	Frequency of the sound stimulus
$L[dB]$	Sound stimulus level
ξ_{sat}	BM saturation displacement (in DS model)
$\dot{\xi}_{sat}$	BM saturation velocity (in AD model)
Q_0	Passive quality factor
α_0	OHCs gain parameter

5.1 The semidiscrete model equations

In Chapter 4 the continuous anti-damping model and the delayed stiffness model have been expressed in the matrix formulation of the state space. Specifically, the spatial partial derivatives of the models equations have been approximated by finite differences on an uniform mesh of the rectified model for the BM. In this way, the corresponding semidiscrete models have been yielded. This technique produces a sequence of N initial value problems (IVPs) parametrized by the space step Δx (see section 4.2 in Chapter 4). In particular, the semidiscrete anti-damping model is defined by the following IVP based on first order ODEs

$$\begin{cases} M_{AD}(t)\,\dot{U}(t) = A_E U(t) + B_E S(t) \quad t \geq 0 \\ U(0) = 0 \end{cases} \tag{5.1}$$

where $U(t)$ is the vector of the states, A_E and B_E are, respectively, the system matrix and the input matrix defined in (4.18), $S(t)$ is the input vector, and $M_{AD}(t)$ is the mass matrix (4.23) for the anti-damping model.

On the other side, the semidiscrete delayed stiffness model is defined by

the following IVP of DDEs

$$\begin{cases} M_{DS}(t)\,\dot{U}(t) = A_E U(t) + B_E\left[S(t) - U_{\tau_s}(t-\tau_s) - U_{\tau_f}(t-\tau_f)\right] & t \geq 0 \\ U(t) = 0 & t \leq 0 \end{cases} \tag{5.2}$$

where, apart from the quantities formerly defined for (5.1), $M_{DS}(t)$ is the mass matrix (4.31) in the delayed stiffness model, while $U_{\tau_s}(t-\tau_s)$ and $U_{\tau_f}(t-\tau_f)$ contain the BM displacement delayed by positive constant lags τ_s and τ_f, respectively, as defined by (4.29) in Chapter 4.

5.2 Numerical approach

Numerical experiments with $N = 500$ have been performed to find the approximate solution of the IVPs (5.1) and (5.2). A greater number N of cochlear partitions might be used in order to obtain more realistic simulations of the models. However, at this stage of the thesis, a discretization of the cochlea in 500 micromechanical elements is sufficient to test the delayed cochlear model (5.2), as well as the problem (5.1), with physically significant results. All the tests have been performed on a Intel(R) Core(TM)2 Duo CPU 6300 1.86 GHz clock, 2 GB RAM and a Intel(R) Core(TM)2 Duo CPU T5550 1.83 GHz clock, 2 GB RAM running Matlab R2014a 32 bit on Windows XP Service Pack 2 platform.

The solution $U(t)$ of the delayed model (5.2) is a continuous function, smoothly linked to the initial function $U(t) = 0$ (for $t \leq 0$). That is, the left hand time derivative $\dot{U}(0)^-$ is equal to the right hand time derivative $\dot{U}(0)^+$, if the input vector $S(t)$ also vanishes for $t = 0$. The N-dimensional vector $S(t)$ represents the stimulus given to the cochlear base, and thus, the only non-null element is the first one (see section 4.2 in Chapter 4). In order to avoid primary discontinuities (see section 2.2 in Chapter 2) generated at the initial time point $t_0 = 0$, sound stimulus functions have been chosen with the condition $S(0) = 0$.

Experimentally, three main typologies of stimulus are employed to investigate the human cochlear response, as suggested by the study of the otoacoustic emissions (OAEs; see section 1.4 in Chapter 1): transient stimulus, single frequency tone, and two simultaneous sinusoidal tones. In the first case the cochlear response measured in the ear canal (namely, the cochlear base, or rather the first partition in the semidiscrete cochlear model) is called *Transient Evoked Otoacoustic Emission* (TEOAE), in the second case *Stimulus Frequency Otoacoustic Emission* (SFOAE), in the last case *Distortion Product Otoacoustic Emission* (DPOAE). Correspondingly, the three follow-

ing kinds of stimuli may be formulated in order to implement the cochlear model (5.2), or also (5.1):

$$\begin{aligned} s_{TE}(t) &= e^{-(t-c)} sin(2\pi f \cdot t) \\ s_{SF}(t) &= sin(2\pi f \cdot t) \\ s_{DP}(t) &= sin(2\pi f_1 \cdot t) + sin(2\pi f_2 \cdot t) \end{aligned} \tag{5.3}$$

where c is a constant, f, f_1, f_2 are the frequencies of the stimulus sinusoidal component. Each function of (5.3) might represent the non-null component (that is, the first one only) of the stimulus vector $S(t)$ in (5.1) or (5.2).

Finally, in order to advance in time, some adjustments are necessary for (5.1) or (5.2).

First, over a length scale of order one tenth of octave, a Gaussian average on $\dot{\xi}^2(x,t)$ or $\xi^2(x,t)$ in the nonlinear coefficient of, respectively, (4.10) for the anti-damping model, or rather (4.12) for the delayed stiffness model, has been introduced with respect to space variable in order to assure the convergence of the integration method. This is because such a nonlinear function, depending pointwise on the BM velocity or displacement, generates fast oscillations of the solution. As a result, very small time steps would be required to integrate the model equation, even leading to failure of the implementation of the numerical code.

In particular, for the anti-damping model, the nonlinear coefficient of (4.10) becomes the following function $C_{nl_{AD}}(x,t)$

$$C_{nl_{AD}}(x,t) = \alpha_0 \left[1 - tanh \left(\frac{1}{\sqrt{\lambda\pi}} \int_0^L e^{-(x-x')^2/\lambda} \frac{\dot{\xi}^2(x',t)}{\dot{\xi}_{sat}^2} dx' \right) \right] \tag{5.4}$$

as suggested in Moleti et al. (2013) [132]. On the other hand, for the delayed stiffness model the nonlinear term of (4.12) becomes the following function $C_{nl_{DS}}(x,t)$

$$C_{nl_{DS}}(x,t) = \alpha_0 \left(\frac{1}{\sqrt{\lambda\pi}} \int_0^L e^{-(x-x')^2/\lambda} \frac{\xi^2(x',t)}{\xi_{sat}^2} dx' \right) \tag{5.5}$$

where L is the length of human cochlea (the value of 35 mm for the human ear has been set in all the models analyzed). In both (5.4) and (5.5), α_0, $\dot{\xi}_{sat}$ and ξ_{sat} are free parameters to be set. The coefficient α_0 is a constant which changes the variation of the cochlear gain. On the other hand, $\dot{\xi}_{sat}$ and ξ_{sat} are constant scales which establishes a saturation amplitude of BM velocity $\dot{\xi}(x,t)$ and displacement $\xi(x,t)$, respectively. In particular, while for the anti-damping model the nonlinear term (5.4) generates two asymptotic

linear regimes of the cochlear amplifier around $\dot{\xi}_{sat}$, for the delayed stiffness model (5.5) introduces a linear growth only below the saturation level ξ_{sat}. Moreover, the integral in (5.4)-(5.5) has been approximated by finite sum of rectangles between two consecutive cochlear partitions, and evaluated by means of the solution at the previous time step. This latter procedure simplifies the numerical calculation of (5.4) or (5.5).

The formulations (5.4)-(5.5) are also preferred for the models at hand in order to make the effective damping function sensitive to the average value of the BM velocity and displacement, respectively. Without such a local cochlear property, at each cochlear place for which the BM amplitude is higher than the saturation amplitude, the active mechanism, driven by the OHCs, is continuously switched on and off by the fast oscillation of $\dot{\xi}(x,t)$ or $\xi(x,t)$.

Second, in order to make faster the numerical integration by `ode15s` package in Matlab, the integrator relative tolerance on the local error (see section 3.3.1 in Chapter 3) has been set to the value of 10^{-2} in both models, thus being effective and at the same time maintaining numeric accuracy and physical properties of the model solution. The speed and accuracy of the numerical code are affected by the physical units of dynamical variables of the model implemented because they introduce a scaling effect on the equation to be solved. As a consequence, at each iterative step, the time step and the spectra of the Jacobian matrix and the transfer matrix are also affected. This influences the number of iterations for the Krylov subspace solvers and computing time of the solution. The implemented code sets the BM displacement in nm, while time variable is expressed in ms, which gives almost the same order of magnitude for BM displacement and velocity in the kHz range (Moleti et al., 2013 [132]).

5.3 Code for the delayed stiffness model

The numerical approximation of the solution of the anti-damping model (5.1) has been found by means of the numerical procedure of Moleti et al. (2009) [135] and Moleti et al. (2013) [132], described in section 4.2 and section 4.3.1 of Chapter 4. On the other hand, the approximate solution of the delayed stiffness model (5.2) has been carried out in this thesis by means of the numerical technique shown in section 4.2 and section 4.3.2. In particular, the following code has been implemented in Matlab (here, a part of the simplified code is reported). Refer to Table 4.2 and section 4.2 - 4.3.2 of Chapter 4 for the quantities recalled in the code.

Code (Delayed stiffness model)

1. Compute the vectors ω_{bm}, τ_f and τ_s, the matrices F, A_E, B_E, C_E, D_E and the stimulus vector S of (5.2) for N micromechanical elements.

2. Choose a constant T such that the integration interval of (5.2) is $[0, T\tau]$, and the parameter Nt such that each of T subintervals $[t_{in}, t_{fin}] \subset [0, T\tau]$ has length τ and $Nt + 1$ time points.

3. Then, implement the following code to obtain the time vector and the solution matrix of the IVP (5.2) in the form `Mass(t)ẏ(t)=f(t,y)` with `y(t)=0` for `t` ≤ 0:

```
% Choose the minimum delay tau
% Let tauf be the delay of fast feedback
% Let taus be the delay of slow feedback
position_index=1;
tau=tauf(position_index); % tauf(1)=0.012 ms

%Compute the lenght tf
%of the integration interval [0,tf]=[0,T*tau]
tf=T*tau;

%Initialize the initial condition y0
y0=zeros(2N,1);

% @Mass is the function handle defined in the next item
options = odeset('Mass',@Mass,'Jacobian', AE,...
         'RelTol', 1e-2, 'AbsTol',1e-6*ones(size(y0)));

for j=1:T
    %Build the integration subinterval tspan=[t_in, t_fin]
    %of length tau and with Nt+1 points
    t_in=(j-1)*tau; %ms
    t_fin=t_in+tau; %ms
    tstep=tau/Nt; %ms/pt
    tspan = t_in:tstep:t_fin; %ms

    if (t_in-tau<0)
        %Define the initial conditions
        y0=zeros(2N,1);
        U_taus=zeros(N,1);
        U_tauf=zeros(N,1);
    else
        y0=y(Nt+1,:);

        % Update the delayed displacements
```

```
            % U_tauf contains the BM displacement delayed of tauf
            % U_taus contains the BM displacement delayed of taus
            % sigma_bm is the BM density
            % rho_f is the fast feedback stiffness coefficient
            % rho_s is the slow feedback stiffness coefficient
            % omega_bm is the BM angular frequency
            for i=1:N
                if t_in>=tauf(i)
                    q=(j-1)*Nt-round(tauf(i)*((j-1)*Nt+1)/t_in)+2;
                    U_tauf(i)=sigma_bm*rho_f*...
                                    solution(q,i*2)*(omega_bm(i))^2;
                end

                if t_in>=taus(i)
                    q=(j-1)*Nt-round(taus(i)*((j-1)*Nt+1)/t_in)+2;
                    U_taus(i)=sigma_bm*rho_s*...
                                    solution(q,i*2)*(omega_bm(i))^2;
                end
            end
        end

        Yds=-(U_tauf+U_taus); % vector of delayed displacements

        % Apply the solver ode15s customized
        % @f is the function handle defined in the next item
        [t,y] = ode15s(@f,tspan,y0,options);

        time((j-1)*Nt+1:j*Nt+1)=t; % time vector
        solution((j-1)*Nt+1:j*Nt+1,:)=y; % solution matrix
    end
```

4. Define the function handle that evaluates the function `f(t,y)` of the IVP to be solved

```
    function yp = f(t,y)
        yp = AE*y+BE*(S+Yds);
    end
```

5. Define the function handle that evaluates the function `Mass(t)` of the IVP to be solved

```
    function M_DS = Mass(t)
        M_DS = speye(2N) - B_E(F\C_E - C_DS DE);
    end
```

where the matrix C_{DS} depends on time and has to be evaluated according to (5.5), while the Matlab function `speye` forms a sparse identity matrix.

5.4 Models approximate solution

In this thesis the delayed stiffness model (5.2) has been tested by simulating the cochlear response to a sinusoidal tone. Namely, a sound stimulus of the following form, defined in (5.3),

$$s_{SF}(t) = sin(2\pi f \cdot t)$$

has been supplied. The sinusoidal tone $s_{SF}(t)$ allows to investigate the cochlear response to a single frequency. Due to the tonotopicity property of the cochlea (see section 1.1 in Chapter 1), the BM oscillates with maximal amplitude in the position which resonates to the stimulus frequency f.

In Figure 5.1 and Figure 5.2 the cochlear response to a 2 kHz-stimulus with 50 dB SPL level is shown, by implementing the anti-damping model and the delayed stiffness model, respectively, on an integration interval of about 20 ms and with $N = 500$. The model approximate solution provides the BM transverse displacement $\xi(x,t)$ and velocity $\dot{\xi}(x,t)$ for each cochlear partition and for each time point simulated. Specifically, the Matlab solver yields a solution matrix where each row contains BM velocity and displacement as function of the spatial mesh points $x_n = n\Delta x$ for $1 \leq n \leq N$ at a fixed time point. The quantities $\xi(x,t)$ and $\dot{\xi}(x,t)$ are oscillating functions and, thus, show the same time-space profile, because they differ only by the angular frequency. In this thesis, the BM velocity will be analyzed. In this way, the results can be compared with the usual measurements of BM velocity on animals.

Both Figure 5.1 and Figure 5.2 show the amplitude of the traveling wave of the BM velocity as function of time and space along the BM. The position $x =$ 0 mm corresponds to the cochlear base, that is the first cochlear partition; the position $x = 35$ mm corresponds to the apex, that is the N^{th} cochlear partition. As you can observe, the BM velocity is an oscillating function with increasing amplitude as the distance from the base increases. Then, at the tonotopic position of about 16 mm the wave reaches its maximal amplitude. In this position a resonance condition occurs because the BM local impedance is minimized at the supplied frequency of 2 kHz. The relationship between the cochlear position and the resonance frequency is defined by the Greenwood Map (1.2), as discussed in section 1.2 and section 1.3 of Chapter 1, or (4.7) of Chapter 4 in the hypothesis of scale invariance. The profile of the BM

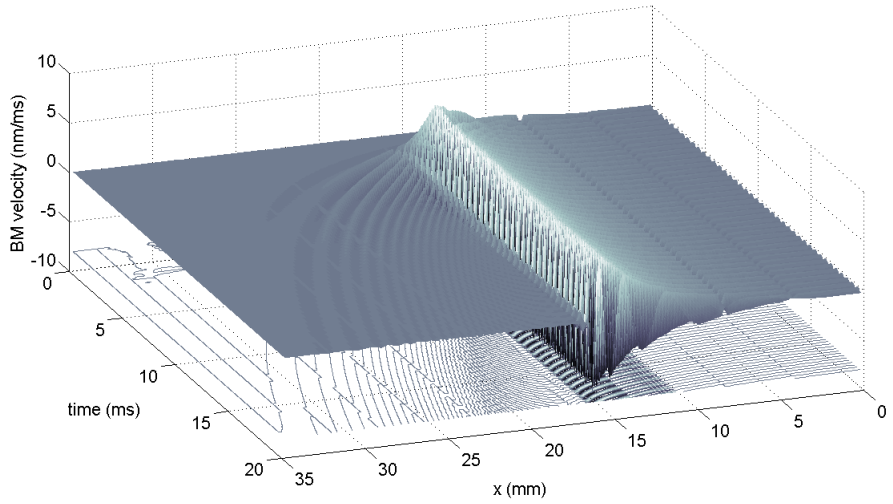

Figure 5.1: Numerical approximate solution of the anti-damping model stimulated by a sinusoidal tone. Model parameters: $N = 500$, $\epsilon = 0.01$, $\alpha_0 = 0.8$, $Q_0 = 4$, $\dot{\xi}_{sat} = 20$ nm/ms, $L[dB] = 50$ dB SPL, $f = 2$ kHz.

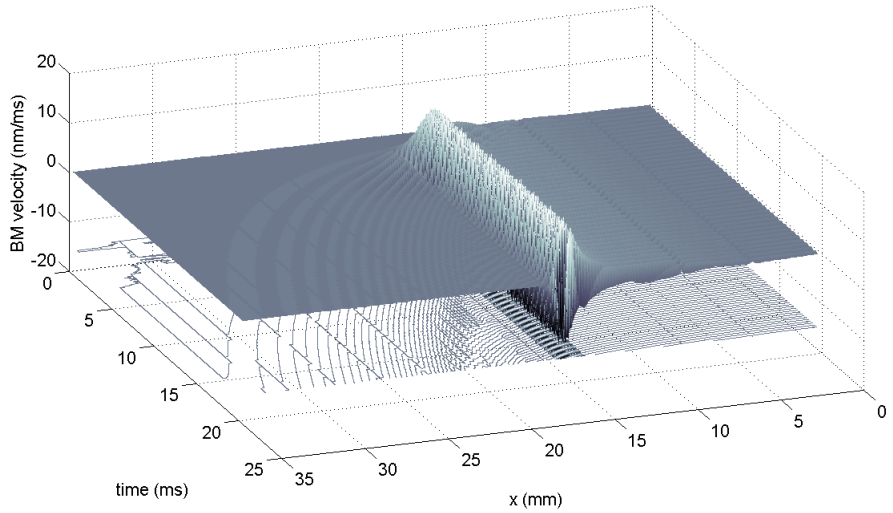

Figure 5.2: Numerical solution of the delayed stiffness model stimulated by a sinusoidal tone. Model parameters: $N = 500$, $\epsilon = 0.01$, $\alpha_0 = 0.8$, $Q_0 = 4$, $\xi_{sat} = 1$ nm, $L[dB] = 50$ dB SPL , $f = 2$ kHz.

velocity falls down after the resonance, as Ren and Nuttall (2001) [149] also observe on animal measurements of BM velocity (see Figure 1.7A in Chapter 1).

Therefore, the approximate solution obtained by the delayed stiffness model is meaningful in terms of the cochlear physical phenomenology and comparable with the results produced by the anti-damping model. This also assures us about the physical soundness of solution obtained by using the integrator for stiff DDEs described in section 4.3.2 in Chapter 4. By means of this integration technique, the physical properties of the delayed stiffness model will be analyzed, as will be discussed in the next sections.

5.5 Properties of the delayed stiffness model

In the previous section the approximate solution of the anti-damping model and the delayed stiffness model, showed that the BM velocity oscillates with increasing amplitude when a single frequency tone is supplied at $x = 0$ mm. In particular, a BM oscillating response at the stimulus frequency is generated with increasing amplitude as the corresponding tonotopic site is approached. In this section some properties of the delayed stiffness model will be analyzed by time integrating the model (5.2) on an interval of 20 ms. All numerical simulations of this section will be performed with the following parameters, unless otherwise specified: $N = 500$, $\epsilon = 0.01$, $\alpha_0 = 0.8$, $Q_0 = 4$, $\xi_{sat} = 1$ nm, $L[dB] = 50$ dB SPL, $f = 2$ kHz.

The approximate solution of (5.2) provides BM displacement and velocity as time function for each cochlear partition. In this way, the response from different cochlear sites can be studied. Figure 5.3 shows the BM velocity as function of time in four different positions along the BM. At $x = 0$ mm a sinusoidal 2kHz-tone is supplied, so an oscillation at the stimulus frequency is caused. In the first three panels of Figure 5.3 an increasing value of the BM velocity amplitude can be noticeable while greater and greater distances from the base ($x = 0$ mm) are observed. When the tonotopic site $x(2\,kHz) \cong 16$ mm is reached (third panel of Figure 5.3), the BM velocity raises to the maximal amplitude. Then, after the resonance condition occurs, the value of the BM velocity amplitude goes down (fourth panel of Figure 5.3). An onset of the response between 0 and about 5 ms is also visible, and it increases with the BM position. During this lag the BM oscillation stabilizes to the value of the regime amplitude. The onset is a consequence of the nonlinear active mechanism driven by the OHCs and the nonlocal property introduced by the Gaussian average (5.5). Namely, the nonlocal nonlinearity makes the cochlear amplifier sensitive to the instantaneous BM displacement level of

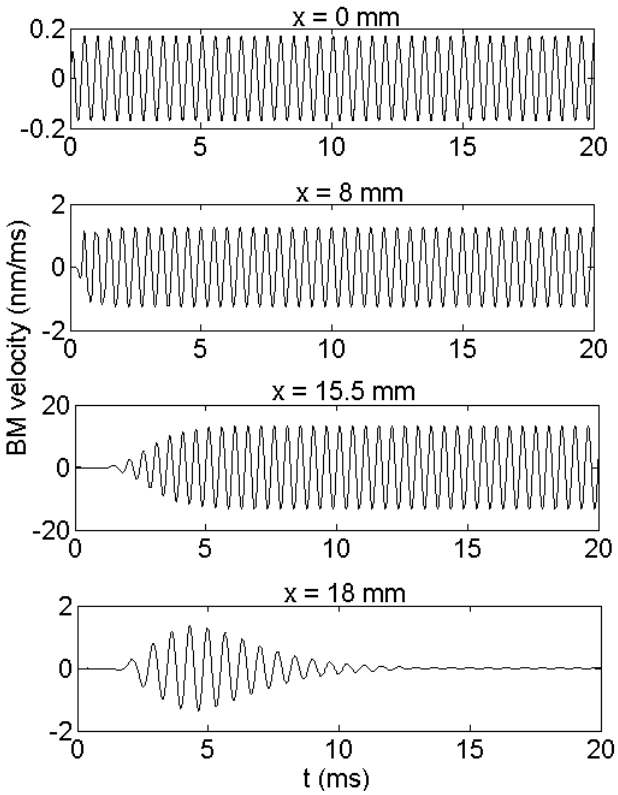

Figure 5.3: Time function of the BM transverse velocity calculated in the approximate solution of the delayed stiffness model (5.2). A sinusoidal tone of 2 kHz has been supplied as sound stimulus at the first cochlear partition $x = 0$ mm. The tonotopic site corresponding to the stimulus frequency is $x(2\,kHz) \cong 16$ mm, displayed in the third panel. Two basal positions and an apical position are also shown in the first two panels and the last one, respectively.

nearby cochlear sites.

In the state space formulation of the model (5.2) (as well as, (5.1)), the cochlear frequency response can be evaluated. Due to the scale invariance cochlear property, the profile of the cochlear response as function of frequency at a fixed cochlear site, has a behavior similar to the cochlear response as function of the space at a fixed frequency. Time-domain solutions of the cochlear model cannot provide frequency profiles with a fine resolution because many hundreds of numerical simulations at different frequencies would be required. However, the fast Fourier transform of the model solution can be considered, and the spectrum of the BM response is then produced for each cochlear site. Consequently, the spectral component of the cochlear

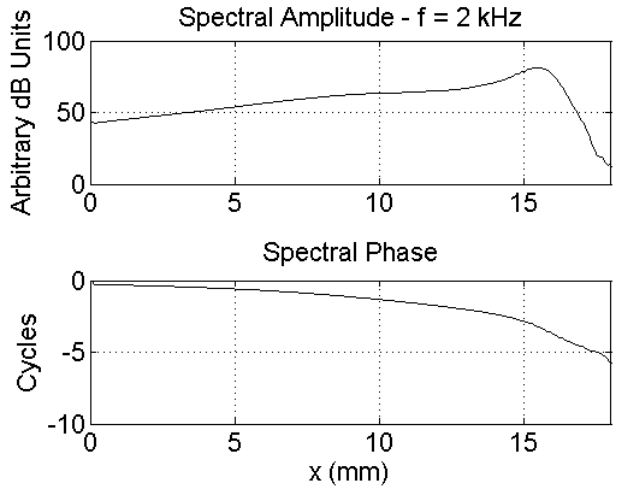

Figure 5.4: Space function of the Fourier component (amplitude and phase) of the BM velocity at the frequency stimulus of 2 kHz in the delayed stiffness model (5.2). Specific ranges of values have been selected on the x-axis and the y-axis. In particular, the values along the x-axis have been limited to the interval [0, 18] mm, because this is the range interested by the resonance phenomenon.

response at a frequency f_0 can be plotted as function of the BM position x. Figure 5.4 shows the Fourier 2 kHz-component of the BM velocity stimulated by a sinusoidal 2 kHz-tone. The BM velocity computed by the same numerical simulation has been displayed in Figure 5.3 as time function. As above discussed, Figure 5.4 also shows a spectral amplitude increasing while the tonotopic place $x(2\,kHz)$ is approached. In $x(2\,kHz)$ a resonance condition occurs, that is a peak of amplitude is reached, and the response falls down beyond $x(2\,kHz)$. The phase of the response is a decreasing function of the position x, as for a forward traveling wave, with a variation of about 5 cycles. If we supply different frequencies, the corresponding tonotopic sites resonate at different positions (see Figure 5.5) according to the Greenwood Map (1.2) (see section 1.2 in Chapter 1) or (4.7) (see section 4.1 in Chapter 4). In particular, higher frequencies resonate at shorter distances from the base, with decreasing amplitude. Such a phenomenology was firstly observed by von Békésy (1960) [203] and de Boer (1980) [49] (see section 1.3 and Figure 1.5 in Chapter 1). On other hand, the phase does not change its slope significantly. Consider that the phase of the cochlear response to a sinusoidal tone is meaningful until the resonance occurs, because beyond the tonotopic position the cochlear response falls down to negligible amplitudes.

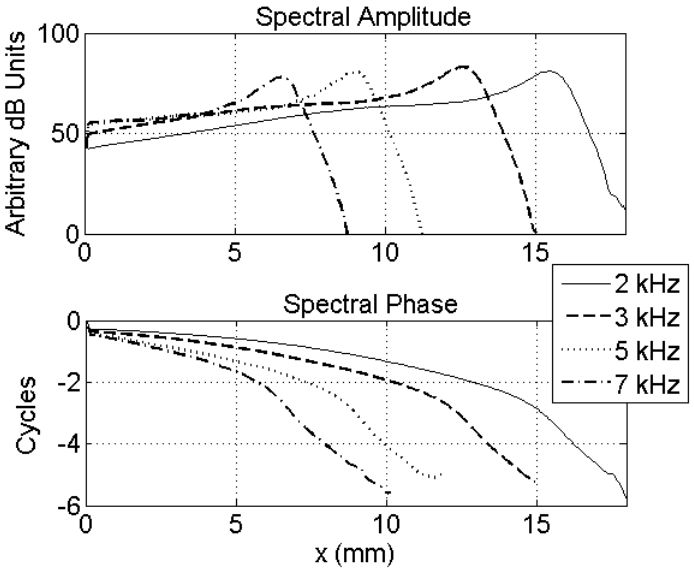

Figure 5.5: Space function of the Fourier component (amplitude and phase) of the BM velocity at stimulus frequencies of 2, 3, 5 and 7 kHz in the delayed stiffness model (5.2). In order to have a better display of the cochlear profiles, specific ranges of values have been selected on the x-axis and the y-axis. In particular, the interval [0, 18] mm has been plotted along the x-axis because the cochlear resonance occurs in this range.

If we observe the BM velocity profile in Figure 5.4, an increasing amplitude (in the form of a "hill") can be also noticeable in the region basal to the tonotopic site $x(2\,kHz)$, with a suppressive effect if the stimulus frequency increases (see Figure 5.5). This basal "hill" is the typical profile in the solution of the delayed stiffness model. It helps to get a broad profile in the cochlear response, as suggested by Zweig and Shera (1991) [210], and then formulated by Talmadge et al. (1998) [189] in the delayed stiffness model.

In order to analyze the action of delayed stiffness terms on the cochlear response, it may be useful to test the effect of each delayed term on the model approximate solution. In Figure 5.6 the cochlear responses by different variants of the delayed cochlear model have been displayed. The Fourier component at the stimulus frequency of 2 kHz has been plotted as a function of the position x. The thin black line represents the approximate solution of the passive model (4.32) (see Chapter 4), that is the model which does not include any additional active nonlinear term. The profile of the BM velocity for a passive cochlea shows a resonance condition with a large bandwidth at a site which is more basal than $x(2\,kHz)$. If the fast delayed term U_{τ_f} is

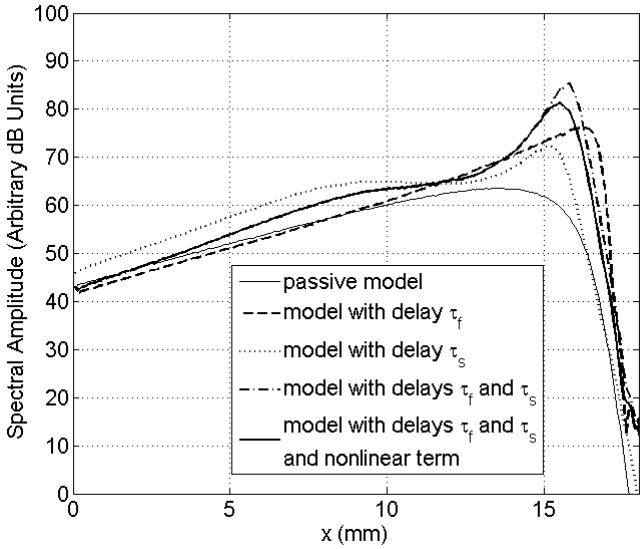

Figure 5.6: Amplitude of the Fourier component at the stimulus frequency of 2 kHz for the approximate solution of the passive model (thin line), the model with the delay τ_f only (dashed line), the model with the delay τ_s only (dotted line), the model with the delays τ_f and τ_s only (dashed and dotted line), the model with the delays τ_f and τ_s and the nonlinear term (the delayed stiffness model (5.2) represented by a bold line). Specific ranges of values have been selected on the x-axis and the y-axis. In particular, the values along the x-axis have been limited to the interval [0, 18] mm, because this is the range interested by the resonance phenomenon.

added to the passive model (called model with delay τ_f in Figure 5.6), then a considerable increase is induced in the response amplitude, with a better tuning of the resonance in $x(2\,kHz)$ and a narrower resonance bandwidth. On the other hand, only the slow delayed term U_{τ_s} causes a shift of the resonance peak towards a more basal position, but also an increase in the oscillation amplitude in a basal region with respect to $x(2\,kHz)$. Therefore, while U_{τ_f} works as an anti-damping force amplifying the BM response, U_{τ_s} helps to create the typical broad BM activity pattern, as already observed in Figure 5.5 and shown in the dotted profile of Figure 5.6 (model with delay τ_s). If also the saturation term is included in the model (model with delays τ_f and τ_s and nonlinear term), then the tonotopic peak decreases its amplitude with respect to the profile of the model with only active delayed terms (model with delays τ_f and τ_s). This is because the saturation level ξ_{sat} of the numerical simulation already works for the 50 dB SPL stimulus

level supplied. Figure 5.7 also shows the effects of the nonlinear active term

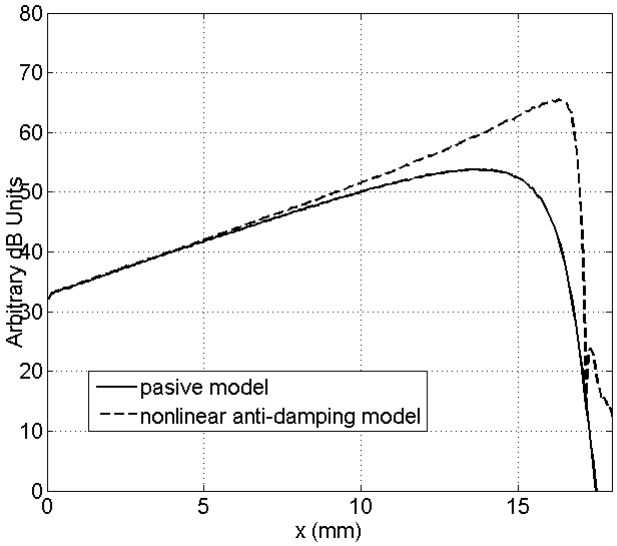

Figure 5.7: Amplitude of the Fourier component at the stimulus frequency of 2 kHz for the approximate solution of the passive model (bold line) and the nonlinear active model (the nonlinear anti-damping model represented by a dashed line). Specific ranges of values have been selected on the x-axis and the y-axis. In particular, the values along the x-axis have been limited to the interval [0, 18] mm, because this is the range interested by the resonance phenomenon.

in the anti-damping model with respect to the passive model (4.32) (see Chapter 4). Analogously to the delayed stiffness model described by Figure 5.6, the active term increases the BM response amplitude and improves the resonance tuning. Note that the profile described by the anti-damping model (dashed line in Figure 5.7) continuously increases from the base ($x = 0$) to the tonotopic site ($x(2\,kHz)$), and power by the active mechanism is released in a region around $x(2\,kHz)$ only. On the other hand, the profile described by the delayed stiffness model (bold line in Figure 5.6) shows that power is also released in a region basal to $x(2\,kHz)$, as caused by the slow feedback delayed term and above discussed.

It is now interesting to study the behavior of the cochlear response by the delayed stiffness model with the stimulus level, as shown in Figure 5.8. The Fourier component at the stimulus frequency of 2 kHz as function of space is involved as above. At low stimulus levels, the BM velocity increases its amplitude linearly, but from 50 dB SPL up the nonlinear term suppresses

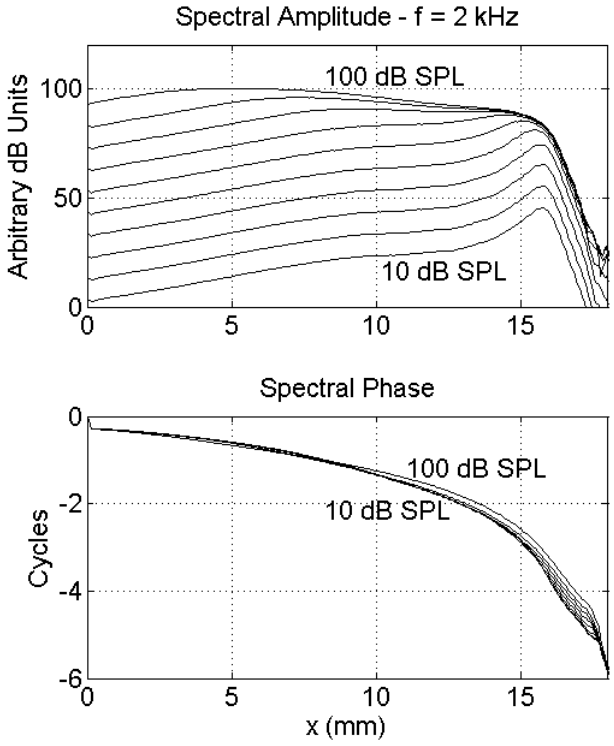

Figure 5.8: Amplitude and phase of the Fourier component at the stimulus frequency of 2 kHz for the approximate solution of the delayed stiffness model, as function of the stimulus level from 10 dB SPL to 100 dB SPL. Specific ranges of values have been selected on the x-axis and the y-axis.

the amplitude in the region around the tonotopic site. This behavior is not physically corresponding to a realistic performance of the inner ear, because a linear regime should again be reached for high stimulus levels. This trend may be performed by means of the nonlinear term of the anti-damping model, as shown in Figure 1.16 reproduced from Moleti et al. (2013) [132] in Chapter 1. On the other hand, tall and broad profiles, observable at low and intermediate stimulus levels in Figure 5.8, are closely similar to the experimental measurements of BM velocity on animals, as reproduced from Ren and Nuttall (2001) [149] in Figure 1.7A (see section 1.3 in Chapter 1).

The approximate solution of the passive model is shown in Figure 5.9, where a linear growth of the cochlear response is observed for all the stimuli, while the amplitude peak and the resonance tuning are remarkably reduced. This phenomenon occurs when the action of the OHCs is lost, as in the insensitive cochlea in the measurements of Ren and Nuttall (2001) [149] re-

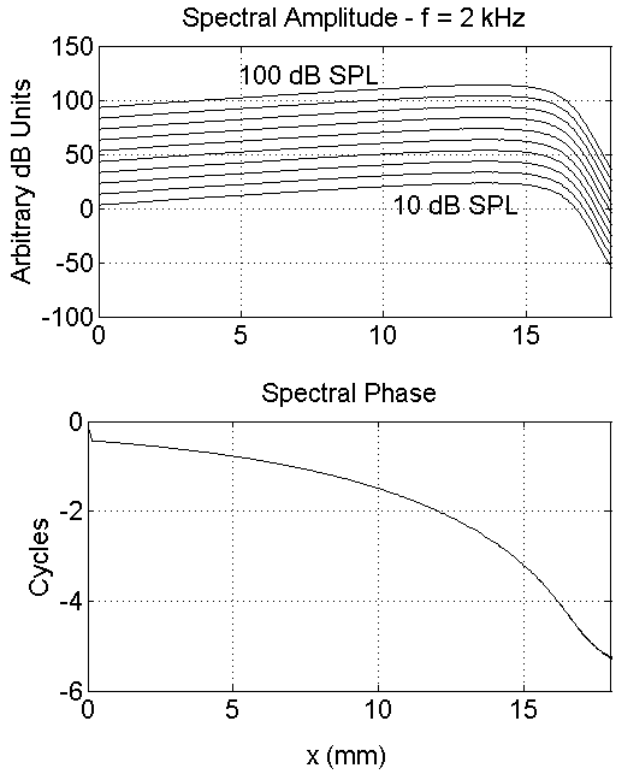

Figure 5.9: Amplitude and phase of the Fourier component at the stimulus frequency of 2 kHz for the approximate solution of the passive model, as function of the stimulus level from 10 dB SPL to 100 d B SPL. Specific ranges of values have been selected on the x-axis and the y-axis. The values along the x-axis have been limited to the interval [0, 18] mm.

produced in Figure 1.7D of Chapter 1. However, if delayed terms are included in the model (Figure 5.8), the cochlear response increases its amplitude peak nonlinearly. Moreover, the phase slope changes with the stimulus level differently from the passive case. This is because now the active mechanism driven by the OHCs is present. Such a mechanism also affects the resonance site by inducing a shift towards more basal positions. This effect is also visible in the measurements on a sensitive cochlea of Ren and Nuttall (2001) [149] and Russell and Nielsen (1997) [157], but it is absent in an insensitive cochlea.

5.6 Some parameters of the delayed stiffness model

Different values for the passive quality factor Q_0 (1.10) (in Chapter 1) or the gain constant α_0 and the saturation amplitude ξ_{sat} in (5.5) may be set in order to change the gain of the active nonlinear mechanism. By means of the next three figures, the effect of Q_0, α_0 and ξ_{sat} on the approximate solution of the delayed stiffness model (5.2) will be analyzed. Unless otherwise specified, all numerical simulations of this section will be performed with the following model parameters: $N = 500$, $\epsilon = 0.01$, $\alpha_0 = 0.8$, $Q_0 = 4$, $\xi_{sat} = 1$ nm, $f = 2$ kHz.

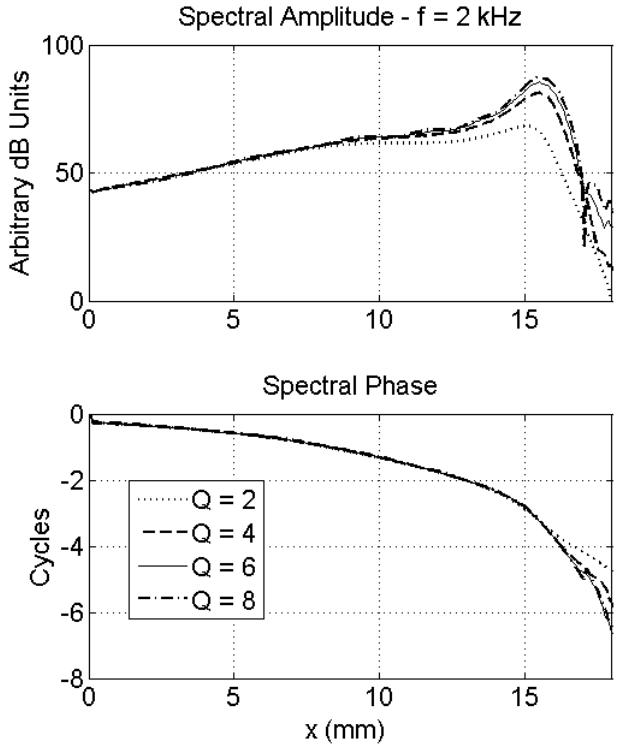

Figure 5.10: Amplitude and phase of the Fourier component at the stimulus frequency of 2 kHz for the approximate solution of the delayed stiffness model as function of the passive quality factor Q_0. The stimulus level is $L[dB] = 50$ dB SPL. Specific ranges of values have been selected on the x-axis and the y-axis.

In Figure 5.10 the BM velocity profile has been plotted as function of

the BM position x for different values of the passive quality factor Q_0. An increasing spectral amplitude of the BM velocity and a decreasing resonance bandwidth are visible as Q_0 increases. The greatest effect occurs when Q_0 increases from 2 to 4.

On the other hand, if the gain constant α_0 is decreased, the BM velocity amplitude increases because the value of the function $C_{nl_{DS}}(x,t)$ (5.5) of the nonlinear term reduces, as shown in Figure 5.11. Note the shift of the resonance site towards apical positions while α_0 decreases, namely, the nonlinearity of the active mechanism reduces.

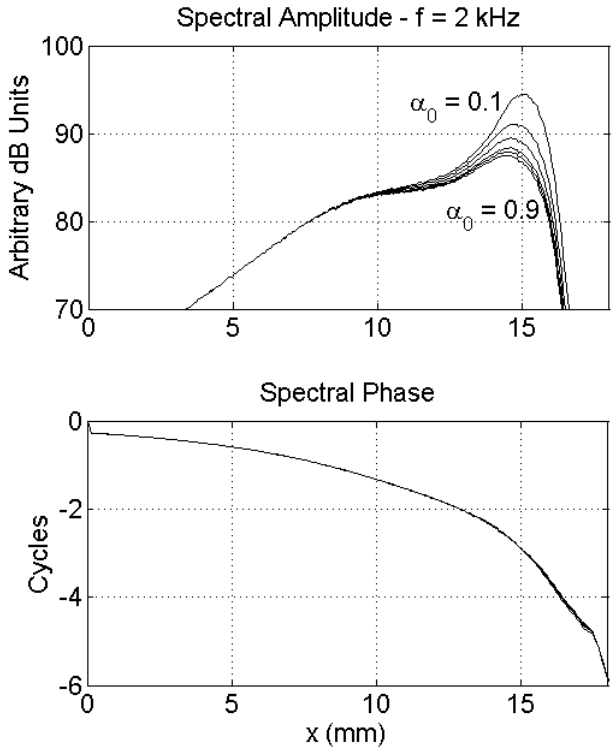

Figure 5.11: Amplitude and phase of the Fourier component at the stimulus frequency of 2 kHz for the approximate solution of the delayed stiffness model as function of the gain constant α_0 (chosen values for α_0 are 0.1, 0.3, 0.5, 0.7, 0.8, 0.9). The stimulus level is $L[dB] = 70$ dB SPL. Specific ranges of values have been selected on the x-axis and the y-axis.

The cochlear nonlinearity is performed by the nonlinear coefficient (5.5), where ξ_{sat} establishes a saturation amplitude. Namely, if $\xi(x,t) << \xi_{sat}$ the cochlear gain is linear, whereas the cochlear response saturates if $\xi(x,t)$ is close to ξ_{sat} or $\xi(x,t) >> \xi_{sat}$ (as is visible in Figure 5.8 from the stimulus

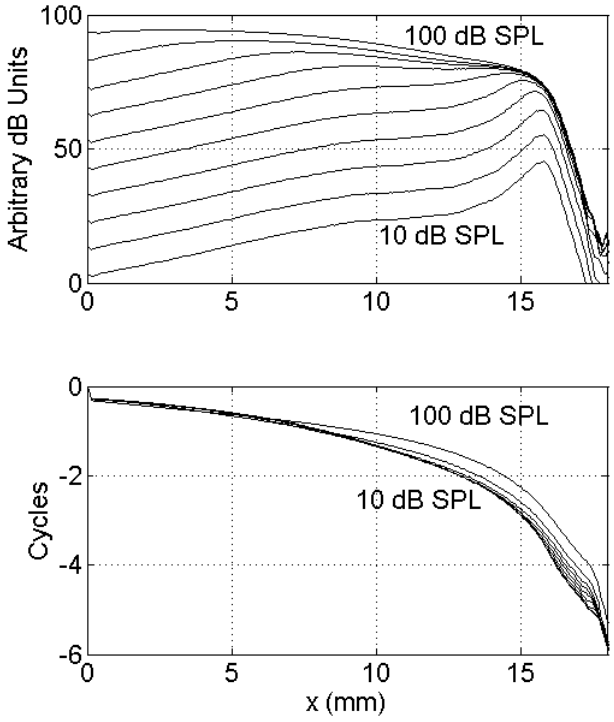

Figure 5.12: Amplitude and phase of the Fourier component at the stimulus frequency of 2 kHz for the approximate solution of the delayed stiffness model, as function of the stimulus level from 10 dB SPL to 100 dB SPL. The value of the saturation amplitude has been set to $\xi_{sat} = 0.33$ nm. Specific ranges of values have been selected on the x-axis and the y-axis.

level of 50 dB SPL). Therefore, the choice about the value of ξ_{sat} is one of the crucial issues for yielding realistic cochlear profiles at different stimulus levels. In Figure 5.8 numerical simulations with $\xi_{sat} = 1$ nm are shown, and a saturation region begins from the stimulus level of 50 dB SPL. In a real cochlea a linear gain is again obtained for high stimulus levels. For example, observe the linear region of the cochlear response for 90 dB SPL and 100 dB SPL in Figure1.7A in Chapter 1, whereas a saturation occurs on the cochlear response of Figure 5.8 at the same stimulus levels. This behavior is a typical characteristic of the nonlinear function (1.30) introduced by Talmadge et al. (1998) [189] in the delayed stiffness model (see section 1.5.4 in Chapter 1). In this thesis, (1.30) has been formulated in the form (5.5), where the saturation amplitude has been considered as a free parameter ξ_{sat}, besides the introduction of the gain constant α_0 and the spatial Gaussian average.

Varying the value ξ_{sat}, different saturation levels are obtained. For example, decreasing the saturation amplitude ξ_{sat} to the value of 0.33 nm, a nonlinear behavior is visible from 40 dB SPL up (see Figure 5.12), while the saturation level was fixed at 50 dB SPL with $\xi_{sat} = 1$ nm (see Figure 5.8).

5.7 The cochlear response of a model with two degrees of freedom

The state space formulation was introduced by Elliott et al. (2007) [61] for the linear active cochlear model formulated by Neely (1981) [137] and Neely and Kim (1986) [138] for the cat cochlea. Elliott et al. also formulated the cochlear nonlinearity in their model. Specifically, each micromechanical

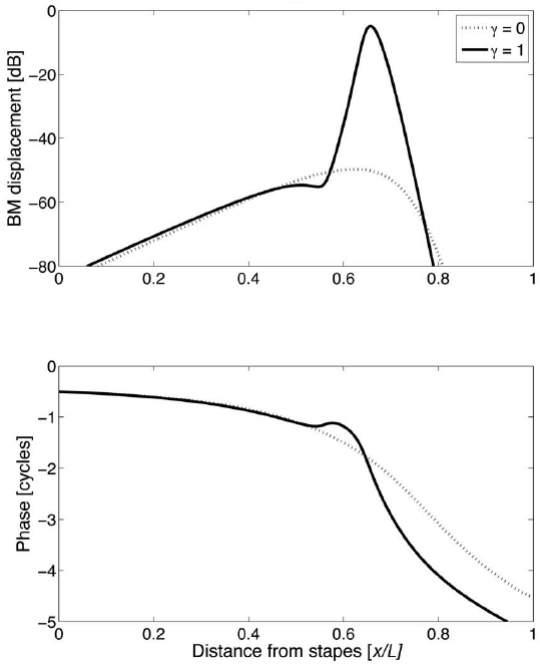

Figure 5.13: Amplitude and phase of the BM displacement computed by means of the state space model by Elliott et al. (2007) [61] with the parameters of Neely and Kim (1986) [138] at 1.6 kHz. The dotted line ($\gamma = 0$) represents the passive model, while the solid line ($\gamma = 1$) represents the active model. This figure has been reproduced from [61].

element is described as a lumped component model with two masses (the tectorial membrane-TM and the BM), three springs and three dampers in an one-dimensional model of the cochlea. A couple spring-damper connects

the two masses and attaches the masses to the rigid bone (see Figure 1.3 in Chapter 1 for a mammalian cross section of cochlea). The differential pressure of the cochlear fluid and an active pressure source, activated by a nonlinear feedback loop between the two masses, are applied to the BM. Moreover the relative motion between BM and TM represents the hair bundle displacement.

The cochlear response of the model of Elliott et al. has been reproduced in Figure 5.13, where the BM displacement is shown for the passive model and the nonlinear active model at 1.6 kHz ($x(1.6\,kHz)/L \cong 0.72$ with $L = 25$ mm for a cat cochlea). The passive BM displacement shows the typical resonance profile with a large bandwidth, as also yielded by the passive delayed stiffness model or the passive anti-damping model (see Figure 5.6 and Figure 5.7, respectively, in section 5.5). On the other hand, active model elements introduce a resonance peak at $x(1.6\,kHz)$.

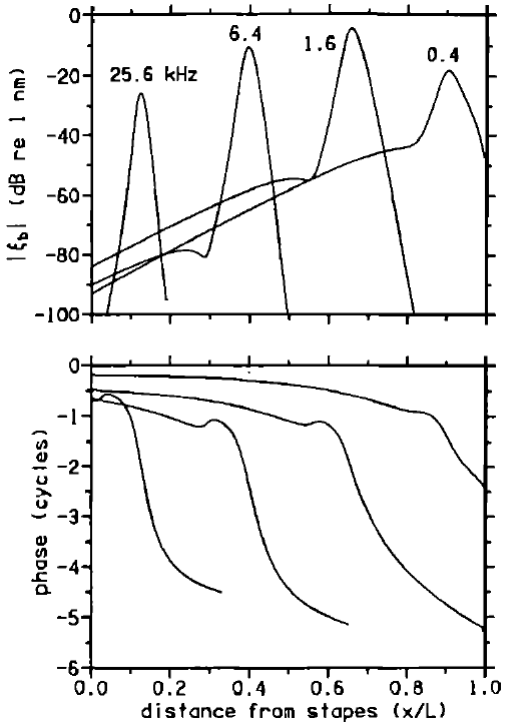

Figure 5.14: Amplitude and phase of the BM displacement in the linear active model of Neely and Kim (1986) [138] at different frequencies. This figure has been reproduced from [138].

The results of Elliott et al., reproduced in Figure 5.13, are similar to those obtained by Neely and Kim. In particular, in Figure 5.14 amplitude

and phase of the BM displacement, computed by Neely and Kim, are shown for different frequencies.

In the double oscillator model of Elliott et al., as well as the model of Neely and Kim, the profile of the cochlear response shows a resonance peak which does not grow from the basal positions monotonically. A depression is caused before the BM displacement increases to reach the maximal amplitude at the tonotopic site, as noticeable in Figure 5.13 or Figure 5.14. Then, a double oscillator model also yields the typical profile of the delayed stiffness model, but without basal release of power by the OHCs. Namely, a basal increase of the oscillation amplitude does not occur in an active model with respect to a passive model. If we observe the cochlear response carried out by Ren and Nuttall (2001) [149] on gerbils (see Figure 1.7 in Chapter 1), a broad and tall behavior is noticeable, but a basal increase does not occur in the sensitive cochlea with respect to the insensitive cochlea. Rather, at the basal positions the BM velocity amplitude is lower when the OHCs are working.

Therefore, both the double oscillator model of Elliott et al. (2007) [61] (or Neely and Kim, 1986 [138]) and the delayed stiffness model of Talmadge et al. (1998) [189] allows to yield realistic profiles of the cochlear response, although the model simplifications can generate some differences in the profiles of the BM displacement, as well as in the anti-damping model. Nevertheless, all the models discussed reproduce many properties of the cochlear phenomenology and, thus, allow to perform reliable numerical experiments of cochlear mechanics.

Conclusions

In this thesis a physical model of the human cochlea based on delay differential equations (DDEs) has been analyzed. Realistic numerical experiments have been performed and comparable results with some model variants have been yielded. All the models discussed include partial differential equations (PDEs), as, in particular, formulated by Neely and Kim (1986) [138], Talmadge et al. (1998) [189], Elliott et al. (2007) [61], Moleti et al. (2013) [132]. In particular, a PDE of the second order with respect to the spatial variable, describes the dynamic of the cochlear fluid in a box model of the cochlea (rectified) divided in two cavities by the basilar membrane (BM). Moreover, a spatial discretization of the cochlea divides the BM in a finite number of micromechanical elements. Each one of such elements is considered a forced damped harmonic oscillator. Forcing terms are the local differential pressure of the cochlear fluid and the additional pressure performed by the outer hair cells (OHCs) through a nonlinear active mechanism. In particular, in the *anti-damping model* this mechanism is performed by a nonlinear function of the BM velocity. On the other hand, in the *delayed stiffness model*, two additional forces, proportional to the BM displacement delayed by constant delays, act as generators of tall and broad profiles of the BM activity pattern.

The delayed model was formulated by Talmadge et al. [189] on the assumptions of Zweig (1991) [210] and Zweig and Shera (1995) [211]. In this thesis a numerical approximation of the model solution has been found in the time domain. The spatial discretization of the continuous model is based on the same approach used for the anti-damping model by Moleti et al. (2009) [135], firstly, generating the semidiscrete model. The latter is given by a sequence of initial value problems (IVPs) of constant DDEs parametrized by the spatial step size. Such IVPs have been then integrated by means of a numerical scheme for DDEs (Bellen and Zennaro, 2003 [10]) and the customized `ode15s` package in Matlab (Bertaccini and Sisto, 2011 [20]).

In particular, as introduced by Elliott et al. (2007) [61], the continuous model has been spatially discretized in the *state space* in a discrete set of micro-elements. The number of these elements has to be quite large, at least

500, as set in this thesis. In this way, a matrix formulation of the continuous model has been obtained, turning the continuous PDE delayed model into a sequence of IVPs based on DDEs.

The state space formalism has many advantages, as pointed out by Elliott et al. (2007) [61]. Firstly, it converts the PDE of the continuous model in sequences of IVPs of differential equations that can be integrated in the time domain. The size of the matrices involved in the state space formulation increases with the number N of cochlear partitions, by using large values of N for performing realistic simulations. Secondly, the problem at hand is an oscillating dynamic system and power is released by means of nonlinear active terms, which simulate the feedback mechanism of the OHCs. Consequently, some numerical instabilities might be generated in the active cochlear model. That is, complex poles of the system matrix might have positive real part for some frequencies and cause exponentially divergent oscillations. An analysis of the model approximate solution for all the individual frequency cannot be carried out in the time domain, because many hundreds of simulations should be performed. On the other hand, a stability analysis of the model solution in the frequency domain may be more difficult to evaluate and interpret, as well as computationally expensive if the cochlear model is strongly nonlinear. However, in the state space formalism the study of stability has an immediate approach because the eigenvalues of the system matrix, that is, the Jacobian of the semidiscrete model, represent the poles of the system for all the micromechanical elements of the cochlea discretized. The position of the poles can be computed by fast algorithms in Matlab, as performed in this thesis for both the anti-damping model and the delayed stiffness model.

In general, for an IVP of ODEs expressed in the state space, the approximate solution can be found by advancing in time by means of a suitable numerical solver (as in the case of the anti-damping model). Then the numerical solution of each discretized element can be found for all the points of the time mesh. The semidiscrete equations of delayed stiffness model are represented by a system of IVPs based on constant DDEs. The integration time interval has been divided in subintervals of length equals to the minimum delay. Then, the semidiscrete model has been turned into a finite number of IVPs based on ODEs for each subinterval. This approach is called *method of steps* in literature (see, for example, Bellen and Zennaro, 2003 [10]), and fixes the initial condition of the IVPs with the approximate solution computed in the last mesh point of the previous subinterval. This procedure here also sets the value of the displacements delayed throughout each subinterval. In the algorithm implemented in this thesis, subintervals of 3 mesh points have been considered, that is, with a time resolution of about 0.006 ms. Consequently, the proposed numerical scheme performs an

approximation of the delayed stiffness on two points for each subinterval. We experienced that this technique seems to be effective for finding a numerical approximate solution of the delayed stiffness model in the state space. In this way, the model solution can be approximated for each micromechanical element and time point with fine spatial and time resolution. The *method of steps* based on the customized `ode15s` has allowed to exploit the benefits of the algebraic properties of the matrices in the semidiscrete method, and yielded comparable results with other models, as the anti-damping model or the model of Elliott et al. (2007) [61]. However, greater numerical advantages might be obtained by a formulation of the continuous model or a technique of time advancing which allow to update the delayed displacement at each time point. Such improvements will be evaluated in forthcoming studies, in order to decrease the approximation error in the evaluation of the delayed displacement, and obtain more accurate results.

Some numerical considerations have been necessary in order to assure the convergence of integrator for the delayed stiffness model. In particular, a spatial Gaussian average of the nonlinear term has been introduced in the model of Talmadge et al. (1998) [189] because of the fast oscillation of the BM displacement. Such an average also introduces the nonlocality in the cochlear response, because the dynamics of every tonotopic site is affected by the activity pattern of the neighboring sites.

The key features of the delayed stiffness model have been tested by supplying a sinusoidal tone as sound stimulus at the first cochlear element. In these simulations, the adopted numerical technique seems to be able to yield a cochlear response which predicts several aspects of the cochlear phenomenology. In particular, properties of tonotopicity, anti-damping and nonlinearity have been tested. The results show a tall and broad BM activity pattern, as evaluated by Zweig (1991) [210] on experimental animal data and Talmadge et al. (1998) [189] on the analytical solution of the model. In this thesis spatial profiles of the BM velocity have been obtained at the stimulus frequency, with a decreasing spectral phase, as expected for a forward traveling wave. Moreover, a resonance condition has been verified at the tonotopic place corresponding to the stimulus frequency. The effect of the free model parameters has been also analyzed, as the passive quality factor, the gain constant and the saturation amplitude of the cochlear amplifier. In this way, a greater confidence on the behavior of the model with the free parameters can help to adjust their value and perform more realistic simulations. Other kinds of stimuli can be implemented, and, for example, distortion products and transient evoked responses might be studied and other properties of the cochlea might be analyzed.

However, the BM activity patterns generated by the delayed stiffness

model as function of the stimulus level, show a behavior which is not in agreement with the experimental data. Namely, after a linear gain at low stimulus levels, an amplitude threshold establishes a saturation effect in the cochlear gain and a linear growth is not recovered at high stimuli. More detailed models have been formulated in literature. For example, the model of Elliott et al. (2007) [61] introduced the OHCs coupling with both the tectorial membrane and the BM. Greater modeling details may be useful in order to reconcile the model solution with the experimental data. At the same time, a more detailed cochlear model includes many free parameters to be handled and makes the interpretation of the model results more complicated. On the other hand, a suitable simplification in the description of the active nonlinear mechanism, driven by the OHCs, may be sufficient if we are interested in the generation mechanisms of the cochlear response, and then, of the otoacoustic emissions. Actually, both the anti-damping model and the delayed stiffness model produce reliable and accurate results. In particular, a fine agreement has been observed in the BM activity pattern between the delayed stiffness model and the model of Elliott et al. . Nevertheless, the cochlear nonlinearity of the delayed stiffness model might need a refinement by means of the formulation of a nonlinear term which works more closely to the compressive function of the real cochlear gain. Such a term has not to release energy, but to generate a saturation region at intermediate stimulus levels only. This is a crucial issue in the modeling of the nonlinearity in the delayed stiffness model, because some numerical instabilities might be generated if further damping or anti-damping functions are added to the fast and slow feedback terms. The nonlinear active term of the anti-damping model produces a more realistic behavior of the cochlear gain with the stimulus level, being linear at low and high stimulus levels, and compressive for intermediate stimulus levels, whereas a monotonic growth of the BM profile is observed while the tonotopic site is approached.

All the models discussed in this thesis are able to predict the main properties of the cochlear response and analyze the generation mechanism. In particular, the delayed stiffness model shows BM activity patterns which raise to the tonotopic resonance through a typical tall and broad profile, as in experimental data (see, for example, Ren and Nuttall, 2001 [149]). Therefore, such a refined model might represent a good theoretical approach to be involved in the analysis of the cochlear mechanisms and the generation of the otoacoustic emissions. In this way, the formulation of more realistic active and nonlinear terms will allow to apply cochlear modeling more efficiently to the study of the cochlear mechanics and the design of hearing diagnostic techniques. For this reason, the improvement of the cochlear properties predicted by the delayed stiffness model, as well as the analysis of such a

model by means of more sophisticated sound stimuli, will be the object of forthcoming studies.

Bibliography

[1] W.E.Arnoldi (1951). The principle of minimized iteration in the solution of the matrix eigenvalue problem. Quart. Appl. Math., 9, 17-29.

[2] U.M.Ascher and L.R.Petzold. Computer methods for Ordinary Differential Equations and Differential-Algebraic Equations. SIAM, Philadelphia, 1998.

[3] O.Axelsson. Iterative Solution Methods. Cambridge University Press, New York, 1994.

[4] C.T.H.Baker. Numerical analysis of Volterra functional and integral equations. In: The state of the art in Numerical Analysis, I.S.Duff and G.A.Watson Eds., Clarendon Press, Oxford 1996.

[5] C.T.H.Baker (2000). Retarded differential equations. J. Comput. Appl. Math. 125, 309-335.

[6] C.T.H.Baker, and C.A.H.Paul (1996). A global convergence theorem for a class of PCERK methods and vanishing lag DDEs. SIAM J. Numer. Anal. 33, 1559-1576.

[7] C.T.H.Baker, C.A.H.Paul, and D.R.Willé (1995). Issue in the numerical solution of evolutionary delay differential equations. Adv. Comput. Math. 3, 171-196.

[8] C.T.H.Baker, C.A.H.Paul, and D.R.Willé. A bibliography on the numerical solution of delay differential equations. NA Report 269, Dept of Mathematics, University of Manchster 1995.

[9] A.Bellen (1985). Constrained mesh methods for functional differential equations. In: Delay equations, approximation and application, ISNM 74, 52-70.

[10] A.Bellen, and M.Zennaro. Numerical methods for delay differential equations. Oxford University Press 2003.

[11] R.Bellmann, and K.L.Cooke. Differential-Difference Equations. Academic Press, New York-London 1963.

[12] C.M.Bender, and S.A.Orszag. Advanced Mathematical Methods for Scientists and Engineers. McGraw-Hill, New York 1978.

[13] D.Bertaccini. Lecture notes of the course "Numerical methods for PDEs". University of Rome Tor Vergata. Unpublished, 2011.

[14] D.Bertaccini. Lecture notes of the course "Time dependent PDEs, structures and preconditioning". The Rome-Moscow School of matrix methods and applied linear algebra 2011. Unpublished.

[15] D.Bertaccini, and D.Calvetti (2007). Fast simulations of solid tumors thermals ablation treatments with a 3D reaction diffusion model. Comput. Biol. Med. 37(8), 1173-1182.

[16] D.Bertaccini, F.Di Benedetto (2007). Spectral analysis of nonsymmetric quasi-Toeplitz matrices with applications to preconditioned multistep formulas. SIAM J. Numer. Anal. 45-6, 2345-2367.

[17] D.Bertaccini, and S.Fanelli (2009). Computational and conditioning issues of a discrete model for cochlear sensorineural hypoacusia. Appl. Num. Mat. 59, 1989-2001.

[18] D.Bertaccini, G.H.Golub, and S.Serra-Capizzano (2007). Spectral analysis of a preconditioned iterative method for the convection-diffusion equation. SIAM J. Matr. Anal. Appl. 29, 260-278.

[19] D.Bertaccini, and M.K.Ng (2003). Band-Toeplitz preconditioned GMRES iterations for time-dependent PDEs. BIT Numerical Mathematics 43(5), 901-914.

[20] D.Bertaccini, and R.Sisto (2011). Fast Numerical solution of nonlinear nonlocal cochlear models. J. Comp. Phys. 230, 2575-2587.

[21] H.G.Bock, and J.Schlöder (1981). Numerical solution of retarded differential equation with state dependent time lags. ZAMM 61, 269-271.

[22] T.Botti (2012). Cochlear Models and Numerical Solution. Unpublished. Poster presentation, 7th Workshop Structural Dynamical Systems: Computational Aspects SDS2012, June 12-15, Hotel-Villaggio Porto Giardino, Capitolo-Monopoli, Bari (Italy).

[23] T.Botti (2014). Delay stiff differential equations in a cochlear model. Unpublished. Poster presentation, 8th Workshop Structural Dynamical Systems: Computational Aspects SDS2014, June 10-13, Hotel-Villaggio Porto Giardino, Capitolo-Monopoli, Bari (Italy).

[24] T.Botti, R.Sisto, A.Moleti, L.D'Amato, and F.Sanjust (2014). DPOAE generation mechanisms and frequency ratio functions. Assoc. Res. Otolaryngol. Abs. 37, 68-69, PS120 (37th Annual Midwinter meeting of the ARO, Manchester Grand Hyatt, San Diego (CA), USA, February 22-26, 2014).

[25] T.Botti, R.Sisto, A.Moleti, L.D'Amato, and F.Sanjust (2014). DPOAE generation dependence on primary frequency ratio. In press on AIP Conf. Proc., 12th International Workshop Mechanics of Hearing, 23-29 June, Cape Sounio (Greece).

[26] R.K.Brayton, F.G.Gustavson, and G.D.Hachtel (1972). A new efficient algorithm for solving differential-algebraic systems using implicit backward differentiation formulas. Proc. IEEE 60, 98-108.

[27] P.N.Brown, G.D.Byrne, and A.C.Hindmarsh (1989). VODE: a variable-coefficient ODE solver. SIAM J. Sci. Comput. 10, 1038-1051.

[28] B.H.Brown, R.H.Smallwood, D.C.Barber, P.V.Lawford, and D.R.Hose. Medical physics and biomedical engineering. Ed. Taylor & Francis 1999.

[29] H.Brunner. Collocation methods for Volterra integral and related functional differential equations. Cambridge University Press 2004.

[30] J.C.Butcher. The numerical analysis of ordinary differential equations. Wiley, London 1987.

[31] J.C.Butcher. Numerical methods for Ordinary Differential Equations. John Wiley, Chichester, UK, 2003.

[32] G.D.Byrne and A.C.Hindmarsh (1975). A polyalgorithm for the numerical solution of ordinary differential equations. ACM Transactions on Mathematical Software 1, 71-96.

[33] R.Chadwick (1980). Studies in cochlear mechanics. In: Mathematical Modeling of the Hearing Process Lecture Notes in Biomathematics, 43. Ed: M.H.Holmes and L.A.Rubenfeld (Springer-Verlag, Berlin, Heidelberg, New York).

[34] R.S.Chadwick, A.Inselberg, and K.Johnson (1976). Mathematical model of the cochlea. II: results and conclusions. SIAM J. Appl. Math. 30, 164-179.

[35] C.C.Cheney. Introduction to Approximation Theory. McGraw Hill, NY, 1966.

[36] Y.Choi, S.Lee, K.Parham, S.T.Neely, and D.O.Kim (2008). Stimulus-frequency otoacoustic emissions: Measurements and simulations with an active cochlear model. J. Acoust. Soc. Am. 123, 2651-2669.

[37] E.A.Coddington and N.Levinson. Theory of Ordinary Differential Equations. McGraw-Hill, New York, 1955.

[38] S.D.Conte and C.de Boor. Elementary Numerical Analysis. McGraw-Hill, New York, 1980.

[39] S.P.Corwin, D.Sarafyan, and R.Thompson (1997). DKLAG6: a code based on continuously imbedded sixth-order Runge-Kutta methods for the solution of state dependent functional differential equations. Appl. Numer. Math. 24, 319-330.

[40] C.W.Cryer. Numerical methods for functional differential equations. In: Delay and functional differential equations and their applications. K.Schmitt Ed., Academic Press, New York 1972.

[41] C.W.Cryer, and L.Tavernini (1972). The numerical solution of Volterra functional differential equations by Euler's method. SIAM J. Numer. Anal. 9, 105-129.

[42] A.R.Curtis. The FACSIMILE numerical integrator for stiff initial value problems. In: Computational Techniques for Ordinary Differential Equations, I. Gladwell and D.K.Sayers, eds., Academic, London, 1980.

[43] C.F.Curtiss and J.O.Hirschfelder (1952). Integration of stiff equations. Proc. Nat. Acad. Sci. USA, 38, 235-243.

[44] G.Dahlquist (1963). A special stability problem for linear multistep methods. BIT, 3, 27-43.

[45] P.Dallos, C.D.Geisler, J.W.Matthews, M.A.Ruggero, and C.R.Steele. Eds. (1990). The Mechanics and Biophysics of Hearing. Lecture Notes in Biomathematics, 87 (Springer-Verlag, Berlin, Heidelberg, New York).

[46] P.Dallos, A.N.Popper, and R.R.Fay, Eds. (1996). The Cochlea. Springer-Verlag, New York.

[47] B.N.Datta. Numerical Linear Algebra and Applications. Brooks/Cole Publishing, Pacific Grove, CA, 1995.

[48] T.A.Davis. Direct methods for sparse linear systems. SIAM, Philadelphia, 2006.

[49] E.de Boer (1980). Auditory physics, Physical principles in hearing theory, I. Physics Reports (Review Section of Physics Letters) 62 (2), 87-174, North-Holland Publishing Company.

[50] E.de Boer (1983). No sharpening? A challenge for cochlear mechanics. J. Acoust. Soc. Am. 73, 567-573.

[51] E.de Boer (1995). On equivalence of locally active models of the cochlea. J. Acoust. Soc. Am. 98, 1400-1409.

[52] E.de Boer (1996). Mechanics of the cochlea: modeling efforts. In "The Cochlea". Ed. P.Dallos, A.N.Popper, R.R.Fay (Springer-Verlag, New York).

[53] E.de Boer, and A.L.Nuttall (2009). Inverse-solution method for a class of non-classical cochlear models. J. Acoust. Soc. Am. 125, 2146-2154.

[54] K.Dekker, and J.G.Verwer. Stability of Runge-Kutta methods for stiff nonlinear differential equations. North-Holland, Amsterdam 1984.

[55] S.Dhar, A.Rogers, and C.Abdala (2011). Breaking away: Violation of distortion emission phase-frequency invariance at low frequencies. J. Acoust. Soc. Am. 129, 3115-3122.

[56] O.Diekmann, S.A.van Gils, S.M.Verduyn-Lunel, and H.O.Walter. Delay equations: functional-, complex-, and nonlinear analysis. AMS series 110. Springer-Verlag, Berlin 1995.

[57] R.D.Driver (1963). Existence theory for a delay differential system. Contributions to differential equations 1, 317-336.

[58] R.D.Driver. Ordinary and delay differential equations. Springer-Verlag, Berlin 1977.

[59] I.S.Duff, A.M.Erisman, and J.K.Reid. Direct Methods for Sparse Matrices. Clarendon Press, Oxford, 1986.

[60] V.M.Eguíluz, M.Ospeck, Y.Choe, A.J.Hudspeth, and M.O.Magnasco (2000). Essential nonlinearities in hearing. Phys. Rev. Lett. 82, 5232-5235.

[61] S.J.Elliott, E.M.Ku, and B.Lineton (2007). A state space model for cochlear mechanics. J. Acoust. Soc. Am. 122, 2759-2771.

[62] L.E.El'sgol'ts. Qualitative methods in mathematical analysis. Amer. Math. Soc., Providence R.I. 1964

[63] L.E.El'sgol'ts, and S.B.Norkin. Introduction to the theory and application of differential equations with deviating arguments. Academic Press, New York 1973.

[64] W.H.Enright, and M.Hu (1995). Interpolating Runge-Kutta methods for vanishing lag delay differential equations. Computing 55, 223-236.

[65] W.H.Enright, T.E.Hull, and B.Lindberg. Comparing numerical methods for stiff systems of ODE's. BIT 15, 10-48.

[66] A.Feldstein, and K.W.Neves (1984). High order methods for state-dependent delay differential equations with nonsmooth solutions. SIAM J. Numer. Anal. 21, 844-863.

[67] H.Fletcher (1951). On the dynamics of the cochlea. J. Acoust. Soc. Am. 23, 637-645.

[68] S.Fox. Human Physiology. Ed. McGraw-Hill 2006.

[69] M.Furst, and M.Lapid (1988). A cochlear model for acoustic emissions. J. Acoust. Soc. Am. 84, 222-229.

[70] C.W.Gear. Numerical Initial Value Problems in Ordinary Differential Equations. Prentice-Hall, Englewood Cliffs, NJ, 1971.

[71] C.W.Gear, and Y.Saad (1983). Iterative solution of linear equations in ODE codes. SIAM J. Sci. Stat. Comput. 4, 583-601.

[72] C.W.Gear and D.S.Watanabe (1974). Stability and convergence of variable order multistep methods. SIAM J. Numer. Anal. 11, 1044-1058.

[73] S.A.Gelfand. Hearing: an introduction to psychological and physiological acoustics. Marcel Dekker Ed., New York 1998.

[74] J.R.Gilbert, C.Moler, and R.Schreiber (1992). Sparse matrices in MATLAB: design and implementation. SIAM J. Matrix Anal. Appl. 13, 333-356.

[75] T.Gold (1948). Hearing. II. The physical basis of the action of the cochlea. Proc. R. Soc. Lond. B. Biol. Sci. 135, 492-498.

[76] G.H.Golub and C.F.Van Loan. Matrix Computations. Third ed. Johns Hopkins University Press, Baltimore, 1996.

[77] A.Greenbaum. Iterative methods for solving linear systems. SIAM, Philadelphia, 1997.

[78] D.D.Greenwood (1990). A cochlear frequency position function for several species-29 years later. J. Acoust. Soc. Am. 87, 2592-2605.

[79] B.Gustafsson, H.O.Kreiss, and J.Oliger. Time dependent problems and difference methods. John Wiley, New York, 1995.

[80] W.Hackbusch. Iterative Solution of Large Linear Systems of Equations. Springer Verlag, New York, 1994.

[81] E.Hairer, S.P.Norsett, and G.Wanner. Solving ordinary differential equations I, Nonstiff problems. Springer-Verlag, Berlin 1993.

[82] E.Hairer, and G.Wanner. Solving ordinary differential equations II, Stiff and differential algebraic problems. Springer-Verlag, New-York 1991.

[83] J.K.Hale. Theory of functional differential equations. Springer-Verlag, New York 1977.

[84] J.K.Hale. Homoclinic orbits and chaos in delay equations. In: Proc. The ninth dundee conference on ordinary and partial differential equations. B.D.Sleeman and R.J.Jarvis Eds, Wiley, New York 1986.

[85] J.K.Hale, and S.M.Verduyn Lunel. Introduction to functional differential equations. Appl. Math. Sc. 99, Springer-Verlag, New York 1977.

[86] J.W.Hall (2000). Handbook of Otoacoustic Emissions. San Diego: Singular Publishing Group.

[87] P. R. Halmos. Finite-Dimensional Vector Spaces. Springer Verlag, New York, 1958.

[88] H.Hayashi, and W.H.Enright. A new algorithm for vanishing delay problems. In: Procedings of Canadian Applied Mathematical Society Annual Meeting, University of York 1993.

[89] P.Henrici. Discrete variable methods in Ordinary Differential Equations. John Wiley, New York, 1962.

[90] D.J.Higham and L.N.Trefethen (1993). Siffness of ODEs. BIT, 33, 285-303.

[91] A.C.Hindmarsh (1980). LSODE and LSODI, two new initial value ordinary differential equation solvers. ACM SIGNUM Newsletter 15, 10-11.

[92] M.H.Holmes (1980). An analysis of a low-frequency model of the cochlea, J. Acoust. Soc. Am. 68, 482-488.

[93] M.H.Holmes (1980). Low frequency asymptotics for a hydroelastic model of the cochlea. SIAM J. Appl. Math. 38, 445-456.

[94] M.H.Holmes (1982). A mathematical model of the dynamics of the inner ear. J. Fluid Mech. 116, 59-75.

[95] M.Holmes, and J.D.Cole (1984). Cochlear mechanics: analysis for a pure tone. J. Acoustic. Soc. Amer. 76, 767-778.

[96] A.S.Householder. Theory of Matrices in Numerical Analysis. Blaisdell Pub. Co.,Johnson, CO, 1964.

[97] A.Inselberg (1978). Cochlear dynamics: the evolution of a mathematical model. SIAM Rev. 20, 301-351.

[98] A.Inselberg, and R.S.Chadwick (1976). Mathematical model of the cochlea. I: formulation and solution. SIAM J. Appl. Math. 30, 149-163.

[99] A.Iserles. Numerical analysis of differential equations. Cambridge University Press, Cambridge, UK, 1996.

[100] D.Kahaner, C.Moler, and S.Nash. Numerical Methods and Software. Prentice-Hall, Englewood Cliffs, NJ, 1989.

[101] R.Kalluri, and C.A.Shera (2007). Near equivalence of human click-evoked and stimulus-frequency otoacoustic emissions. J. Acoust. Soc. Am. 121, 2097-2110.

[102] L.J.Kanis, and E.de Boer (1993). Self-suppression in a locally active nonlinear model of the cochlea: A quasilinear approach. J. Acoust. Soc. Am. 94, 3199-3206.

[103] A.Karoui, and R.Vaillancourt (1994). Computer solution of state-dependent delay differential equations. Comput. Math. Appl. 27, 37-51.

[104] A.Karoui, and R.Vaillancourt (1995). A numerical method for vanishing-lag delay differential equations. Appl. Numer. Math. 17, 383-395.

[105] J.Keener, and J.Sneyd. Mathematical physiology. Springer 1998.

[106] D.T.Kemp (1978). Stimulated acoustic emissions from within the human auditory system. J. Acoust. Soc. Am. 64, 1386-1391.

[107] D.T.Kemp (1979). Evidence of mechanical nonlinearity and frequency selective wave amplification in the cochlea. Arch. Oto-Rhino-Laryngol. 224, 37-45.

[108] D.T.Kemp (1986). Otoacoustic emissions, travelling waves and cochlear mechanisms. Hear. Res. 22, 95-104.

[109] D.T.Kemp, and R.A.Chum (1980). Properties of the generator of stimulated acoustic emissions. Hear. Res. 2, 213-232.

[110] D.T.Kemp, S.Ryan, and P.Brah (1990). A guide to the effective use of otoacoustic emissions. Ear Hear. 11, 93-105.

[111] J.Kevorkian. Partial Differential Equations. Wadsworth & Brooks/-Cole, Pacific Corove, CA, 1990.

[112] H.Kim, and D.M.Barrs (2006). Hearing aids: a review of what's new. Otolaryngology-Head and Neck Surgery 134, 1043-1050.

[113] D.O.Kim, S.T.Neely, C.E.Molnar, and J.W.Matthews (1980). An active cochlear model with negative damping in the partition: Comparison with Rhode's ante- and post-mortem observations. In: Psychophysical and Behavioral Studies in Hearing. Edited by G.V.d.Brink and F.A.Bilsen (Delft U.P., Delft), pp. 7-14.

[114] Y.Kim, and J.Xin (2005). A two-dimensional nonlinear nonlocal feed-forward cochlear model and time domain computation of multitone interactions. Multiscale Model. Simul. 4(2), 664-690.

[115] R.W.Klopfenstein (1971). Numerical differentiation formulas for stiff systems of ordinary differential equations. RCA Review 32, 447-462.

[116] R.D.Knight, and D.T.Kemp (2001). Wave and place fixed DPOAE maps of the human ear. J. Acoust. Soc. Am. 109, 1513-1525.

[117] V.Kolmanovskii, and A.Myshkis. Applied theory of functional differential equations. Kluwer, Dordrecht 1992

[118] V.Kolmanovskii, and V.Nosov. Stability of functional differential equations. Academic Press, London 1986.

[119] M.A.Krasnoselskii, G.M.Vainikko, P.P.Zabreico, Ya.B.Rutitskii, and V.Ya.Stetsenko. Approximate Solutions of Operator Equations. Wolters-Nordhoff, Groningen, 1972.

[120] F.T.Krogh (1973). Algorithms for changing the step size. SIAM J. Numer. Anal. 10, 949-965.

[121] E.M.Ku (2008). Modelling the human cochlea. Ph.D. thesis, University of Southampton, United Kingdom.

[122] Y.Kuang. Delay differential equations with applications in populations dynamics. Academic Press, Boston 1993.

[123] J.D.Lambert. Computational methods in Ordinary Differential Equations. John Wiley, New York, 1973.

[124] J.D.Lambert. Numerical methods for ordinary differential systems: the initial value problem. John Wiley 1993.

[125] M.B.Lesser, and D.A.Berkley (1972). Fluid mechanics of the cochlea. Part I. J. Acoust. Soc. Am. 51, 497-512.

[126] R.J. LeVeque. Finite Difference Methods for Ordinary and Partial Differential Equations. Steady-State and Time-Dependent Problems. SIAM 2007.

[127] K.M.Lim, and C.R.Steele (2002). A three-dimensional nonlinear active cochlear model analyzed by the WKB-numeric method. Hear. Res. 170, 190-205.

[128] G.R.Long, C.L.Talmadge, and J.Lee (2008). Measuring distortion product otoacoustic emissions using continuously sweeping primaries. J. Acoust. Soc. Am. 124, 1613-1626.

[129] M.C.Makey, and L.Glass (1977). Oscillation and chaos in physiological control systems. Science 197, 287-289.

[130] D.McFadden, and R.Mishra (1993). On the relation between hearing sensitivity and otoacoustic emissions. Hear. Res. 71, 208-213.

[131] G.Meinardus, and G.Nürnberger (1985). Approximation theory and numerical methods for delay differential equations. In: Delay equations, approximation and application, ISNM 74, 13-40.

[132] A.Moleti, A.M.Al-Maamury, D.Bertaccini, T.Botti, and R.Sisto (2013). Generation place of the long- and short-latency components of transient evoked otoacoustic emissions in a nonlinear cochlear model. J. Acoust. Soc. Am. 133, 4098-4108.

[133] A.Moleti, D.Bertaccini, T.Botti, and R.Sisto (2013). Numerical simulations of the transient-evoked otoacoustic response. AIA-DAGA Abs., pp. 425 (Conference on Acoustics 2013, Merano, Italy).

[134] A.Moleti, T.Botti, and R.Sisto (2012). Transient-evoked otoacoustic emission generators in a nonlinear cochlea. J. Acoust. Soc. Am. 131, 2891-2903.

[135] A.Moleti, N.Paternoster, D.Bertaccini, R.Sisto, and F.Sunjust (2009). Otoacoustic emissions in time-domain solutions of nonlinear nonlocal cochlear models. J. Acoust. Soc. Am. 126, 2425-2436.

[136] K.W.Morton and D.F.Mayers. Numerical solution of partial differential equations. Cambridge University Press, Cambridge, UK, 1994.

[137] S. T. Neely (1981). Finite difference solution of a two-dimensional mathematical model of the cochlea. J. Acoust. Soc. Am. 69, 1386-1393.

[138] S.T.Neely, and D.O.Kim (1986). A model for active elements in cochlear biomechanics. J. Acoust. Soc. Am. 79, 1472-1480.

[139] K.W.Neves, and A.Feldstein (1976). Characterization of jump discontinuities for state dependent delay differential equations. J. Math. Anal. Appl. 56, 689-707.

[140] R.Nobili, and F.Mammano (1996). Biophysics of the cochlea II: Stationary nonlinear phenomenology. J. Acoust. Soc. Am. 99, 2244-2255.

[141] R.Patuzzi (1996). Cochlear micromechanics and macromechanics. In: Springer Handbook of Auditory Research, Volume 8: The Cochlea. Edited by P.Dallos, A.N.Popper, and R.R.Fay (Springer-Verlag, New York), pp. 186-257.

[142] C.A.H.Paul (1992). Developing a delay differential equation solver. Appl. Numer. Math. 9, 403-414.

[143] L.C.Peterson and B.P.Bogert (1950). A dynamical theory of the cochlea. J. Acoust. Soc. Am. 22, 369-381.

[144] J.C.Polking. MATLAB Manual for Ordinary Differential Equations. Prentice-Hall, Englewood Cliffs, NJ, 1995.

[145] R.Probst, B.L.Lonsbury-Martin, and G.K.Martin (1991). A review of otoacoustic emissions. J. Acoust. Soc. Am. 89, 2027-2066.

[146] S.Puria (2003). Measurements of human middle ear forward and reverse acoustics: Implications for otoacoustic emissions. J. Acoust. Soc. Am. 113, 2773-2789.

[147] O.F.Ranke (1950). Theory of operation of the cochlea: A contribution to the hydrodynamics of the cochlea. J. Acoust. Soc. Am. 22, 772-777.

[148] T.Reiher. Statilitätsuntersuchungen bei rückwärtigen differentiationsformeln in Abhängigkeit von einem parameter. Tech. Report 11, Sektion Mathematik, Humboldt Universität zu Berlin, 1978.

[149] T.Ren, and A.L.Nuttall (2001). Basilar membrane vibration in the basal turn of the sensitive gerbil cochlea. Hearing Research 151, 48-60.

[150] W.S.Rhode (1971). Observations of the vibration of the basilar membrane in squirrel monkeys using the Mössbauer technique. J. Acoust. Soc. Am. 49, 1218-1231.

[151] W.S.Rhode (2007). Basilar membrane mechanics in the 6-9 kHz region of sensitive chinchilla cochleae. J. Acoust. Soc. Am. 121, 2792-2804.

[152] R.D.Richtmyer and K.W.Morton. Difference methods for Initial-Value Problems. Wiley-Interscience, New York, 1967.

[153] T.J.Rivlin. The Chebyshev Polynomials: from Approximation Theory to Algebra and Number Theory. J. Wiley and Sons, New York, 1990.

[154] M.S.Robinette, and T.J.Glattke. Otoacoustic Emissions: Clinical Applications. Third Edition. New York, Thieme Medical Publishers 2007.

[155] L.Robles, and M.A.Ruggero (2001). Mechanics of the Mammalian Cochlea. Physiol. Rev. 81(3), 1305-1352.

[156] J.R.Rosowski (1995). Models of external- and middle-ear function. In: Springer Handbook of Auditory Research, Volume 6: Auditory Computation. Edited by H.L.Hawkins, T.A.McMullen, A.N.Popper, and R.R.Fay (Springer-Verlag, New York), pp. 15-61.

[157] I.J.Russell, and K.E.Nielsen (1997). The location of the cochlear amplifier: Spatial representation of a single tone on the guinea pig basilar membrane. Proc. Natl. Acad. Sci. USA 94, 2660-2664.

[158] Y.Saad (1981). Krylov subspace methods for solving large unsymmetric linear systems. Mathematics of Computation, 37, 105-126.

[159] Y.Saad. Iterative methods for sparse Linear Systems. PWS Publishing Company, Boston, MA, 1995.

[160] Y.Saad and M.H.Schultz (1986). GMRES: a generalized minimal residual algorithm for solving nonsymmetric linear systems. SIAM Journal on Scientific and Statistical Computing, 7, 856-869.

[161] E.Schloth (1983). Relation between spectral composition of spontaneous otoacoustic emissions and fine structure of threshold in quiet. ACUSTICA, Vol. 53.

[162] L.F.Shampine (1980). Implementation of implicit formulas for the solution of ODE's. SIAM J. Sci. Statist. Comput. 1, 103-118.

[163] L.F.Shampine (1981). Evaluation of a test set for stiff ODE solvers. ACM Trans. Math. Software 7, 409-420.

[164] L.F.Shampine. Numerical Solution of Ordinary Differential Equations. Chapman & Hall, New York, 1994.

[165] L.F.Shampine and L.S.Baca (1984). Error estimators for stiff differential equations. J. Comp. Appl. Math. 11, 197-207.

[166] L.F.Shampine and M.K.Gordon. Computer solution of ordinary differential equations: the Initial Value Problem. W.H.Freeman, San Francisco, 1975.

[167] L.F.Shampine, and M.W.Reichelt (1997). The Matlab Ode Suite. SIAM J. Sci. Comput. 18, 1-22.

[168] L.F.Shampine, and S.Thompson (2001). Solving DDEs in MATLAB. Appl. Num. Math. 37, 441-458.

[169] C.A.Shera, and J.J.Guinan (1999). Evoked otoacoustic emissions arise by two fundamentally different mechanisms: A taxonomy for mammalian OAEs. J. Acoust. Soc. Am. 105, 782-798.

[170] C.A.Shera, A.Tubis, and C.L.Talmadge (2005). Coherent reflection in a two-dimensional cochlea: Short-wave versus long-wave scattering in the generation of reflection-source otoacoustic emissions. J. Acoust. Soc. Am. 118, 287-313.

[171] C.A.Shera, and G.Zweig (1993). Dynamic symmetry creation: The origin of spectral periodicity in evoked otoacoustic emissions. In: Biophysics of Hair Cell Sensory Systems. Edited by H.Duifhuis, J.W.Horst, P.van Dijk, and S.M.van Netten (World Scientific, Singapore), pp. 54-63.

[172] C.A.Shera, and G.Zweig (1993). Noninvasive measurements of the cochlear traveling wave ratio. J. Acoust. Soc. Am. 93, 3333-3352.

[173] W.M.Siebert (1974). Ranke revisited - a simple short-wave cochlear model. J. Acoust. Soc. Am. 56, 594-600.

[174] R.Sisto, T.Botti, A.Moleti, and D.Bertaccini (2010). Numerical simulations of otoacoustic emissions from a non-linear non-local cochlear model. AIP Conf. Proc. 1281, 1047-1050 (ICNAAM 2010).

[175] R.Sisto, and A.Moleti (1999). Modeling otoacoustic emissions by active nonlinear oscillators. J. Acoust. Soc. Am. 106, 1893-1906.

[176] R.Sisto, and A.Moleti (2007). Transient evoked otoacoustic emission latency and cochlear tuning at different stimulus levels. J. Acoust. Soc. Am. 122, 2183-2190.

[177] R.Sisto, and A.Moleti (2008). Transient evoked otoacoustic emission input/output function and cochlear reflectivity: Experiment and model. J. Acoust. Soc. Am. 124, 2995-3008.

[178] R.Sisto, A.Moleti, T.Botti, D.Bertaccini, and C.A.Shera (2011). Distortion product otoacoustic emissions and backward traveling waves in nonlinear active models of the cochlea. J. Acoust. Soc. Am. 129, 3141-3152.

[179] R.Sisto, A.Moleti, and M.Lucertini (2001). Spontaneous otoacoustic emissions and relaxation dynamics of long decay time OAEs in audiometrically normal and impaired subjects. J. Acoust. Soc. Am. 109, 638-647.

[180] R.Sisto, A.Moleti, N.Paternoster, T.Botti, and D.Bertaccini (2010). Different models of the active cochlea, and how to implement them in the state-space formalism. J. Acoust. Soc. Am. 128, 1191-1202.

[181] R.Sisto, A.Moleti, and C.A.Shera (2007). Cochlear reflectivity in transmission-line models and otoacoustic emission characteristic time delays. J. Acoust. Soc. Am. 122, 3554-3561.

[182] R.Sisto, F.Sanjust, and A.Moleti (2013). Input/output functions of different-latency components of transient-evoked and stimulus-frequency otoacoustic emissions. J. Acoust. Soc. Am. 133, 2240-2253

[183] C.R.Steele (1974). Behavior of the basilar membrane with pure-tone excitation. J. Acoust. Soc. Am. 55, 148-162.

[184] T.Steihaug and A.Wolfbrandt (1979). An attempt to avoid exact Jacobian and non-linear equations in the numerical solution of stiff differential equations. Math. Comp. 33, 521-534.

[185] G.W.Stewart. Introduction to matrix computations. Academic Press, New York, 1973.

[186] G.W.Stewart, J.G.Sun. Matrix Perturbation Theory. Academic Press, NY, 1990.

[187] J.C.Strikwerda. Finite difference schemes and partial differential equations. Second ed. SIAM, Philadelphia, 2004.

[188] C.Talmadge, and A.Tubis (1993). On modeling the connection between spontaneous and evoked otoacoustic emissions. In: Biophysics of Hair Cell Sensory Systems. Edited by H.Duifhuis, J.W.Horst, P.van Dijk, and S.M.van Netten (World Scientific, Singapore), pp. 25-32.

[189] C.L.Talmadge, A.Tubis, G.R.Long, and P.Piskorski (1998). Modeling otoacoustic emission and hearing threshold fine structure. J. Acoust. Soc. Am. 104, 1517-1443.

[190] C.L.Talmadge, A.Tubis, G.R.Long, and C.Tong (2000). Modeling the combined effects of basilar membrane nonlinearity and roughness on

stimulus frequency otoacoustic emission fine structure. J. Acoust. Soc. Am. 104, 1517-1543.

[191] C.Talmadge, A.Tubis, P.Piskorski, and G.R.Long (1997). Modeling otoacoustic emission fine structure. In: Diversity in Auditory Mechanics. Edited by E.Lewis, G.Long, R.Lyon, P.Narins, and C.Steele (World Scientific, Singapore), pp. 462-471.

[192] L.Tavernini (1971). One-step methods for the numerical solution of Volterra functional differential equations. SIAM J. Numer. Anal. 4, 786-795.

[193] L.Tavernini (1973). Linear multistep methods for the numerical solution of Volterra functional differential equations. Applicable Anal. 3, 169-185.

[194] L.Tavernini (1978). The approximate solution of Volterra differential systems with state dependent time lags. SIAM J. Numer. Anal. 15, 1039-1052.

[195] G.Teschl. Ordinary differential equations and dynamical systems. American Mathematical Society, 2012.

[196] G.Tognola, F.Grandori, and P.Ravazzani (2001). Data processing options and response scoring for OAE-based newborn hearing screening. J. Acoust. Soc. Am. 109, 283-290.

[197] L.Torelli (1989). Stability of numerical method for delay differential equations. J. Comput. Appl. Math. 25, 15-26.

[198] L.N.Trefethen and D.Bau, III. Numerical Linear Algebra. SIAM, Philadelphia, 1997.

[199] A.Tveito and R.Winther. Introduction to partial differential equations: a computational approach. Springer, New York, 1998.

[200] P.van Hengel (1993). Comment on 'periodicity in otoacoustic emissions'. In: Biophysics of Hair Cell Sensory Systems. Edited by H.Duifhuis, J.W.Horst, P.van Dijk, and S.M.van Netten (World Scientific, Singapore), p. 62.

[201] R.S.Varga. Matrix Iterative Analysis. Prentice Hall, Englewood Cliffs, NJ, 1962.

[202] G.von Békésy. (1949). The vibration of the cochlear partition in anatomical preparation and in models of the inner ear. J. Acoust. Soc. Am. 21, 233-245.

[203] G.von Békésy. Experiments in Hearing. McGraw-Hill, New York 1960.

[204] S.E.Voss, and C.A.Shera (2004). Simultaneous measurement of middle ear input impedance and forward/reverse transmission in cat. J. Acoust. Soc. Am. 116, 2187-2198.

[205] D.R.Willé, and C.T.H.Baker (1992). The tracking of derivative discontinuities in systems of delay differential equations. Appl. Numer. Math. 9, 209-222.

[206] D.R.Willé, and C.T.H.Baker (1992). DELSOL - a numerical code for the solution of systems of delay differential equations. Appl. Numer. Math. 9, 223-234.

[207] D.R.Willé, and C.T.H.Baker. Some issues in the detection and location of derivative discontinuities in delay differential equations. NA Report 238, Dept of Mathematics, University of Manchester 1994.

[208] D.M.Young. Iterative Solution of Large Linear Systems. Academic Press, New York, 1971.

[209] M.Zennaro. Delay differential equations: theory and numerics. In: Theory and numerics of ordinary and partial differential equations, M.Ainsworth, J.Levesley, W.A.Light and M.Marletta Eds., Clarendon Press, Oxford 1995.

[210] G.Zweig (1991). Finding the impedance of the organ of Corti. J. Acoust. Soc. Am. 89, 1229-1254.

[211] G.Zweig, and C.A.Shera (1995). The origins of periodicity in the spectrum of evoked otoacoustic emissions. J. Acoust. Soc. Am. 98, 2018-2047.

[212] E.Zwicker, and E.Schloth (1984). Interrelation of different oto-acoustic emissions. J. Acoust. Soc. Am. 75, 1148-1154.

[213] J.Zwislocki (1953). Review of recent mathematical theories of cochlear dynamics. J. Acoust. Soc. Am. 25, 743-751.